HYDROCARBON RESERVOIR POTENTIAL OF THE MISSISSIPPIAN CHAINMAN SHALE, WESTERN UTAH

by S. Robert Bereskin, John D. McLennan, Thomas C. Chidsey, Jr., and Peter J Nielsen

MISCELLANEOUS PUBLICATION 15-4
UTAH GEOLOGICAL SURVEY
a division of
UTAH DEPARTMENT OF NATURAL RESOURCES
2015

HYDROCARBON RESERVOIR POTENTIAL OF THE MISSISSIPPIAN CHAINMAN SHALE, WESTERN UTAH

by S. Robert Bereskin [1], John D. McLennan [2], Thomas C. Chidsey, Jr. [3], and Peter J Nielsen [3]

[1]Bereskin and Associates, Inc., Salt Lake City, Utah
[2]University of Utah, Salt Lake City, Utah
[3]Utah Geological Survey, Salt Lake City, Utah

Cover photo: *Typical outcrop of the Chainman Shale, Camp Canyon, central Confusion Range, western Utah.*

ISBN 978-1-55791-910-6

MISCELLANEOUS PUBLICATION 15-4
UTAH GEOLOGICAL SURVEY
a division of
UTAH DEPARTMENT OF NATURAL RESOURCES
2015

STATE OF UTAH
Gary R. Herbert, Governor

DEPARTMENT OF NATURAL RESOURCES
Michael Styler, Executive Director

UTAH GEOLOGICAL SURVEY
Richard G. Allis, Director

PUBLICATIONS
contact
Natural Resources Map & Bookstore
1594 W. North Temple
Salt Lake City, UT 84114
telephone: 801-537-3320
toll-free: 1-888-UTAH MAP
website: mapstore.utah.gov
email: geostore@utah.gov

UTAH GEOLOGICAL SURVEY
contact
1594 W. North Temple, Suite 3110
Salt Lake City, UT 84114
telephone: 801-537-3300
website: geology.utah.gov

The Miscellaneous Publication series provides non-UGS authors with a high-quality format for documents concerning Utah geology. Although review comments have been incorporated, this document does not necessarily conform to UGS technical, editorial, or policy standards. The Utah Department of Natural Resources, Utah Geological Survey, makes no warranty, expressed or implied, regarding the suitability of this product for a particular use. The Utah Department of Natural Resources, Utah Geological Survey, shall not be liable under any circumstances for any direct, indirect, special, incidental, or consequential damages with respect to claims by users of this product.

CONTENTS

ABSTRACT 1
INTRODUCTION 1
Purpose 1
Previous Work 1
Methods of Study and Scope 4
REGIONAL OVERVIEW 4
Chainman Shale 4
Confusion Range 7
GEOLOGIC DISCUSSION 7
Measured Section 7
Microscopic Observations 11
Laboratory Testing 12
Total Organic Carbon and Programmed Pyrolysis 12
Tight Rock Analysis 13
X-Ray Fluorescence and X-Ray Diffraction 13
Sample collection and preparation 13
Overview 14
Results 14
Discussion 15
Interpretation 17
RESOURCE EVALUATION 18
Overview of Exploration Wells Penetrating the Chainman Shale, Western Millard County, Utah 18
Hand-Held Gamma Logging 20
Petrophysical Techniques 20
Results 21
Camp Canyon Measured Section Petrophysics 21
Geochemistry 23
Porosity 23
Resource Calculations 23
CONCLUSIONS 26
ACKNOWLEDGMENTS 28
REFERENCES 28
APPENDICES
Appendix A—Measured Section ..... on CD
Appendix B—Geophysical and Petrophysical Logs ..... on CD
Appendix C—Thin Section Analysis ..... on CD
Appendix D—Scanning Electron Microscopy ..... on CD
Appendix E—X-Ray Fluorescence and X-Ray Diffraction ..... on CD

FIGURES

Figure 1. Location map of the Camp Canyon study site and measured section for the Mississippian Chainman Shale, central Confusion Range, western Utah 2
Figure 2. Stratigraphic column of the Chainman Shale, Confusion Range, comparing stratigraphic nomenclature 3
Figure 3. Schematic west to east cross section from eastern Nevada through Utah during Mississippian time 6
Figure 4. Paleogeography of Utah and eastern Nevada during Mississippian time 6
Figure 5. Geologic map of the central Confusion Range, western Millard County, Utah 8
Figure 6. Overview from the Willow Gap Member to the lower part of the Chainman Shale, Camp Canyon area 10
Figure 7. View north along the topographically resistant Willow Gap Member 11
Figure 8. Contact of resistant Willow Gap limestone beds with the overlying recessive mixed rocks of the Jensen Member 12
Figure 9. Plot of the Chemical Index of Alteration and Chemical Index of Weathering from samples of the Chainman Shale 15
Figure 10. Plot of whole-rock, weight-percent ratios from members of the Chainman Shale 16
Figure 11. Vertical thickness plot of the percentages of carbonates, non-clay mineral silicates, and clay minerals from samples collected in the Chainman Shale 16

Figure 12. Ternary plot of average percentages of carbonates, non-clay mineral silicates, and clay minerals from members of the Chainman Shale 18
Figure 13. Location of selected deep exploration wells in and adjacent to Millard County, western Utah 19
Figure 14. Trenching for fresh samples in portions of recessive units—Jensen Member 20
Figure 15. Spectral gamma ray components and total gamma ray 20
Figure 16. Van Krevelen diagram showing total organic carbon (TOC) measurements from the samples collected from the Confusion Range and legacy data from Aminoil No. 1-23 Land Co. well, Pine Valley, Nevada 24
Figure 17. Hydrocarbon generation versus TOC plot suggesting that the kerogen is gas to dry-gas prone 24
Figure 18. Hydrogen index versus Tmax suggesting the possibility of oil as well as dry gas 24
Figure 19. Production index versus Tmax, suggesting dry gas, wet gas, and oil are possibilities in the Chainman Shale 24
Figure 20. Total gamma-ray track from hand-held scintillometer measurements and the laboratory measured values for vitrinite reflectance 25
Figure 21. Total gamma-ray track from hand-held scintillometer measurements and the laboratory measured values for TOC 25
Figure 22. Inferred vitrinite curve for the lower members of the Chainman Shale 26
Figure 23. Gas-filled porosity and inferred porosity over the hypothesized hydrocarbon-bearing zones of the Chainman Shale 27
Figure 24. Possible cumulative volumes (recoverable estimate) of oil and gas for a hypothetical Chainman completion 27

TABLES

Table 1. Total organic carbon and programmed pyrolysis data of Chainman Shale from the Camp Canyon section 5
Table 2. Tight rock analysis data of Chainman Shale. 5
Table 3. List of exploration wells penetrating the Chainman Shale in and adjacent to Millard County, western Utah 19

HYDROCARBON RESERVOIR POTENTIAL OF THE MISSISSIPPIAN CHAINMAN SHALE, WESTERN UTAH

by S. Robert Bereskin, John D. McLennan, Thomas C. Chidsey, Jr., and Peter J Nielsen

ABSTRACT

Examination and sampling of a 500-meter surface section of Mississippian Chainman Shale from the Confusion Range of western Utah indicate that it possesses clear potential for hydrocarbon production. Although good stratigraphic and geochemical work has been published, this evaluation of the Chainman revealed previously unrecognized reservoir potential as an unconventional resource, particularly in the lower 300 meters of the formation.

Whole-rock chemistry and mineralogy of samples from the Chainman Shale indicate variations in sea level and proximal/distal sediment source. Although total organic carbon measurements are uniformly modest (1 to 2 weight percent), new laboratory analyses reveal adequate mudrock porosity (3 to 9% effective) and oil saturation for largely liquid hydrocarbon production. One surface sample surprisingly contained substantial amounts of mobile oil (8%). Of the four major unconventional reservoir types recognized (organic siltstone, argillaceous mudstone, calcareous mudstone, and siliceous mudstone), the siliceous mudstone and organic siltstone most likely represent the "sweet spot" lithologies in the Chainman of western Utah. If some gross subsurface reservoir assumptions are made, including a normally pressured well at 1600-meter drilling depth, a 20% water saturation, and a 20% recovery factor, estimations of recoverable oil on an 80-acre spacing would amount to 270,000 barrels of oil and 1.5 billion cubic feet of gas over a 20-year lifespan. This estimate is based on surface mapping and geochemical testing exclusively.

INTRODUCTION

Purpose

Because of recent interest in the petroleum potential of numerous mudrock sequences during the last decade or so, particularly in North America, this study embarked on a preliminary analysis of the Mississippian Chainman Shale of western Utah. While this organic-rich mud rock formation is known to geochemically source mid-Paleozoic, oil-bearing carbonates in nearby Nevada, little effort has been dedicated to the Chainman in terms of its own reservoir potential. This effort subsequently focused on outcrops of the Chainman exposed in Camp Canyon (also known informally as Skunk Springs canyon), central Confusion Range, western Utah (figure 1).

Previous Work

The Chainman Shale is well known as the source for most of the oil produced in Nevada's Railroad Valley fields (e.g., Meissner and others, 1984; Meissner, 1995), and much work has been published concerning that specific area. However, research is more limited for the Chainman in western Utah because good outcrops and well penetrations are very sparse, and there is no hydrocarbon production at this time to serve as the typical impetus for detailed studies.

The Chainman Shale was named by Spencer (1917) for outcrops near the Chainman mine west of Ely in eastern Nevada. The most comprehensive regional stratigraphic study of the Chainman was conducted by Sadlick (1965) in which five members were named and described in the cental Confusion Range, in acending order: Needle Siltstone, Skunk Spring Limestone, and Camp Canyon, Willow Gap, and Jensen Members (figure 2). The stratigraphy of the Chainman in the region was further refined and described by Sandberg and others (1980), Sandberg and Gutschick (1984), Webster and others (1984), Hintze (1986, 1997), and Hintze and Davis (2003). Sandberg and others (1980) reduced the Skunk Spring Limestone Member in rank to the Skunk Spring Limestone Bed (figure 2) and proposed several informal members. They did not recognize the Camp Canyon Member and divided it into two informal members: the lower 34 meters of the section is referred to as the concretionary shale member (with the Skunk Spring Limestone Bed at the base) and the remaining 290-meter section above is the middle member (figure 2). In addition, Sandberg and others (1980) identified a 5-meter-thick, phosphate-rich unit at the base of the Chainman, which they informally named the phosphatic member (figure 2). Sandberg and Gutschick (1984) also recognized this phosphatic zone in the Chainman as well as in the basal part of other Mississippian formations in northern Utah and southeastern Idaho, and therefore formally elevated it to the Delle Phosphatic Member. Hintze (1986) and Hintze and Davis (2003) mapped and described all five members as named by Sadlick (1965), as well as the Delle Phosphatic Member, in Chainman exposures throughout Millard County. Therefore, we use these member names in this report.

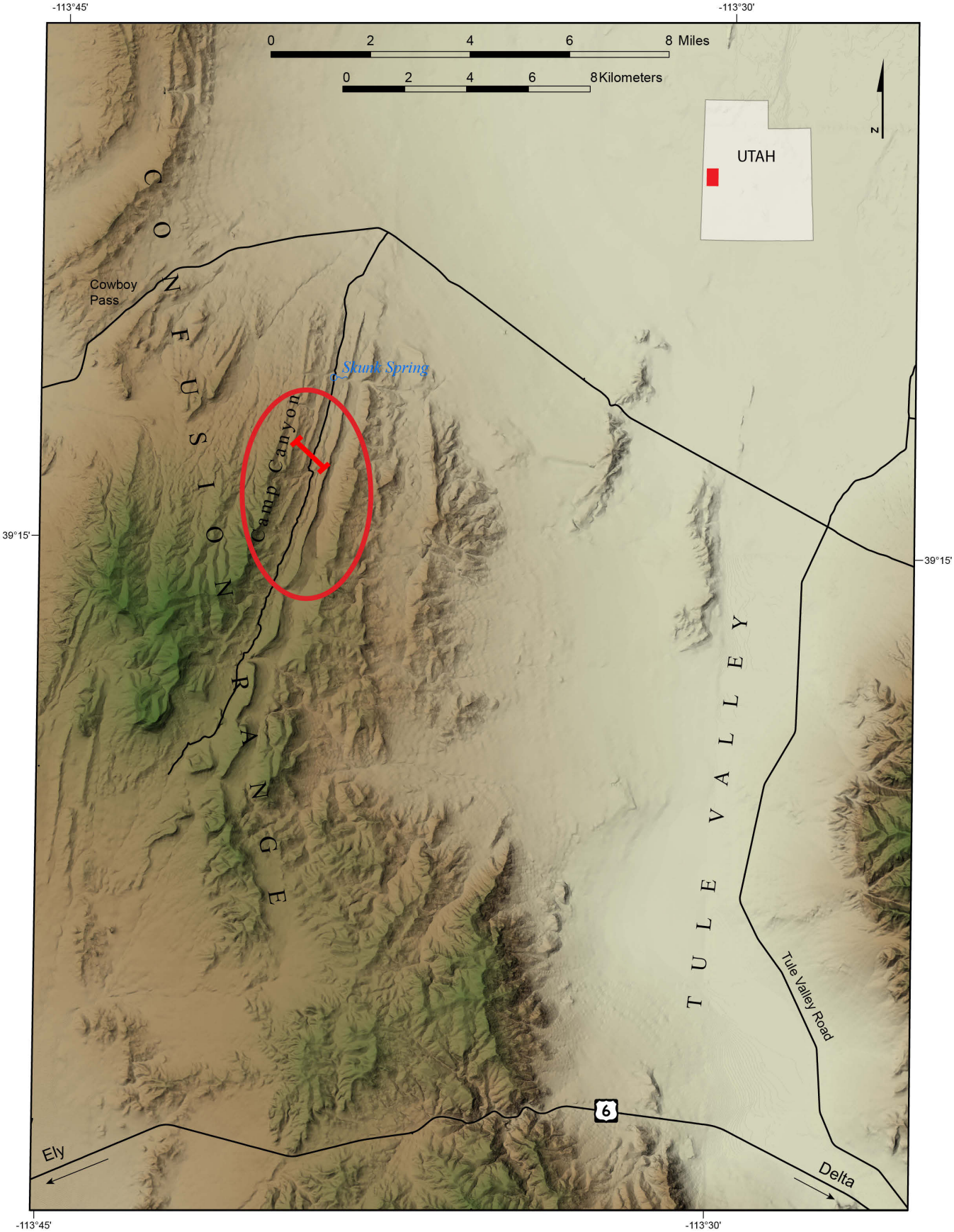

Figure 1. *Location of the Camp Canyon study site and measured section (approximate line of section indicated by the solid red line within the circle) for the Mississippian Chainman Shale, central Confusion Range, western Utah.*

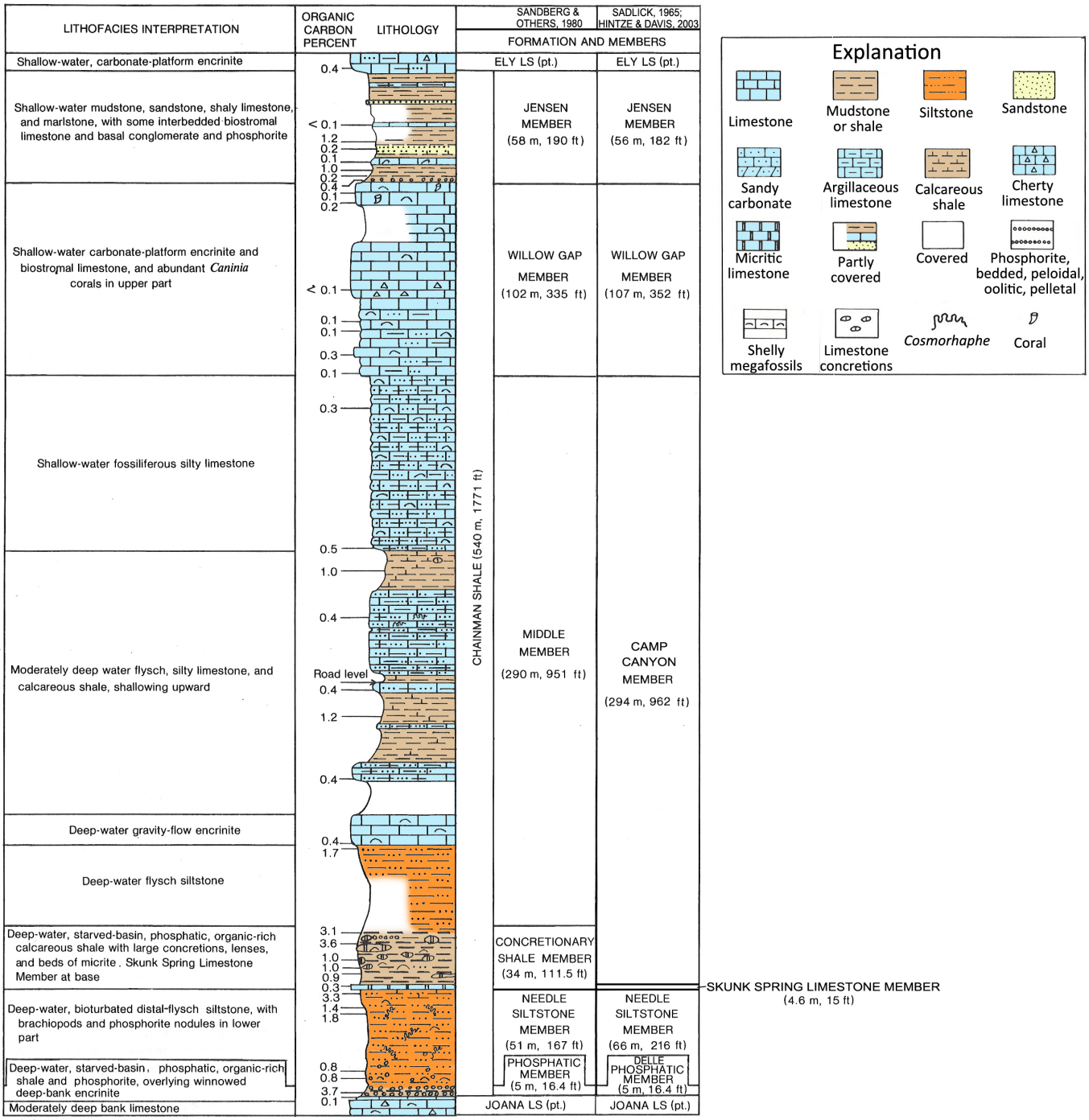

Figure 2. *Stratigraphic column of the Chainman Shale, Confusion Range, comparing stratigraphic nomenclature of Sadlick (1965), Sandberg and others (1980), and Hintze and Davis (2003). This report uses the nomenclature shown on the right-hand column. Note: the higher values of organic carbon, from Sandberg and others (1980), are in the lower part of the Chainman (Camp Canyon, Needle Siltstone, Delle Phosphatic Members). Modified from Sandberg and others (1980).*

The paleogeography of the Mississippian rocks in the eastern Great Basin has been analyzed and interpreted by Craig and Varnes (1979), Skipp (1979), Welsh and Bissell (1979), Gutschick and others (1980), Sandberg and others (1982), and Blakey and Ranney (2008). Fossils identified within the Chainman are included in studies by Sadlick (1965), Karklins (1986), and Gordon and Yochelson (1987).

The surface geology of the central Confusion Range was mapped by Hose (1963a, 1963b, 1965a, 1965b), Hose and Ziony (1964), Hose and Repenning (1964), and Hintze (1974). Our study area is located within the Cowboy Pass SW quadrangle mapped by Hose and Repenning (1964). The geologic map of the Tule Valley 30′ x 60′ quadrangle, which includes the Confusion Range, was compiled by Hintze and Davis (2002). Most recently, Greene and Herring (2013) and Greene (2014) described the structural geology, using a series of balanced cross sections, and petroleum potential of the Confusion Range.

The source rock potential of the Chainman Shale has been the focus of several regional studies covering western Utah and eastern Nevada (e.g., Meissner and others, 1984; Poole and Claypool, 1984). Sandberg and others (1980) provided total organic carbon analysis for samples from the study area. The U.S. Geological Survey (Anna and others, 2007) assessed the undiscovered oil and gas potential of the eastern Great Basin in 2004. Analysis of Paleozoic source rocks, including the Chainman, was a major part of this assessment.

Methods of Study and Scope

Trips to the study area in 2011 were designed to acquire a lithostratigraphic perspective; the entire formation was measured by Jacob staff and Brunton compass, and samples were collected for a variety of geologic/geochemical analyses. Additionally, the measured section was concurrently gamma-ray logged by the field team.

Whereas previous surface stratigraphic, biostratigraphic, and geochemical work has been done in the Confusion Range and environs, this study pays particular attention to the various mudrock facies, to gain a better perspective on these mudrock lithotypes. The surface gamma-ray log should provide an analog to any downhole logs for wells drilled in the region, and the engineering/economic calculations derived from the geologic and geochemical work allow oil-in-place estimates, as well as assessment of additional economic parameters, that might govern future oil and gas exploration efforts in western Utah.

The following geologic and geochemical tasks were accomplished:

- lithostratigraphic compilation of an approximately 500-meter measured section—in appendix A,
- surface gamma-ray logging—provided in appendix B,
- surface mudrock samples analyzed for basic pyrolisis data (table 1),
- samples collected for thin section analysis (appendix C), scanning electron microscopy (SEM) (appendix D), and X-ray fluorescence (XRF) and X-ray diffraction (XRD) (appendix E), and
- mudrock samples collected for reservoir quality testing, tight rock analysis (TRA), in laboratory: porosity, permeability, saturations (table 2).

REGIONAL OVERVIEW

Chainman Shale

The Chainman Shale was deposited over a very long period of geologic time during the Mississippian, early Osagean to late Chesterian (North American stage names found in Davydov and others, 2004) (Hintze and Kowallis, 2009). The thickness of the Chainman in western Utah generally ranges from about 300 to 800 meters. This is a relatively thin interval of sedimentary rocks, considering the 30 million years for its deposition. It can be accounted for by subsidence exceeding the rate of sedimentation during middle Osagean and Meramecian time, resulting in a starved basin (Gutschick and Sandberg, 1983; Sandberg and Gutschick, 1980, 1984; Stokes, 1986; Cook and Corboy, 2004; Hintze and Kowallis, 2009). Beginning in the Late Devonian, north-south-trending highlands formed in central Nevada as part of the Antler orogeny. East-vergent thrusting created the foredeep or foreland basin into which the Chainman, as well as the underlying Early Mississippian (late Kinderhookian through early Osagean) Joana and overlying Late Mississippian through Middle Pennsylvanian (late Chesterian through Desmoinesian) Ely Limestones, were deposited (figures 3 and 4). The foredeep basin was separated from the shallow-shelf carbonate platform of eastern Utah, Arizona, Wyoming, and Colorado, by a foreslope (Gutschick and Sandberg, 1983). By the Late Mississippian (late Chesterian) the carbonate platform to the east was exposed to subaerial erosion; however, the foreland basin in western Utah and eastern Nevada continued to receive sediments from the eroding Antler highlands to the west.

The Chainman Shale was initially deposited in deep water (greater than 300 meters) under dysaerobic conditions (Gutschick and Sandberg, 1983), ideal for the preservation of organic matter. This environment was conducive to the development of organic-rich shale beds and phosphate accumulations deposited, in part, through oceanic upwelling (figure 3). Fine-grained detritus (clastic mud and silts) in this basinal facies was derived from the Antler highlands. Thus, the Chainman contains less limestone than its stratigraphic equivalents on the platform to the east, such as the Deseret, Humbug, Great Blue, Redwall, and Leadville Formations

Table 1. *Total organic carbon (TOC) and programmed pyrolysis data of Chainman Shale from the Camp Canyon section. Measured section provided in appendix A indicates sample locations (in meters).*

Sample ID	As-Received Bulk Density (g/cc)	TOC[1] (wt.%)	S1[2] (mg/g)	S2[3] (mg/g)	S3[4] (mg/g)	Tmax[5] (°C)	HI[6]	OI[7]	S1/ TOC	PI[8]	Calc R_o[9] (%)
Sample 486	2.325	0.70	0.02	0.11	0.46	NA	16	66	3	0.15	NA
Mc-8-51	NA	0.68	0.04	0.07	0.22	NA	10	32	6	0.36	NA
Mc-8-49	2.399	0.61	0.04	0.18	0.15	NA	30	25	7	0.18	NA
Mc-7-42	NA	1.27	0.04	0.28*	0.29	468	22	23	3	0.13	1.26
Mc-7-39	NA	1.57	0.19	1.08	0.28	438	69	18	12	0.15	0.72
Mc-9-86	2.504	1.26	0.08	0.74	0.38	448	59	30	6	0.10	0.90
Mc-6-16b	2.409	1.63	0.04	0.16	0.55	NA	10	34	2	0.20	NA
Mc-6-9	NA	1.17	0.03	0.23	0.35	NA	20	30	3	0.12	NA
Mc-6-6	2.633	1.58	0.32	1.59	0.17	446	101	11	20	0.17	0.87
Mc-6-2	2.593	0.94	0.20	1.02	0.36	445	108	38	21	0.16	0.85
Basal Chainman	NA	3.40	0.04	0.92	0.97	511*	27	29	1	0.04	2.04

[1] TOC = total organic carbon (wt.%)
[2] S1 = amount of free hydrocarbons in the sample (mg HC/g rock)
[3] S2 = amount of hydrocarbons generated by pyrolitic degradation of kerogen (mg HC/g rock)
[4] S3 = amount of CO_2 (mg CO_2/g rock) produced during pyrolysis of kerogen
[5] Tmax = temperature (°C) of maximum release of hydrocarbons from cracking of kerogen during pyrolysis
[6] HI = hydrogen index
[7] OI = oxygen index
[8] PI = production index
[9] R_o = calculated vitrinite reflectance
NA = not available
* Data questionable due to outcrop sampling conditions

Table 2. *Tight rock analysis data of Chainman Shale from the Camp Canyon section. Measured section provided in appendix A indicates sample locations (in meters).*

Sample ID	As-Received Bulk Density (g/cc)	As-Received Grain Density (g/cc)	Effective Dry Grain Density (g/cc)	Effective Porosity (% of BV*)	Water Saturation (% of PV†)	Gas Saturation (% of PV)	Mobile Oil Saturation (% of PV)	Gas-Filled Porosity (% of BV)	Bound Hydrocarbon Saturation (% of BV)	Bound Clay Water (% of BV)	Pressure-Decay Permeability (nD)
Sample 486	2.325	2.349	2.542	13.42	91.71	7.72	0.58	1.04	0.08	21.02	177
Mc-8-49	2.399	2.615	2.637	9.48	11.71	87.45	0.84	8.29	0.01	7.90	51
Mc-9-86	2.504	2.604	2.627	5.14	23.59	74.79	1.62	3.84	0.15	4.35	106
Mc-6-16b	2.409	2.558	2.573	6.74	11.90	86.91	1.19	5.85	0.01	9.09	112
Mc-6-6	2.633	2.710	2.716	3.16	2.47	89.81	7.72	2.83	0.10	2.48	173
Mc-6-2	2.593	2.676	2.682	3.46	8.29	90.32	1.38	3.13	0.01	4.02	78

* BV – bulk volume
†PV – pore volume

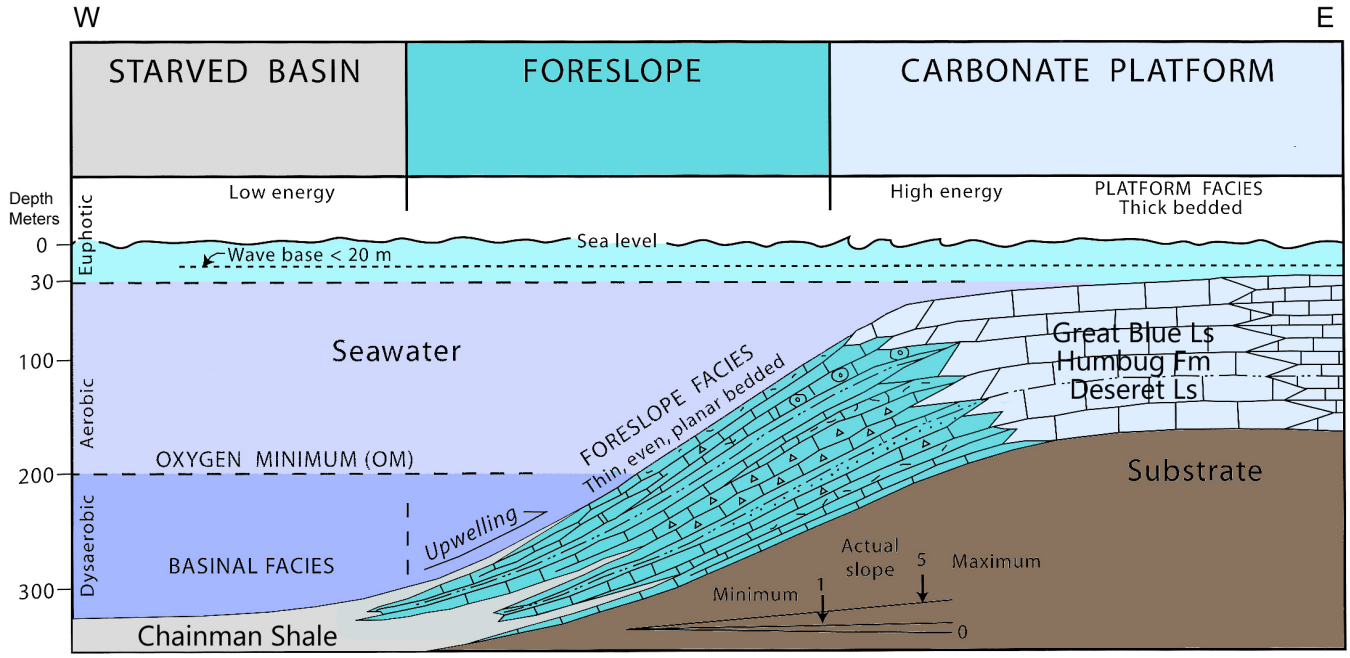

Figure 3. *Schematic west-to-east cross section from eastern Nevada through Utah during Mississippian time displaying the deep starved basin (in which the Chainman Shale was deposited), foreslope, and shallow carbonate platform. Vertical scale is exaggerated. Modified from Gutschick and Sandberg (1983) and Hintze and Kowallis (2009).*

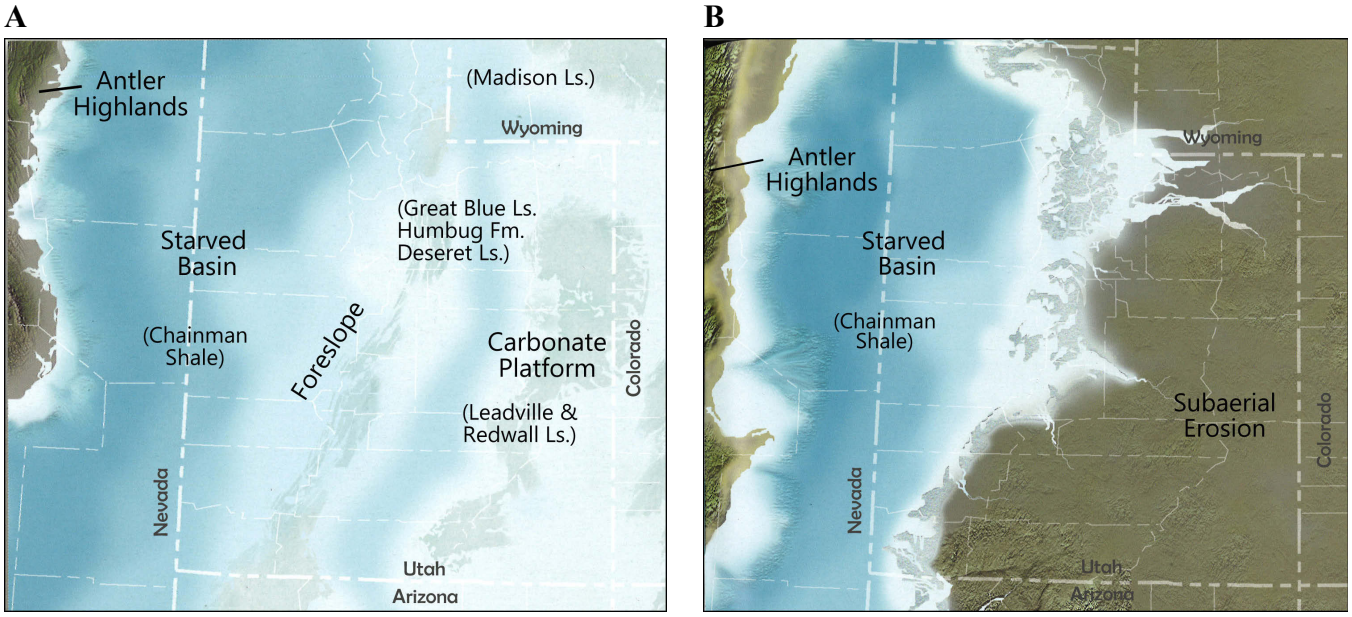

Figure 4. *Paleogeography of Utah and eastern Nevada during Mississippian time. A – A warm shallow sea covered much of Utah during the early Meramecian (340 Ma). Western Utah and eastern Nevada was the site of a deep starved basin and organic-rich sediment deposition that formed the Chainman Shale. Note the Antler orogenic belt farther to the west. B – During the Late Mississippian (Chesterian) the carbonate platform was exposed whereas Chainman deposition continued in the starved basin of western Utah and eastern Nevada. In addition, erosion of the Antler highlands provided a significant influx of clastic sediments into the basin. Modified from Blakey and Ranney (2008).*

(Stokes, 1986; Hintze and Kowallis, 2009). However, limestone units are present in the upper Chainman and contain crinoids, horn corals, and brachiopods, suggesting an easterly supply of carbonate debris (not present in central Neveda) and a change to shallow-shelf deposition in the foreland basin rather than the deep, sediment-starved conditions of its early history (figure 3).

The Chainman depositional environments, from oldest to youngest, were identified by Sadlick (1965), Sandberg and others (1980), and Sandberg and Gutschick (1984) as: (1) deep-water, sediment-starved basin (Delle Phosphatic Member of Sandberg and Gutschick, 1984), (2) low-energy, neritic or sublittoral (Needle Siltstone Member of Sadlick, 1965), (3) low-energy, outer-sublittoral, shallow-marine (Skunk Spring Limestone Member of Sadlick, 1965), (4) deep-water, sediment-starved basin at the base to shallow marine at the top (Camp Canyon Member of Sadlick, 1965), (5) shallow-marine, lime-sand bank (Willow Gap Member of Sadlick, 1965), and (6) moderate-energy, inner-sublittoral, shallow-marine (Jensen Member of Sadlick, 1965).

Confusion Range

The Confusion Range is a typical north-south-trending Basin and Range uplift bounded by Quaternary-covered, large normal fault zones (some with over 1000 meters of displacement) adjacent to Tule and Snake Valleys on the east and west sides, respectively. Regional extension began in the Miocene and continues to the present (Dickinson, 2006; Hintze and Kowallis, 2009). As the west-moving North American continental plate migrated over a deep-seated mantle upwelling, the extension broke the weak Phanerozoic rocks into horsts and grabens (Wernicke, 1992; Anna and others, 2007).

The general structure of the Confusion Range is part of a 130-kilometer-long, 24-kilometer-wide synclinorial feature extending through western Millard County (Hintze and Davis, 2003). However, in the Confusion Range the geology is structurally complex (figure 5). Prior to Basin and Range extension, the region was one of compression during the Sevier orogeny, primarily in Late Cretaceous time as the Farallon oceanic plate was subducting along the western edge of the North American plate (Armstrong, 1968; Hintze and Kowallis, 2009). The Confusion Range contains numerous, stacked or imbricated, "thin skinned," east-vergent, thrust faults as part of the hinterland of the Cordilleran thrust belt that resulted from the Sevier orogeny (Hintze, 1974; Hose, 1977; Hintze and Davis, 2002; Greene and Herring, 2013; Greene, 2014). Horizontal shortening from Sevier compression in the range is about 10 kilometers (Greene and Herring, 2013).

The central part of the Confusion Range contains several thrust faults, some of which have leading edges exposed along their eastern boundary (figure 5). Typically thrusts cut up section in competent, carbonate-dominated formations, such as the Ordovician House Limestone and Devonian Guilmette Formation, and sole into shale (for example, in the Cambrian Orr Formation or Upper Devonian–Lower Mississippian Pilot Shale). Thrust imbricates in the area have created generally north-south-trending, short- to long-axis, tight, overturned to low-amplitude, fault-propagation/fault-bend anticlines and associated synclines (e.g., the Conger Springs anticline and Conger Mountain syncline, figure 5). Local normal faults with small throws, indeterminate ages, short horizontal lengths, and various orientations are common (figure 5).

Rocks ranging in age from Ordovician (Pogonip Group) to Triassic (Thaynes Formation) are exposed in the Confusion Range (figure 5). The Chainman Shale is between 490 and 550 meters thick (Hintze and Davis, 2003), although Hose (1977) suggested it is commonly attenuated structurally. The Chainman forms a major strike valley, Camp Canyon (including the study section), along the gently west dipping east flank of the Conger Mountain syncline (figures 5 and 6). The underlying Joana and overlying Ely Limestones form prominent ridges (figure 6); these formations are 60 to 118 meters and 560 to 610 meters thick, respectively, in the Confusion Range (Hintze and Davis, 2003). The contacts with the intervening Chainman are conformable.

The Chainman Shale generally consists of interbedded shale, limestone, mudstone, siltstone, and sandstone with some calcarenite and calcisiltite. Organic-rich shale beds are black, whereas other lithologies weather light brownish gray, medium to light gray, medium grayish black, and dark, pale yellowish or orangish brown. Shale beds may also be silty, calcareous, and/or fossiliferous; some basal units contain distinct limestone concretions. Limestone beds are variable, locally cross-laminated, fossiliferous, silty, clayey, finely crystalline, or contain scattered chert nodules. They may be thin to thick bedded, in places forming prominent resistant ledges and cliffs. Sandstone beds are very fine grained, calcareous, and thin bedded. Sandstone, siltstone, and clayey to silty limestone beds form low ledges and blocky talus slopes. Though typically covered, the base of the Chainman is marked by a phosphatic siltstone to shale bed (the Delle Phosphatic Member of Sandberg and Gutschick, 1984). Shale exposures are extremely poor, confined to areas of incised gullies and side canyons. Much of the Chainman is covered by unconsolidated Quaternary colluvium and alluvial fan deposits consisting of poorly sorted silt, sand, and pebble/cobble gravels.

GEOLOGIC DISCUSSION

Measured Section

We measured a complete lithostratigraphic section of Chainman Shale (appendix A) about 3.4 kilometers south of Skunk Spring (section 8, T. 18 S., R. 16 W., Salt Lake Base Line &

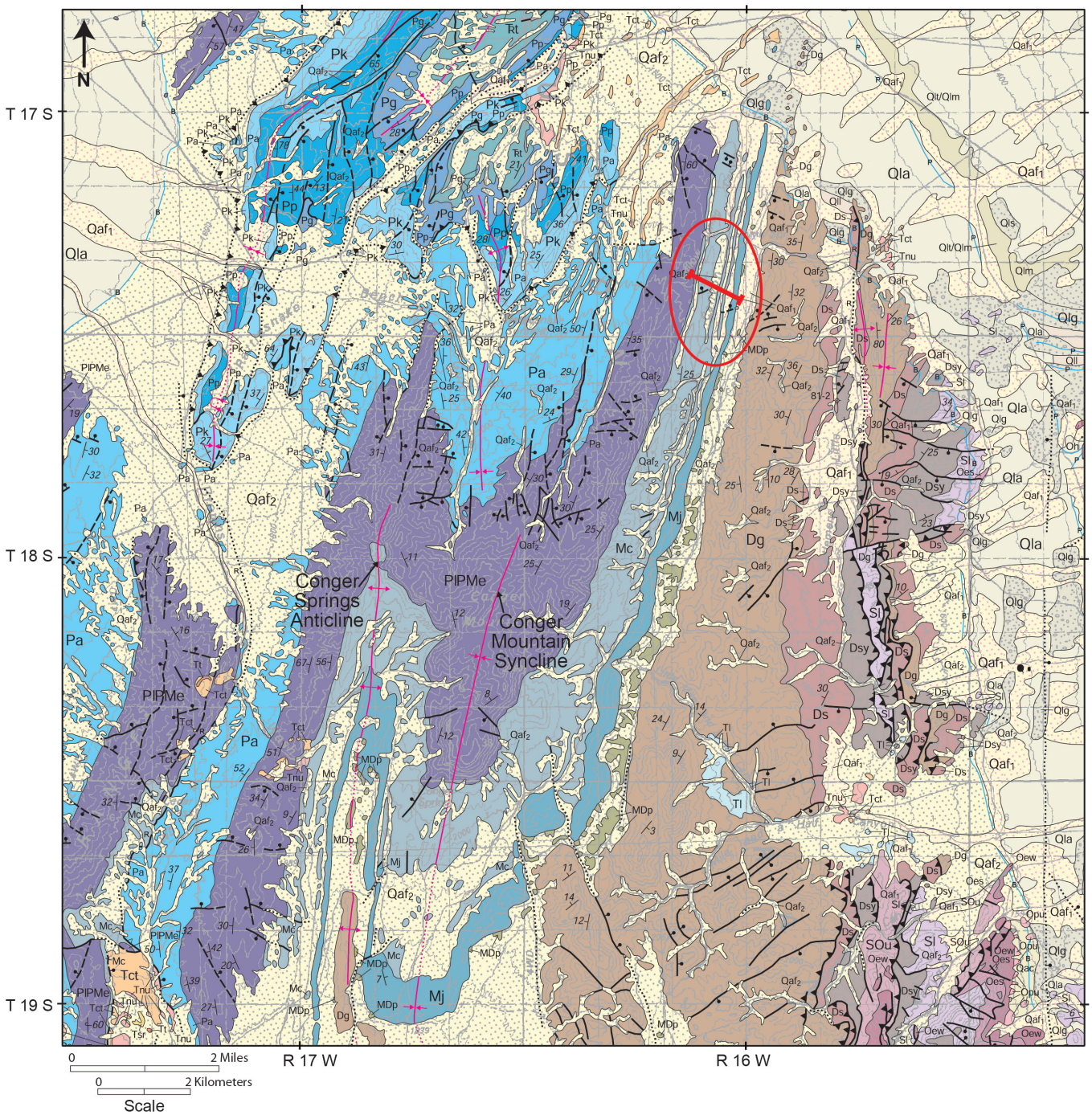

Figure 5. *Geologic map of the central Confusion Range, western Millard County, Utah. Approximate line of the Chainman Shale measured section in the Camp Canyon study area indicated by the solid red line within the circle. Modified from Hintze and Davis (2002).*

Figure 5. *Legend.*

Figure 6. *Overview from the Willow Gap Member (mostly bioclastic limestones in foreground) looking northeast towards the lower portion of the Camp Canyon area Chainman Shale section. The resistant Joana Limestone can be seen in the middle distance, and the recessive units upsection contain the basal phosphorite (Delle Phosphatic Member), the Needle Siltstone Member, and the organic-rich mudrocks of the Camp Canyon Member. Within this deeply eroded interval, one can discern locally resistant ridges and/or beds; these "ribs" belong to the deeper water, micritic, organic limestone beds of the Camp Canyon Member.*

Meridian [SLBL&M]) in the northern Confusion Range in what is called Camp Canyon or (informally) Skunk Spring canyon (figure 1). A surface gamma-ray profile (appendices A and B) was taken, using a hand-held scintillometer, as a supplement to the measured stratigraphic section.

The best line of section was selected using Google Maps™, topographic maps, and an early reconnaissance survey of the study area from unimproved dirt roads. Outcrops were fairly good as a general east-southeast to west-northwest line of section was irregularly pursued, but alluvium obscured portions of the section, particularly where recessive shale beds likely exist just beneath the alluvium. In many cases, we hand trenched the section to reveal bedrock—mostly shale and siltstone.

Details of the measured section can be found in appendix A, but in general the Chainman Shale at this location can be subdivided into the following major units from bottom to top (figure 2): (1) basal, dark gray phosphatic zone (Delle Phosphatic Member) resting on the underlying Mississippian Joana Limestone (most phosphate is covered by alluvium), (2) orange-brown weathering organic muddy siltstone or silty mudstone unit with sporadic bioturbation (Needle Siltstone Member) (figure 6), (3) medium gray, thin- to thick-bedded limestone that forms a distinct ledge about 6 meters thick with the top covered by alluvium (Skunk Spring Limestone), (4) interbedded succession of recessive dark gray to brown-gray, calcareous and noncalcareous mudrock (shale) alternating with resistant "ribs" of mostly micritic (lime mud) organic limestone that become more bioclastic upsection (Camp Canyon Member) (figure 6), (5) very thick and resistant shallowing-upward succession of bioclastic limestone beds (Willow Gap Member) (figures 6 and 7), (6) phosphatic zone of the basal Jensen Member capping perhaps a karstic and erosional surface developed on the subjacent limestone beds (upper-most Willow Gap Member) (figure 8), and (7) pebble conglomerate that progressively leads to an orange-weathering recessive interval composed of silty and sandy limestone, calcareous siltstone, and intermittent mudstone beds (Jensen Member) (figures 7 and 8). The phosphatic zones are commonly present at or near the bases of transgressive systems tracks (TSTs), for example, within the Delle Phosphatic and above the top of the Willow Gap Members, respectively (appendix A). The contact with the overlying, mainly Pennsylvanian, Ely Limestone is usually obscured by float and is located approximately where the orange-weathering Chainman float ends up-section.

As noted on the measured section, samples were collected at intervals selected for specific characteristics. Many samples were not analyzed because of limited funding for laboratory tests; thus, additional samples are available for future study at the Utah Core Research Center at the Utah Geological Survey (UGS) in Salt Lake City, Utah. Finally, appendix A describes

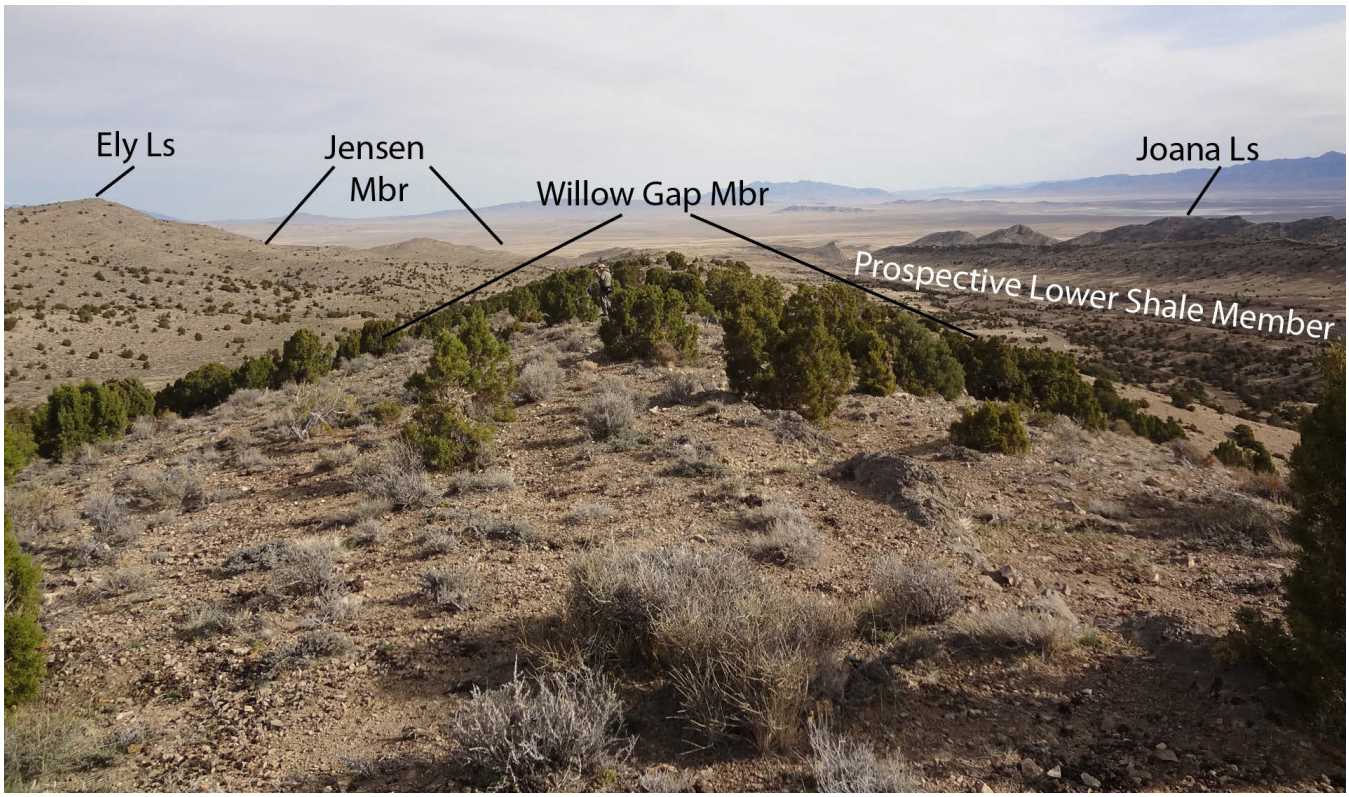

Figure 7. *View north along the topographically resistant Willow Gap Member, the unit that markedly contrasts with the two recessive Chainman units above (left) and stratigraphically below (right). On the right, one can readily see the locally resistant organic limestone ridges or "ribs," characteristic within the mudrock-rich section. The boldly resistant ridge on the right is reflective of the underlying Joana Limestone. The recessive unit to the left is the Jensen Member and to the right is the Camp Canyon Member (Sadlick, 1965). The Chainman Shale is overlain by Ely Limestone (resistant material on left just beneath the skyline).*

the basic lithologies and comments on depositional environments. In reality, the work of Sadlick (1965), Sandberg and others (1980), and Sandberg and Gutschick (1984) was very thorough, and this study makes no attempt to seriously alter their previous findings. What we hope to accomplish is a more detailed description of the potential unconventional reservoirs.

Microscopic Observations

Most thin section and scanning electron microscopy work focuses on the phosphate beds, siltstone beds of the Needles Member, and the mudrocks. Individual thin section details are provided on plates in appendix C, and SEM data are in appendix D of this report.

Phosphatic beds are mainly composed of ooids, lumps, and cements, and pertinent details can be found in plate I (all views) and in plate VII (views A and B) of appendix C. Interestingly, a single sample from the basal phosphate is also highly organic (~3.5% total organic carbon [TOC]). The siltstone facies lying above the basal phosphate comprises various ingredients, including dolomite, quartz, some feldspar, organic matter, pyrite, muscovite, illitic clay, and microfossils. What is interesting and important to this study is the fair amount of organic content (~1.0 to 1.5%) combined with some observable, but comparatively low, porosity (appendix C, plate II, view D) and some stratigraphic thickness. SEM microscopy also shows some void space in the various photomicrographs—especially so in SEM plate 6 (appendix D). These observations indicate that this dolomitic siltstone facies should be incorporated into any potential reservoir assessment using the quantitative data available (TOC and TRA assessments, along with a measured thickness). In fact, the siltstone lithofacies is somewhat lithologically analogous to certain reservoir portions of the Triassic Montney Formation of western Canada—a known oil and gas producer. Quantitative analysis of the basal phosphate is also a possibility although the complete thickness is conjectural in our study because of cover; however, the reported thickness by Sandberg and others (1980) could be used for this facies' reservoir calculation.

Three basic varieties of dark-gray to black mudrocks were discovered in the Camp Canyon Member: (1) an argillaceous (or clay-rich) mudrock (sample 6-16b), (2) a volumetrically dominant calcareous mudstone (samples 7-42 and 8-49), and (3) a compositionally curious siliceous-calcareous mudrock (sample 9-86) in which the silica content consists of microaggregates of quartz. We identified and collected a fourth type of mudrock with a limited stratigraphic extent from a deeply trenched part of the section at 486 meters. It is a dark gray to black, organic claystone that seems to contain a good deal of bound water.

Figure 8. *Approximate contact in gully separates the resistant Willow Gap limestone beds from the overlying recessive mixed rocks of the Jensen Member. The contact appears "slightly" karstic upon the limestone beds, and a distinct phosphate bed directly and disconformably overlies the questionable karstic surface. View is to the northeast.*

All three major mudrock types possess varying and distinct textural characteristics (see plate descriptions, appendix C), but all seem modestly organic rich even from thin sections. The absolute TOC values (see table 1) are certainly subdued due to the presence of insoluble terrigenous materials and dolomite. However, the moderately acceptable TOC values can be compensated through the total thickness of the mudrock interval in terms of calculating in-place hydrocarbons. All types also possess porosity to varying degrees: (1) leaching of fossils (Radiolaria) and additional microporosity in the argillaceous mudrock, (2) interparticle voids and microporosity in the calcareous mudrock facies, and (3) intercrystalline microporosity among the authigenic quartz microaggregates in the siliceous-calcareous mudrock (see SEM images). The exact vertical stratigraphic extent of the siliceous-calcareous mudrock facies, particularly as detected by SEM imaging, is not known from this limited geologic study; perhaps a future downhole logging suite and/or a continuous coring program could delineate the vertical extent of each major mudrock type.

Laboratory Testing

Laboratory work done for this project included: (1) Total Organic Carbon (TOC), (2) programmed pyrolysis (RockEval pyrolysis), (3) Tight Rock Analysis (TRA), which is a newly designed process for determining porosity, permeability, and saturations in mudrocks, and (4) XRF and XRD analysis.

Total Organic Carbon and Programmed Pyrolysis

The TOC data (table 1) reveal that eight of the eleven samples analyzed are within an acceptable range of values for the Chainman Shale to be considered a potential source rock in this area. Apart from the comparatively high TOC value for the dark phosphate sample at the formation base, most values fall between 1.0 and 1.5 weight percent (wt.%). These values are not particularly high, mostly due to the abundant minerals not successfully dissolved away prior to the measurement (mostly terrigenous clastics and dolomite). However, in spite of deep trenching for fresh samples, these values should be considered as minimal because of the unknown severity of near-surface weathering. Also, the thickness of a Chainman organic-rich interval in the basal phosphate, dolomitic siltstone, and mudrock might be as much as 260 meters in this location—an adequate thickness to provide a reasonable oil-in-place calculation. In fact, the lower limestone ridges appear organic rich as well; unfortunately no TOC measurements were run on these dark carbonates. Finally, analysis of

the programmed pyrolysis work reveals that most Chaiman samples fall in the oil window here, possibly in an oil window associated with "wet" gas. One should keep in mind that any nearby hydrothermal activity, common to both Nevada and Utah, could alter the Tmax (the temperature [°C] at which maximum release of hydrocarbons from cracking of kerogen during pyrolysis occurs) appropriately and substantially into the gas window.

Tight Rock Analysis

Data from TRA measurments also provide some interesting insight into Chainman petroleum potential (table 2). Apart from a sample at 486 meters, which was very thin and isolated stratigraphically, the other five samples possess adequate effective porosities (3.16 to 9.48%), with maximum porosity found in the siliceous-calcareous mudstone sample (Mc 8-49). The relected ultra-violet image of that sample (appendix C, plate VI, view B), which shows both dissolution (leached) pores and micropores, makes it optically clear that this lithofacies may be an optimal production sweetspot if a substantially thick (at least 3 meters for individual zones, 15 meters total in the wellbore for an economic well) zone could be detected through logging or continuous coring. All measured permeabilities are relatively modest, but based on similar TRA measurements performed on thousands of mudrock samples elsewhere, these numbers exceed the minimally acceptable 100 nanodarcy (nD) level recognized for adequate hydrocarbon production. One should remember that any surface weathering can affect the porosity/permeability numbers, both positively (dissolution causing elevated void space) and negatively (enhanced authigenic clays clogging pre-existing pores). A final interesting observation concerns the elevated mobile oil saturation of 7.72% for sample Mc 6-6 (dolomitic siltstone). This was a surprise because these surface samples have inherent surface weathering potential. Still, the number of natural seeps in nearby Nevada instructs all potential observers that the 7.72% value should not be all that astonishing. This observation is very encouraging to any potential Chainman production in Utah.

X-Ray Fluorescence and X-Ray Diffraction

Sample collection and preparation: Thirty-six samples from members of the Chainman Shale were collected from the stratigraphic section in Camp Canyon. Samples were collected from the base of the Chainman near the underlying Joana Limestone contact through near the contact with the overlying Ely Limestone. Several samples were collected from slope-forming shale units. The shale samples were very fissile and had obvious weathering rinds around individual rock pieces. These shale samples were processed by carefully selecting rock samples and removing the weathering rind.

About 40 to 50 grams of rock was used for crushing from each individual sample. Many samples required crushing in mechanical jaws to rock pieces of approximately 2 centimeters in diameter. The shale rock pieces were rinsed in a methanol solution to help remove any surface weathering minerals. The samples were milled between one and three minutes to less than 45 microns using a ring and puck machine.

The samples were statistically split into two analytical and two reserve portions. The analytical samples were placed in a 105°C oven for eight hours to remove unbound surface water. The samples were weighed before and after dehydration in the oven. Generally between 2 and 8 wt.% surface water was removed from the samples. The dehydrated sample splits were hand milled in a porcelain mortar and pestle to remove clumps and to thoroughly mix the powder. One analytical split was prepared into a pressed pellet for XRF analysis using standard pellet preparation techniques. Several samples of different rock types (i.e., variable amounts of expected Si and Ca content) had a second pressed pellet prepared from the powder to provide a preparation-analytical split. The second analytical sample was individually prepared in aluminum sample holders using standard XRD preparation techniques.

The Chaiman samples were analyzed using a Rigaku ZSX-mini XRF instrument. Universally known shale, whole-rock, and limestone standards were used to determine accuracy. The preparation-analytical split pellets, some run in multiple machine runs, provided an estimate of the reproducibility of the analytical process. The individual- and multiple-run samples showed less than 4% variability in the sampling results. The oxide wt.% totals from the multiple analytical runs were greater than 99% indicating that water was sufficiently removed from the samples and that CO_2 loss from the carbonates was not a significant factor. Sample duplicates indicate that Na variability probably accounts for the low and variable oxide wt.% totals.

The mineralogical samples were analyzed using a Rigaku Miniflex II XRD instrument. The Miniflex II is capable of analyzing six individual samples in an analytical run. The instrument was calibrated for positional accuracy and beam alignment using a quartz powder standard. The quartz standard was processed several times during the analytical runs. The mineralogical samples were measured between 3.5 and 110° 2-theta angles using 0.15° 2-theta steps and a 0.25-second sample time. Several samples were selected and analytical splits were analyzed to determine the reproducibility and accuracy of the mineralogical sample preparation. We found that both peak 2-theta and peak intensity were nearly identical between duplicate samples and within analytical sample runs, indicating that sample preparation did not introduce errors into the mineralogical analysis. The International Centre for Diffraction Database (2010) and the Crystallographic Open Database (COD) pattern databases were used to identify minerals in the whole-rock diffraction patterns. The Reference-Intensity-Ratio (RIR) method was used to estimate, with a 10% error, the relative percentages of minerals in the powder samples.

Overview: Major minerals and elements identified by whole-rock XRF and XRD conform fairly well to the lithologic assessments in the megascopic and microscopic analyses. The results of the whole-rock and mineralogical data suggest variations in the sea level and sediment source.

Elemental XRF concentrations in whole-rock samples indicate depositional environments and sediment source (Sageman and Lyons, 2003). Ratios of Si/Al and Al/K and Fe content indicate types of minerals, their source, and possible conditions at the time of deposition and compaction. Continental weathering leaches Na, Mg, Si, and Ca from many minerals and matrix, which concentrates Al and Ti in soils and paleosols. K and Fe leaching is more complicated since it depends on the oxidation state of Fe and the electrical affinity of K to clay minerals at the weathering location (Nesbitt and Young, 1982; Harnois, 1988). Clay minerals form during weathering of igneous and metamorphic minerals during the development of soils. One exception is direct precipitation during hydrothermal alteration. Natural waters, river sediments, and nearly all igneous and metamorphic minerals have higher concentrations of Ca and Na compared to Al and K (Taylor and McLennan, 1985). Plagioclase and K-feldspars start at a 50% ratio of Ca and Na to Al and a 0 to 50% ratio to K. As feldspar minerals weather, Ca, Na, and K are quickly leached leaving higher concentrations of Al and some chemically rebonded K in clay minerals. As weathering continues, illite and montmorillonite are reorganized to kaolinite and smectites (McLennan 1993). Two weathering indexes, the Chemical Index of Weathering (CIW; Harnois, 1988) and the Chemical Index of Alteration (CIA; Nesbitt and Young, 1982) have been devised. These indices have been extensively used on whole-rock element analysis from sedimentary rocks to determine possible sediment sources and the degree of weathering of the source sediments (Price and Velbel, 2003). The CIW (Al_2O_3/ Al_2O_3+CaO+Na_2O) does not include potassium in the ratio, but CIA (Al_2O_3/Al_2O_3+CaO+Na_2O+K_2O) does. Higher ratios in both indices indicate more weathered clay minerals in the sediments. The type of clay minerals in the sediments indicate the degree of weathering on either continental terrain or soils (Price and Velbel, 2003).

Sandberg and Gutschick (1984) suggested that the Delle Phosphatic Member was deposited in a deep-water, sediment-starved basin. The Camp Canyon Member through the upper Jensen Member are thought to represent sediments deposited in shallow marine, clastic to lime-sand banks with possible subaerial parts. Mississippian carbonate banks formed in shallow seas to the east whereas the Antler orogeny and associated subduction zone were active to the west.

The Chainman Shale contains clay minerals identified by XRF and XRD analyses. Clay minerals like illite and montmorillonite are generally considered allogenic minerals that form in paleosols where there is dissolution of minerals and movement of cations. Allogenic kaolinite and chlorite are generally products of weathering and development of soils on volcanic rocks. The weathering of feldspars and silicates in soils that develop on continental granitic, metamorphic, and volcanic terrains is generally believed to be the source of most clay minerals in sedimentary rocks. Exceptions to this are the development of clay minerals as part of hydrothermal alteration or metamorphism; however, no hydrothermal alteration was observed in the Chainman in the Camp Canyon section. In general, higher concentrations of Al or higher aluminum-bearing clay minerals indicate a higher degree of weathering (Sageman and Lyons, 2003). The ratios of bulk minerals like quartz, feldspars, biotite, and other allogenic grains in comparison to the percentage of allogenic clay minerals can be used to determine possible sources of sediment and estimate the degree of weathering of the sediments.

Appendix E shows the XRF, whole-rock chemical analyses of samples from the various members of the Chainman Shale. These data are juxtaposed alongside the column depths such that stratigraphic control is maintained. The mineralogical analyses from whole-rock, XRD patterns are also presented in appendix E, as are sample preparation and analysis techniques.

Results: The Chainman mineralogy is predominately allogenic quartz, with lesser amounts of muscovite and clay minerals and authigenic carbonate. Three phosphatic layers were identified in the Chainman Shale. The basal Delle Phosphatic Member has the highest concentration of phosphate in the form of fluorapatite. The second highest phosphate concentration of fluorapatite was found at 12 meters in a layer in the lower part of the Needle Siltstone Member. A third phosphatic layer was identified at the base of the Jensen Member at 458 meters. The phosphatic zones at 1 and 12 meters are 75 and 76% fluorapatite respectively, with quartz concentrations of 24 and 25%, respectively. The third phosphatic zone at 458 meters has 70% fluorapatite, with 15% calcite or limestone, 9% mica, and 6% quartz. Micas are not considered to have high Fe concentrations and contribute only a small amount of Fe to the whole-rock composition at the third phosphatic zone. According to Sageman and Lyons (2003), Fe from seawater is concentrated as FeO in sediments during organic reduction. The FeO is likely oxidized to Fe_2O_3 during lithification or during weathering by oxygen-bearing meterotic water. High P and Fe concentrations suggest a deep-water with upwelling currents, reduced, and organic-rich depositional environment (Sheldon and others, 1967; Sageman and Lyons, 2003), which were found in the third phosphatic zone. The first and second phosphatic zones have low Fe, the cause of which is not understood. It is possible that Fe may not have been highly concentrated in the seawater when the phosphate and organics of these zones were developing in the bottom sediments. It is also possible that a leaching mechanism has occurred in the lower part of the Chainman Shale that has not occurred in the upper part. Further sampling and study of the phosphatic zones in the Chainman would help to understand the relationship between high phosphate and variable Fe concentration.

Concentrations of S are not high in any of the samples; the highest typically occur at, or above, the phosphatic zones. The highest concentration of S occurs at 99 meters, just above the top of the concretionary black shale unit in the Camp Canyon Member. Concentrations of Mg, Al, K, Ti, and Fe are elevated at the same location, due to the clay minerals and muscovite. Most elements are depleted above and below the 99-meter sample, indicating the zone received different sediments for a brief period of time.

Sheet silicates, including micas and clay minerals, are found in most samples from the Chainman Shale. These silicates also contribute K and Al to whole-rock elemental concentrations and may not reflect the actual degree of weathering of the sediment source of the Chainman.

Discussion: A plot of the CIW and the CIA versus thickness through the Chainman Shale shows a large difference in the weathering indices or in the K concentration in the sediments (figure 9). The CIW indicates that most samples from the Needle Siltstone and Camp Canyon Members are in the montmorillonite to kaolinite weathering range representing more mature, weathered sediments from the Antler orogenic belt to the west. Less weathered sediments, represented in the average shale to illite range of the CIW in the upper parts of the Camp Canyon and Jensen sections, reflect erosion of more siliceous terrain with less paleosol development.

Samples from the Chainman generally have very minor amounts of K-feldspar and no plagioclase. Three feldspar-rich samples, at 14 meters in the Needle Siltstone Member, 175 meters in the Camp Canyon Member, and at 515 meters in the Jensen Member, contain 37%, 29%, and 34% feldspar, respectively. These high feldspar concentrations probably reflect periodic erosion of continental volcanic rocks or deposition of aerial volcanic ash associated with the Antler orogeny.

A plot of Si/Al, Ti/Al, K/Fe+Mg, and Ca/Si ratios from the Chainman Shale (figure 10) and a plot of percentages of carbonate, silicate (quartz and micas), and clay minerals (figure 11) reflect results comparable to the CIW and CIA plots. Only six samples are classified as non-calcareous with less than 4% carbonate; these samples are predominately quartz with lesser amounts of clay minerals. Their whole-rock com-

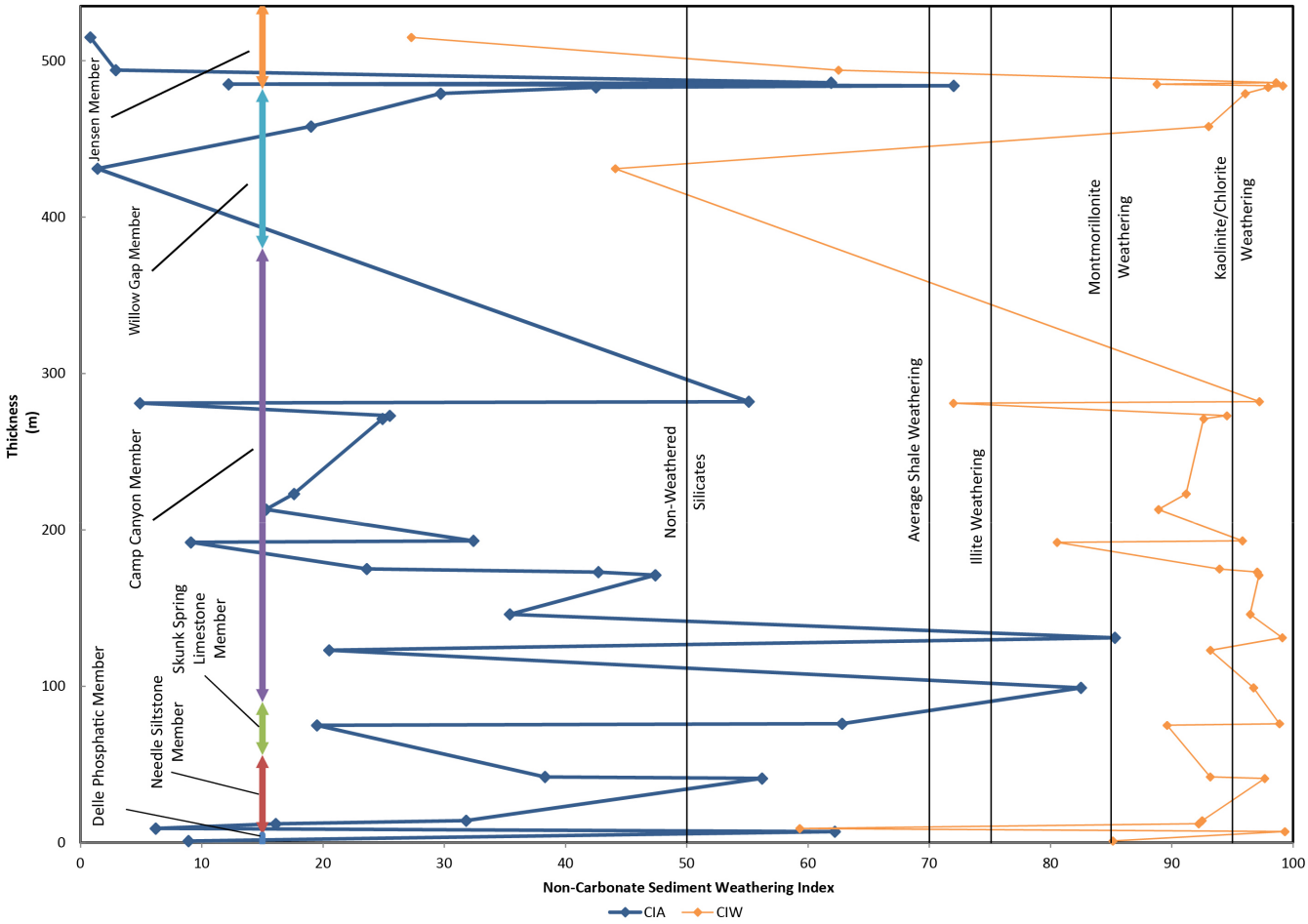

Figure 9. *Plot of the Chemical Index of Alteration (CIA) and Chemical Index of Weathering (CIW) from samples of the Chainman Shale. The indices are calculated from whole-rock oxide concentrations tabulated in appendix E. The indices reflect the degree of weathering by the concentration of Al in clay minerals within soil sediments. See text for discussions of the indices and the degree of weathering.*

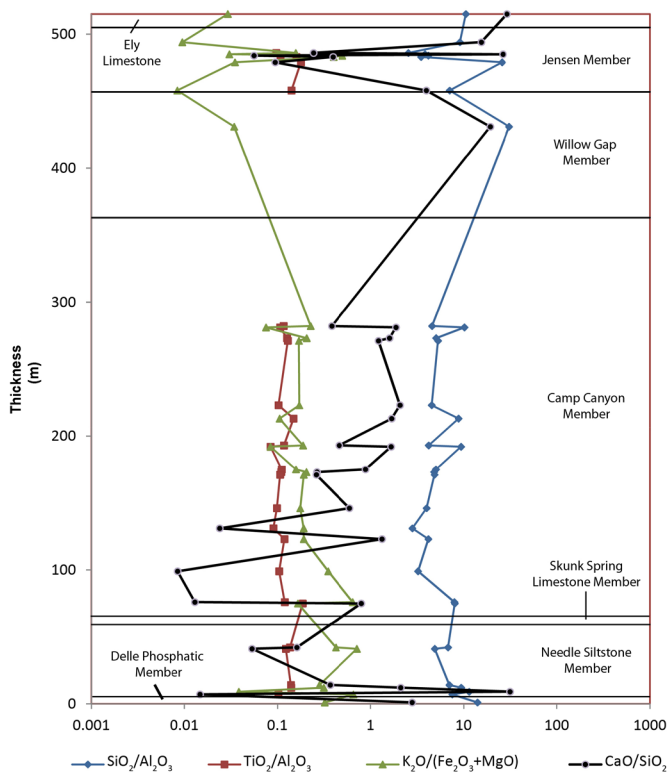

Figure 10. *Plot of whole-rock, weight-percent ratios from members of the Chainman Shale. Ratios are calculated from oxide weight concentrations in appendix E. Weight percent oxide ratios reflect the mineralogy of the samples and suggest possible modes of deposition and sources of sediment. High SiO_2/Al_2O_3 and TiO_2/Al_2O_3 ratios suggest more continental sources of the sediment, K_2O/Fe_2O_3+MgO suggest weathered sediments, and CaO/SiO_2 indicate the carbonate content of the sample.*

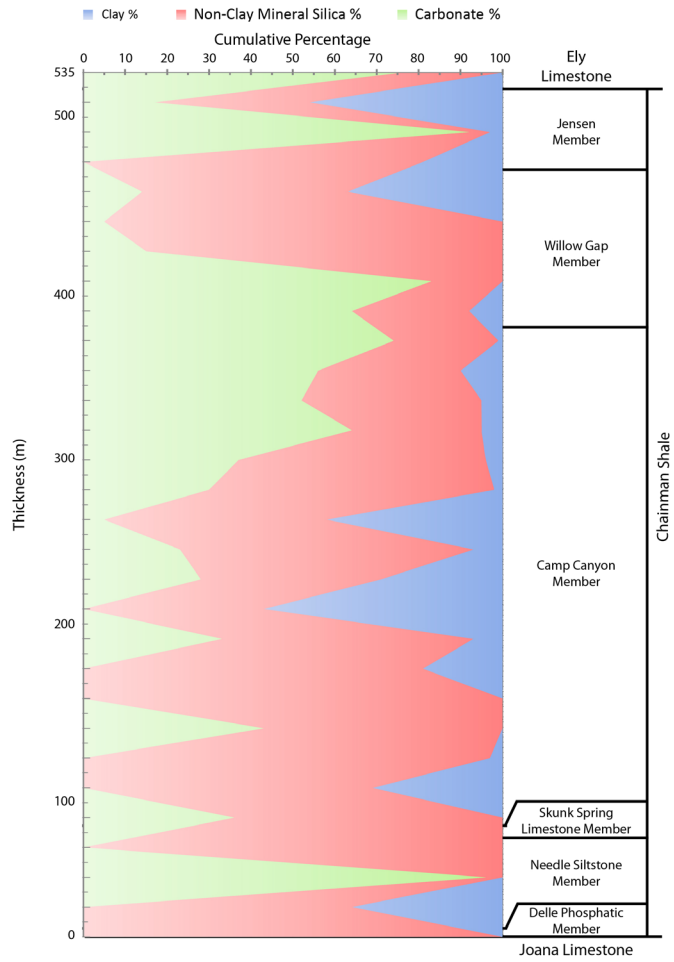

Figure 11. *Vertical thickness plot of the percentages of carbonates, non-clay mineral silicates, and clay minerals from samples collected in the Chainman Shale. Mineral percentages are shown in appendix E. The basal Delle Phosphatic Member is at the bottom of the chart and the top shows the contact between the Jensen Member and the Ely Limestone.*

position and mineralogy suggest a less weathered sediment source. The sediments in these intervals could have been derived from either a western volcaniclastic sediment source or a volcanic ash or air fall into the starved basin. During late Devonian, sediments derived from the transcontinental arch to the east were deposited into a western foreland basin east of the island arc and proto-highlands of the approaching Antler subduction zone. As the Antler orogeny developed in the west, it exposed basin sediments and possibility provided a source of quartz, mica, and clay minerals.

The Chainman Si/Al and K/Fe+Mg ratios show a nearly vertical trend through the Needle Siltstone Member to the upper 60 meters of the Camp Canyon Member (figure 10). The ratios then shift to slightly greater Si/Al and Ca/Si whereas K/Fe decreases, suggesting declining clay and silicate mineral influx. Figure 11 shows a similar trend of upward decrease of clays and silicates relative to carbonate. These trends suggest reduced siliciclastic sediment input, possibly a result of erosional leveling of the western Antler highlands. The elemental ratios along with the mineralogy suggest that the Needle Siltstone and the concretionary black shale facies of the Camp Canyon were deposited in a deep-water, low-energy, and organic-rich starved basin with siliciclastic input from a distal continental source. The spikes of high-percentage clay minerals indicate that increased weathered continental sediment was sporadically supplied to the basin. This possibly reflects changes in the fluvial system periodically dumping more sediment into the starved basin. Since only carbonate banks lay to the east during Mississippian time, the source of clay minerals, which typically develop as soil horizons, is fluvial systems that eroded western continental soils and deposited them into the sedimentary basin.

The K/Fe+Mg ratio spikes at 76 meters, which coincides with an increase in the amount of continental-derived silicates (figure 10). This likely represents a geologically short change or episodic pulse in the type of sediment coming into the basin at this time. Detrital micas typically derive from intrusive and extrusive igneous rocks, but the Chainman micas are probably recycled from western eugeosynclinal sediments containing detrital micas. Their original source may have been erosion of Archean rocks from the eastern continental highlands into the early Paleozoic sea, followed by compac-

tion and uplift by the Antler orogeny. A similar example occurs in shale of the Uinta Mountain Group, which contains detrital mica eroded from Archean rocks and deposited into a Neoproterozoic basin (Douglas A. Sprinkel, Utah Geological Survey, written communication, 2014). Since the Chainman micas have not weathered to kaolinite or montmorillonite, they were likely quickly transported to and deposited in the sedimentary basin.

Decreasing K_2O/Fe_2O_3+MgO coupled with increasing CaO/SiO_2 ratios, starting at approximately 28 meters and continuing through the top of the Camp Canyon section, suggest a decrease in the terrigenous sediment supply (figure 10). The mineralogical composition of silicates and carbonate in figure 11 also show this same trend. Apart from a spike in the amount of clay minerals in the sediment in the lower part of the Camp Canyon Member, their abundance in the overlying samples is very small. The trend indicates a decrease in the amount of sediment coming into the basin, either as a result of relative sea level rise or a shift of the western sediment source towards the north or south along the coastline. Conversely, the sediment source may have had less soil and more sedimentary or siliceous parent material available for erosion.

The basin during Camp Canyon time was predominately the site of carbonate deposition with decreasing amounts of quartz and clay minerals towards the top of the Camp Canyon Member and up through the lower Willow Gap Member. An abrupt increase in the amount of siliciclastic sediment relative to carbonate is observed starting at the top of the Willow Gap and the basal and middle parts of the Jensen Member. This sudden change suggests an increase in the sediment supply by renewed fluvial transport of sediment into the starved basin, possibly reflecting a decrease in sea level. The whole-rock percentage of carbonate decreases during this interval, but the sediments are still calcareous (4 to 15%) to carbonate-rich (> 15%). The amount of clay minerals was miniscule during the Willow Gap and lower Jensen time then started increasing towards the top of the Jensen Member. The percentage of clay minerals in the Jensen spikes twice, following the decreasing silicate and increasing carbonate trend. The spikes and trends in the siliciclastic sediments probably indicate a change in supply of sediment as the distance from provenance to basin increased and the source terrain became more silicic.

Several samples contain significant amounts of dolomite as compared to predominately calcite or limestone found in most of the samples. Dolomite is easily distinguished from calcite in whole-rock XRD patterns so its occurrence is certain. Dolomite occurs in the members of the Chainman Shale near beds with high iron and phosphate content. As mentioned earlier, the high concentration of phosphate is likely related to high TOC and a reducing alkaline environment, probably caused by bacterial reduction (Machel and Mountjoy, 1986). Several models of dolomitization require high concentrations of organic carbon and a reduced alkaline environment. However, two dolomitic samples at 75 and 213 meters in the Camp Canyon Member are not associated with higher phosphate. It is possible that concealed phosphatic layers associated with these samples were not identified or collected in the field. Alternatively, the organic carbon content and alkalinity could have been sufficient for dolomitization but not sufficient to concentrate phosphate at that interval. The localized occurrence of dolomite in the Camp Canyon section suggests that dolomitization occurred at or slightly after deposition of primary limestone. It also suggests that the conditions for dolomitization occurred episodically during the deposition of siliciclastic sediment into the starved basin. This may again reflect changing sea level and distance to the sediment source, and a variation in the sediment source material.

Figure 12 is a ternary plot of the average mineralogical group compositions of the various members of the Chainman Shale and comparison to several productive North American shale reservoirs (Horton, 2012). All members of the Chainman, except the Willow Gap Member, have higher silicate and less carbonate than other shale reservoirs. This suggests the Chainman was deposited in a more proximal part of the basin relative to the sediment source than the other shale plays. The overall high clay mineral concentration in the Haynesville, Fayetteville, Bakken, Barnett, and Mancos Shales suggests they had more distal, deep-water depositional environments that were supplied with deeply weathered sediment. The Willow Gap Member has less silicate and higher carbonate mineral percentages suggesting that its source was predominately from a carbonate bank, likely to the east (figure 3), with less influence of siliciclastic input from the western Antler orogenic belt.

Interpretation: Changes in relative sea level and sediment supply from the western Antler orogeny are reflected in the Chainman Shale starting in the deep-water, low-energy sediments of the earliest Delle Phosphatic Member, and progressing up through the low-energy, siliciclastic, carbonate-rich environment of the Needle Siltstone Member, and then to the silty to sandy carbonate banks of the upper parts of the Camp Canyon and Willow Gap Members. Phosphatic zones represent deep water environments with upwelling currents. Carbonate debris and sediment, particularly in the Willow Gap Member, were likely supplied from an eastern source. Finally, the Jensen reflects interaction between an eastern distal carbonate bank environment and continued variation in sediment supply from the western highlands. Carbonate was deposited with various amounts of siliciclastics coming in from sources to the west through most of the depositional history of the Chainman. The organic-rich bedded phosphates along with the variety of marine fossils found in the Chainman (Hintze and Davis, 2003) suggest that organic carbon sources were plentiful in the seas that deposited the Camp Canyon section.

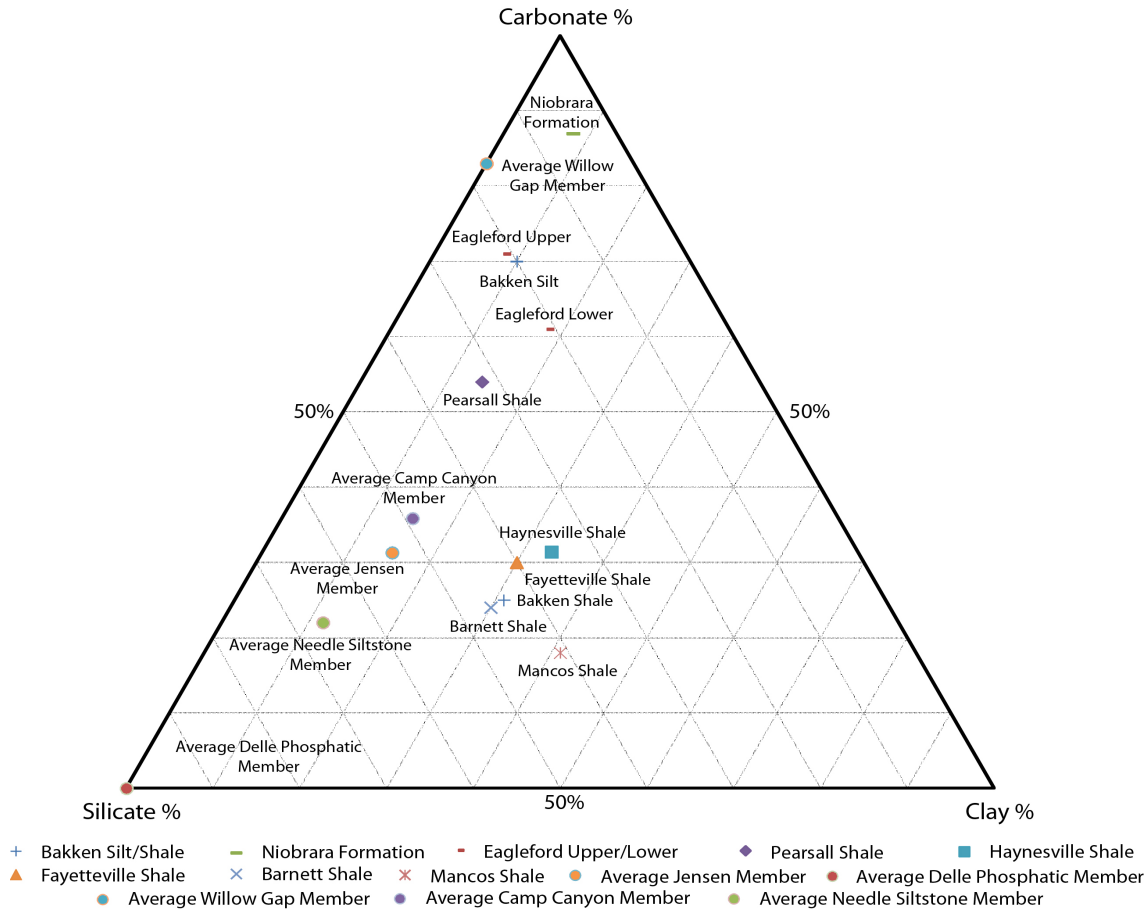

Figure 12. *Ternary plot of average percentages of carbonates, non-clay mineral silicates, and clay minerals from members of the Chainman Shale. Mineral percentages are shown in appendix E. Averages from other North American shale plays (from Horton, 2012) have been included for comparison.*

RESOURCE EVALUATION

Overview of Exploration Wells Penetrating the Chainman Shale, Western Millard County, Utah

Exploratory drilling is extremely sparse in western Utah. In the vicinity of the Confusion Range and surrounding areas (western Millard County and easternmost White Pine County, Nevada), only 14 deep wells have been drilled. Early exploration wells (1950s) tested surface anticlines identified by basic geologic mapping. Following the discovery of oil and gas in the northern Utah thrust belt during the 1970s and 1980s, drilling in the region targeted complex subsurface structures identified principally by seismic data. The locations of the deep wells, along with interpreted formation tops, faults, total depths, completion dates, and other information, are summarized by Hintze and Davis (2003).

Five wells penetrated the Chainman Shale in the region (figure 13 and table 3); other deep wells encountered formations older than Chainman beneath relatively thin surficial deposits. The thickness of the Chainman in these wells varies from 570 to 680 meters (Hintze and Davis, 2003). In 1952, Standard Oil of California drilled the Desolation Anticline well (NE1/4NW1/4 section 8, T. 15 S., R. 17 W., SLBL&M) to test a surface structure near the northern end of the Confusion Range approximately 35 kilometers north of the Camp Canyon study area; a closer well about 4 kilometers to the east of the measured section, the Cities Service Oil Company State AB No. 1 (SW1/4NW1/4 section 2, T. 18 S., R. 16 W., SLBL&M), spudded in the Devonian section. The Desolation well drilled the Chainman Shale at 826 meters. The entire Chainman section was penetrated and four named members, described in the Camp Canyon section, were identified based on geophysical and well cuttings (in descending order): Jensen Member – 174 meters, Willow Gap Member – 40 meters, Camp Canyon Member – 213 meters, and Needle Siltstone Member – 143 meters (Hintze and Davis, 2003).

The members of the Chainman Shale are typically difficult to identify in many of the other geophysical well logs or drill cuttings; faulting further complicates the stratigraphic interpretations. However, they are important to recognize as some members contain significant organic-rich units whereas others could serve as potential reservoirs. Thus, regional correlation, thickness, and distribution of the Chainman members are critical factors in exploration efforts. Although none of the five wells that penetrated the Chainman tested hydrocarbons, the new

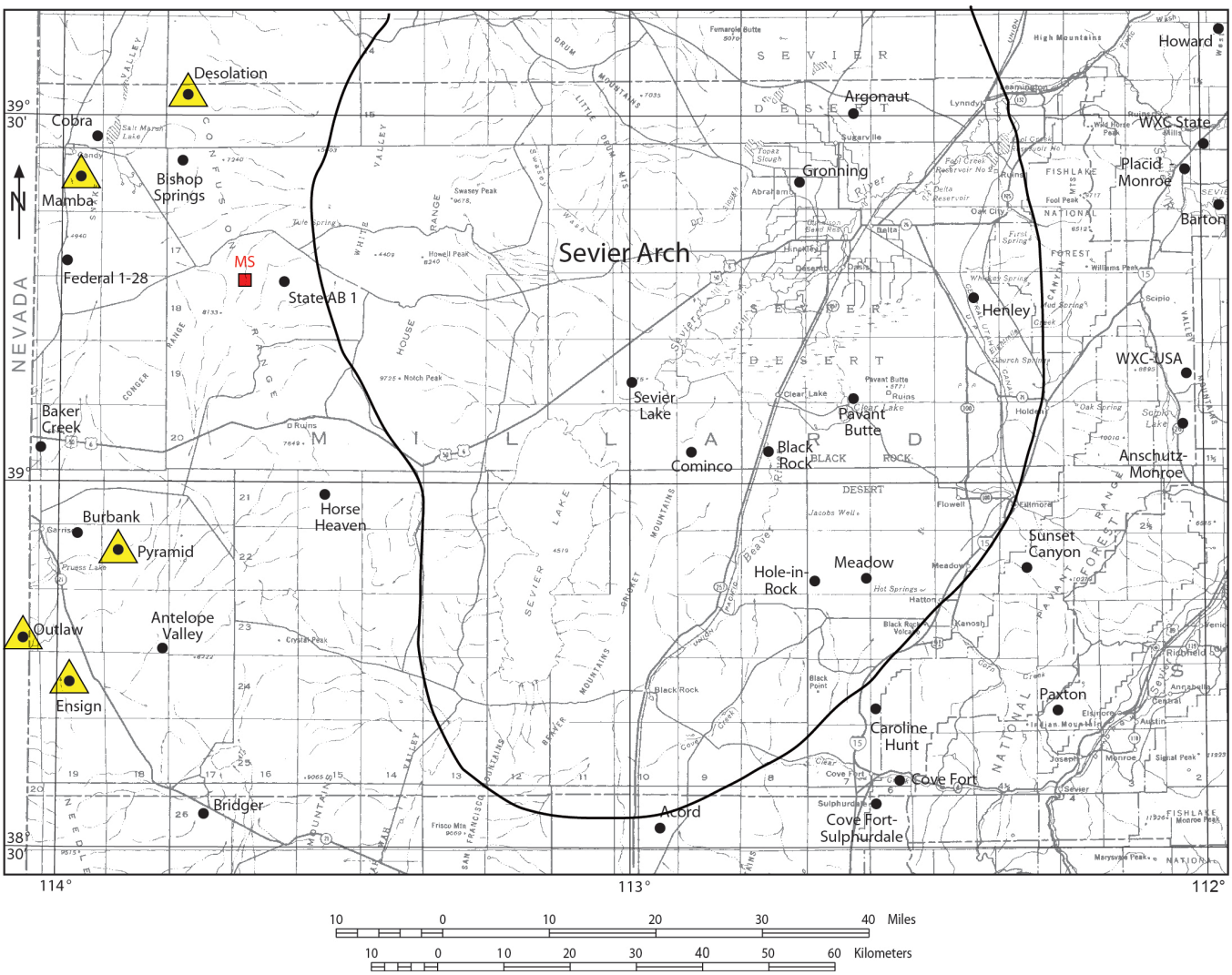

Figure 13. *Location of selected deep exploration wells in and adjacent to Millard County, western Utah. Wells penetrating the Chainman Shale are identified with a yellow highlighted triangle; the Camp Canyon measured section (MS) is also shown. Also shown is the Sevier arch, a broad structural culmination formed during the Late Cretaceous Sevier orogeny. Early Ordovician rocks are overlain by Tertiary volcanics on the arch in this area; all younger sedimentary rocks are missing. From Hintze and Davis (2003).*

Table 3. *List of wells penetrating Chainman Shale in western Utah-eastern Nevada. See figure 13 for well locations in relation to the Camp Canyon measured section.*

Well Name	Operator	Section	Township	Range	County	State	T.D. (m)	Chainman Depth (m)	Year Drilled
Desolation Anticline	Standard Oil of California	8	15S	17W	Millard	Utah	1890	826	1952
Cedar Pass	Pyramid Oil & Gas	17	22S	18W	Millard	Utah	2289	878	1968
Ensign #1-16	Commodore Resources	16	24S	19W	Millard	Utah	3730	649	1980
Outlaw #1 Federal	Commodore Resources	1	10N	70E	White Pine	Nevada	3962	741	1982
Mamba Federal 31-32	Equitable Resources Energy	22	16S	19W	Millard	Utah	992	860?	1996

resource evaluation provided in this study combined with the latest drilling and completion techniques (horizontal drilling and state-of-the-art hydraulic fracturing) could lead to renewed exploration efforts and potential discoveries in western Utah.

Hand-Held Gamma Logging

Two sets of data were available for inferring Chaiman oil or gas in place: hand-held spectral gamma-ray data (figures 14 and 15) and the suite of laboratory information on surface samples. The surface gamma-ray profile (appendix B) proved to be a useful complement to the measured stratigraphic section (appendix A), and for the most part, gamma radiation responses correspond to overall lithological patterns. In general, phosphate beds show high radiation, limestone intervals exhibit low responses, and mudrocks can respond variably, depending mainly on calcium carbonate content.

The gamma-ray (GR) curve generated along the measured section (figure 15 and appendix B) and the organic geochemistry of samples collected from the outcrop allow comparison to other Chainman Shale sections in the area. The Outlaw Federal No. 1 (NE1/4NE1/4 section 1, T. 10 N., R. 70 E., White Pine County, Nevada) located 65 kilometers southwest of the Camp Canyon section at the Utah–Nevada border (figure 13), has been identified for a type Chainman well. The Outlaw Federal No. 1 was drilled in 1982 to a depth of 3962 meters (table 3). A complete, unfaulted section of Chainman is identified in the well. A good suite of geophysical logs, including gamma ray, caliper, interval transit time, sonic porosity, spontaneous potential, and deep resistivity (deep laterolog), is available. Other wells near the Camp Canyon section have penetrated the Chainman, but they have either an incomplete suite of geophysical logs or thickened or thinned sections due to Sevier thrust faulting (Hintze and Davis, 2003), and thus they are less favorable as a type Chainman well.

Figure 14. *Trenching for fresh samples was often necessary in some portions of recessive units—Jensen Member in this instance; trenching was also essential for accurate surface gamma-ray logging results.*

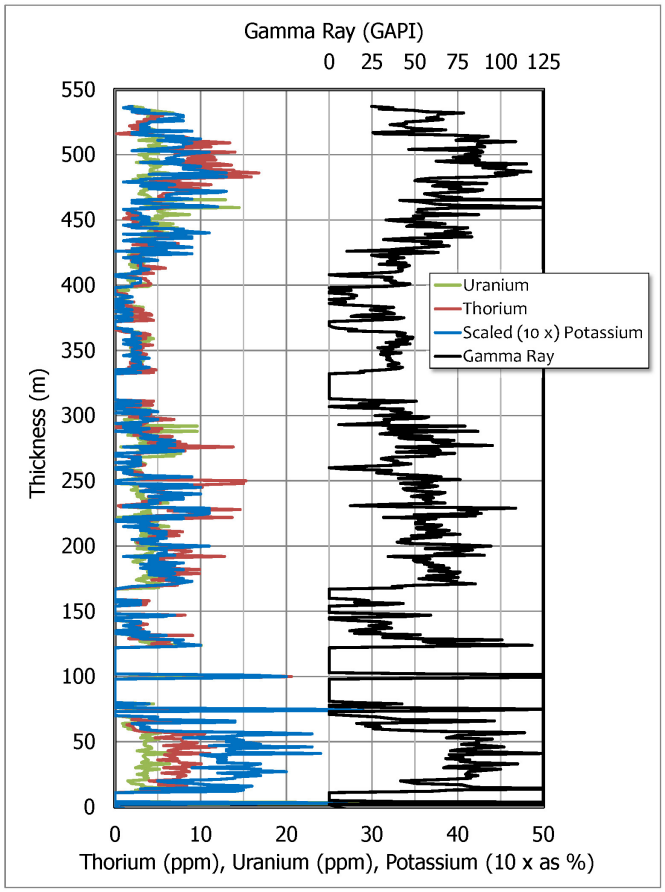

Figure 15. *Spectral gamma ray components and total gamma ray (from hand-held scintillometer measurements).*

Petrophysical Techniques

The Outlaw type well GR curve was normalized by identifying high and low GR picks from a GR histogram and scaling the curve using the picks and the average GR value. Normalization removes potential of error introduced by downhole sensors and plotting equipment. The caliper curve, showing borehole diameter, was used to generate a "Badhole" curve identifying borehole diameters greater than 38 centimeters. Borehole diameter affects geophysical tools, particularly sonic tools, which have pads intended to move along the sides of the borehole. Large diameter boreholes and high-density drilling mud can dampen the GR response. Thus, the normalized GR curve was also corrected using borehole diameter. The calibrated GR curves from the type well and the Camp Canyon section were used to calculate the gamma-ray index and the volume of shale (Vsh) as a percentage of the total rock volume.

The sonic porosity curve was reverse calculated from delta transit time (DT) or the compressional wave velocity by solving the Raymer-Hurt-Gardner (RHG) equation (an empirical velocity/porosity relationship) for matrix velocity using limestone (47.6 µsec/ft) and fresh water (189 µsec/ft) velocities as a check to the DT curve. The measured DT curve was used to calculate a bulk density (RHOB) curve applying the

standard RHOB from DT equation used in synthetic well log generation. The relationship works because the velocity of a compressional wave propagating through a combined fluid and rock matrix is related to the elasticity of the fluid and the matrix, or the bulk density.

The deep resistivity (LLD) curve was determined to not need normalization. Most resistivity curves are only normalized if there are obvious scale changes or extreme bad-hole conditions.

The GR curve from the Camp Canyon measured section was also normalized since the hand-held outcrop instrument has a different cross sectional area compared to downhole well-logging tools. A histogram of the GR curve at Camp Canyon was generated for the entire Chainman Shale section. The high and low GR picks were selected from the histogram and were used to normalize the curve similar to the Outlaw type well GR data, essentially stretching the curve between the high and low points and enhancing curve changes between rock types. The normalized and corrected GR curves from the Outlaw type well and the Camp Canyon measured section are referenced as standard GR curves in the following discussions.

Results

The tops of the various members of the Chainman were identified in the type well. Generally, each member is thicker in the Outlaw type well than the Camp Canyon measured section, which would be expected since the well is more proximal to the sediment source of the subsiding basin. The Chainman GR curves for the Outlaw type well and the Camp Canyon section are displayed in plate 2 of appendix B. They show comparable trends within members and similar areas of high GR shaley or phosphatic intervals, along with similar intervals of increasing sand or limestone. The good correlation between Outlaw type well and Camp Canyon measured section GR curves suggests that petrophysical and correlation variables generated using the Outlaw type well should have a very good correlation to synthetic curves and petrophysical variables at the Camp Canyon section. This correlation concept is used to generate synthetic RHOB, density LOGR (RLOGR), and TOC curves for the Camp Canyon section. The density LOGR, or RLOGR, is a method to estimate TOC or organic matter concentration from overlays of DT and RHOB and the log of the deep resistivity (Passey and others, 1990).

Individual GR histograms of the Chainman intervals from the Outlaw type well and from the Camp Canyon section show a typical bell curve distribution indicating a mixture of various lithologies. Bimodal histograms suggest that two rock types dominate the stratigraphic section. Each histogram shows extremely high GR zones, which correlate to identified and suspected phosphatic zones. At least four phosphatic zones are identified on the GR curve from the Outlaw type well. The GR curve from Camp Canyon has some missing covered sections, but the three phosphatic zones identified in the outcrop correlate with high GR zones. Similarly, high GR log intervals are observed within the Chainman on GR logs from other wells in the region. Therefore, we anticipate that at least four phosphatic zones would be identified on a complete GR curve from the Camp Canyon section. The phosphatic zones at the Outlaw type well are generally thicker and have higher GR signatures than similar sections found to the east in Utah.

The Vsh curves for the Outlaw type well and the Camp Canyon section are presented in track 1 of plate 2, appendix B. The Vsh percentage at the Outlaw type well varies from 0% in the limestone units to 48% in the phosphatic zones. The phosphatic-zone Vsh is high due to the higher GR counts from uranium. The highest Vsh is probably in the 35 to 40% range. The Vsh at Camp Canyon ranges from 0% in the limestones to 27% in the phosphatic zones. Again, the uranium concentration has boosted the Vsh higher in the phosphatic zones. The highest Camp Canyon Vsh is probably 18 to 22%. Curves from both locations show the same general trends with highest shale percentage in the middle section of the Jensen Member, high Vsh spikes in the upper portion of Camp Canyon Member, and higher average Vsh in the black shale interval of the lower Camp Canyon.

The scintillometer used at Camp Canyon also measured thorium, potassium, and uranium radiation, and generated a spectral gamma-ray curve (SGR) (figure 15). Only total gamma-ray data are available at Outlaw Federal No. 1. The SGR data from Camp Canyon suggest that potassium and to a lesser degree thorium are the predominant sources of radiation, outside of the phosphatic zones, which have high concentrations of uranium. Increased uranium often corresponds with high concentrations of organic matter, which is found in the shales, siltstones, and silty sandstones in the Chainman Shale, but the phosphatic zones probably contain the highest organic material and are the best source rock intervals. The high uranium concentrations in the phosphatic zones affect the GR curve and result in increased GR counts and lower bulk density, RLOGR, and TOC. Neither SGR nor TOC values were available for the Outlaw Federal No.1 well so only a general statement about possible TOC concentrations there can be made. The actual TOC measurement (sample Basal Chainman, table 1) from the Delle Phosphatic Member has the highest TOC measured in at the Camp Canyon section, but the gamma-ray survey did not include that part of the section. The phosphate zones in the Camp Canyon Member were not sampled, so it is not possible to state a correlation between TOC in the Delle Phosphate Member and the phosphatic zones farther up section.

Camp Canyon Measured Section Petrophysics

The Outlaw type well was used to generate a linear correlation between GR and DT and GR and RHOB curves. The correlation between GR and DT generally resulted in a goodness-of-fit (R^2) between 0.6 and 0.8. A synthetic RHOB curve

was calculated for the Outlaw type well using the standard DT – RHOB relation equation. The synthetic RHOB curve showed problems in the oversized zones and in the high GR phosphatic spike areas, as expected. Generally, the synthetic RHOB curve reflected the anticipated bulk density of the sandstone, limestone, and siltstone known to exist in the Chainman Shale. An RLOGR curve was generated from the density equation from Passey and others (1990):

$$RLOGR = log\left(\frac{RESD}{RESDBASE}\right) - 2.5\left(\frac{RHOB}{RHOBBASE}\right) \quad (1)$$

where:

RLOGR =	density LogR.
RESD =	deep resistivity (ohmm).
RESDBASE =	baseline resistivity in (ohmm).
RHOB =	bulk density (g/cm^3).
RHOBBASE =	bulk density baseline (g/cm^3).

The deep resistivity baseline (RESDBASE) and RHOB baseline (RHOBBASE) values were identified from overlaying the RHOB and LLD curves and identifying overlapping areas in non-source shales or siltstones. A baseline value of 90 ohmm for RESDBASE and 2.4 g/cm^3 for RHOBBASE were identified between depths 1164 and 1201 meters in the Outlaw type well. The baseline values, along with the LLD and synthetic RHOB were used to generate a RLOGR curve for the Chainman and are shown in plate 3, appendix B.

The RLOGR curve is plotted adjacent to the LLD curve, and several areas of separation between the two curves suggest zones containing organic material. Small separation zones are observed in the Jensen and Camp Canyon Members. The Willow Gap Member has small zones of separation, but generally shows very little organic matter. Starting with the black shale interval in the lower Camp Canyon Member, separation begins to increase down to the top of the Skunk Spring Limestone Member. However, no separation is observed in the Skunk Spring Limestone. Large separation is observed in the upper part of the Needle Siltstone Member down to the top of the sandier lower part. The separation increases at the contact between the Skunk Spring Limestone and the Delle Phosphatic Members. The high phosphatic zone in the Delle Phosphatic Member shows a cross over and separation suggesting both a source area and high organic matter content. It is anticipated that the RLOGR curve for the Camp Canyon section, using the correlation between GR and RLOGR from the Outlaw type well, will resemble the curve trends seen in the Outlaw type well.

A cross plot between the synthetic RHOB and RLOGR for the Outlaw well displays a linear relationship with a correlation coefficient $R^2 > 0.6$. Plate 3, appendix B shows the normalized, corrected GR, DT, and LLD curves as well as the synthetic RHOB and RLOGR curves for the Outlaw type well. The Outlaw well linear equation was used to calculate the synthetic RLOGR curve for the Camp Canyon section. As discussed previously, 11 samples were collected and analyzed for TOC and programmed pyrolysis (table 1). A calculated vitrinite reflectance (R_o) is available for six of the ten samples. The calculation of a TOC curve using the RLOGR and level-of-maturity (LOM) data is shown in track 4 of plate 2, appendix B. The LOM is unitless and is estimated for organic matter (including oil, gas, and coal) from R_o using charts presented in Hood and others (1975). LOM for the TOC analyses with R_o are 9 in the Jensen Member, 10 in the Camp Canyon Member, 11 in the Needle Siltstone Member, and 12 in the Delle Phosphatic Member. The Willow Gap and the Skunk Spring Limestone Members did not have an R_o, so they were assigned a value of 10. The top of the oil window is approximately 8.5 and the top of the gas window is 11.5. The LOM correlates with other maturity indices, suggesting that organic matter in the Chainman Shale is beyond the oil window, definitely in the gas window, and possibility overmature in the lower part of the unit. The Camp Canyon RLOGR curve shows similar trends and spikes as found in the type well. However, the Camp Canyon section's lower synthetic baseline values for RHOB and RESD suggest lower TOC or organic matter concentrations relative to the Outlaw type well. The potential resource of oil and gas from the Chainman is discussed in the geochemistry section.

A TOC curve can be generated using the RLOGR and LOM variables (Passey and others, 1990). The equation is as follows:

$$TOC = RLOGR * 10(2.297 - 0.1688 * LOM) \quad (2)$$

where:

TOC =	total organic carbon (wt.%).
RLOGR =	density LogR (unitless).
LOM =	Level of Maturity (unitless).

The calculated TOC curve and the sample TOC points are shown in track 4, plate 2, appendix B. Since the LOM was estimated directly from calculated R_o in the geochemical analyses, the RLOGR curve was shifted in the different members so that the calculated TOC curve more closely fit the measured values. The average TOC in the Jensen Member is less than 1 wt.%. The Camp Canyon Member is approximately 1.3 wt.% and the average TOC in the Needle Siltstone Member is slightly higher at 1.5 wt.%. The Delle Phosphatic Member shows high TOC at 3 wt.%. These number compare favorably with the measured TOC values. The TOC curve trend suggests very low organic matter concentration in this part of the Chainman Shale. The left shift of the RLOGR curve suggests that there is organic matter in the Chainman as discussed in the geochemistry section.

The DT was measured and limestone sonic porosity (SPHL) calculated for the Chainman Shale at the Outlaw type well.

The SPHL at the Outlaw type well will overestimate porosity when compared to sandstone porosity. Density porosity can underestimate the actual porosity because TOC and water have large amounts of hydrogren, which can skew the density porosity to lower values. DT was recalculated to sonic porosity with sandstone units (SPHS) and is presented in plate 3, appendix B. Density porosity for sandstone (DPHS) was calculated from RHOB for the Camp Canyon section. The SPHS and DPHS porosity curve trends from the Outlaw type well and Camp Canyon section correlate well with each other and generally have the same sample average and spike values. The SPHS porosity in the Jensen Member varies from 0 to 10% with a few spikes over 20%. The DPHS at Camp Canyon shows highly variable porosity, generally averaging 5%, but ranging between 0 and 30%. The Willow Gap Member SPHS averages 10%, but is shifted to 13% when calculated in limestone units. Willow Gap DPHS averages 7% and ranges between 0 and 12%. The Camp Canyon Member SPHS is highly variable, particularly in the oversized-hole intervals where there is possible bad DT curve data due to borehole sloughing. The average Camp Canyon SHPS is 8% and ranges from 0 to 18%. Several shaley and phosphatic zones are very tight with porosities <1%. The DPHS at Camp Canyon has an average porosity of 10% with similar lower porosity zones in shale and phosphatic intervals. The SPHS and DPHS for the Skunk Spring Limestone Member are 5% and 10%, respectively. The Needle Siltstone and the Delle Phosphatic Members have highly variable SPHS and DPHS porosities ranging from 0 to 17% and 0 to 5%, respectively. Average Chainman porosities are 5% at the Outlaw type well and 1% at the Camp Canyon section.

Geochemistry

Sandberg and others (1980, p. 76) acknowledged reasonable organic content in the Chainman Shale as follows:

> Possible petroleum source rocks in the Chainman Shale occur mainly in the lower three members (figure 2). Twelve samples from these members averaged 1.8% organic carbon, but all four samples of organic-rich phosphatic mudstone exceeded 3.0% organic-carbon. Hydrocarbon content of three samples (two siltstones and one mudstone) ranged from 23 to 907 parts per million (ppm).
>
> Organic-carbon content of the upper three members of the Chainman Shale is relatively low in comparison to that of the lower three members (figure 2). Twenty-three samples from the higher members averaged 0.45% organic carbon. Only four samples, two of which came from the lower part of the middle member, contained 1.0% or more organic carbon. Several mudstone units in the lower, deeper water part of the middle member may be marginal petroleum source rocks.

Our geochemical data (table 1) support the conclusions of Sandberg and others (1980). In addition, the Chainman Shale kerogen is predominantly type III (dry gas prone) to slightly gas prone as suggested by standard geochemical diagrams and plots (figures 16 and 17); however, some oil production may be feasible (figures 18 and 19).

Figure 20 shows the variation in R_o with position in the Camp Canyon measured section, and figure 21 shows a similar plot for TOC. Notice that in figures 20 and 21 the measured values have been fit to the spectral gamma-ray and total gamma-ray data, using multivariate regression. The quality of these analyses is naturally poor due to the limited amount of data and interdependence of some of the variables. Nevertheless, this provides some quantitative representation of parameters that would be useful for estimating hypothetical resources.

There is some evidence of the organic matter being in the oil window as well as in the gas window based on R_o. To characterize this, a multivariate regression of vitrinite reflectance data was performed and regions with vitrinite reflectance greater than 0.6 and 1.1 were identified as lower limits of the oil and gas windows, respectively. The multivariate regression to estimate vitrinite reflectance (dependent variable) was based on the only other parameters available—Th, K, U, and total gamma-ray values (independent variables in the regression). The number of laboratory measurements is small and some of the independent variables are not exclusively independent, but no other options were available. Figure 22 shows vitrinite reflectance values over the depth range identified by Sandberg and others (1980) as having the best source potential (Delle Phosphatic Member through the lower section of the Camp Canyon Member).

Porosity

In a fashion similar to the vitrinite reflectance analysis above (designating potential oil and gas generating zones), porosity from laboratory measurements was regressed using spectral gamma-ray data. The same limitations and assumptions apply. Specifically, multivariate regression was used to estimate laboratory porosity values. The porosity measurements are shown in table 2 and figure 23. Figure 23 also shows the prediction of porosity that arose from estimating porosity from spectral gamma-ray values.

Resource Calculations

We made certain inferences to estimate the oil and gas in place in more moderately deeply buried Chainman Shale in western Utah and eastern Nevada. Vitrinite reflectance data were only available from programmed pyrolysis that was correlated with the hand-held gamma-ray data to indicate of R_o with depth. This was used as the criterion for oil versus gas as shown on figure 22. Total organic carbon data from certain samples were regressed (multivariate linear regression using the measured TOC and spectral gamma-ray data) with the original-gas-in-place and original-oil-in-place calculations by specifying a lower threshold for commercial production as

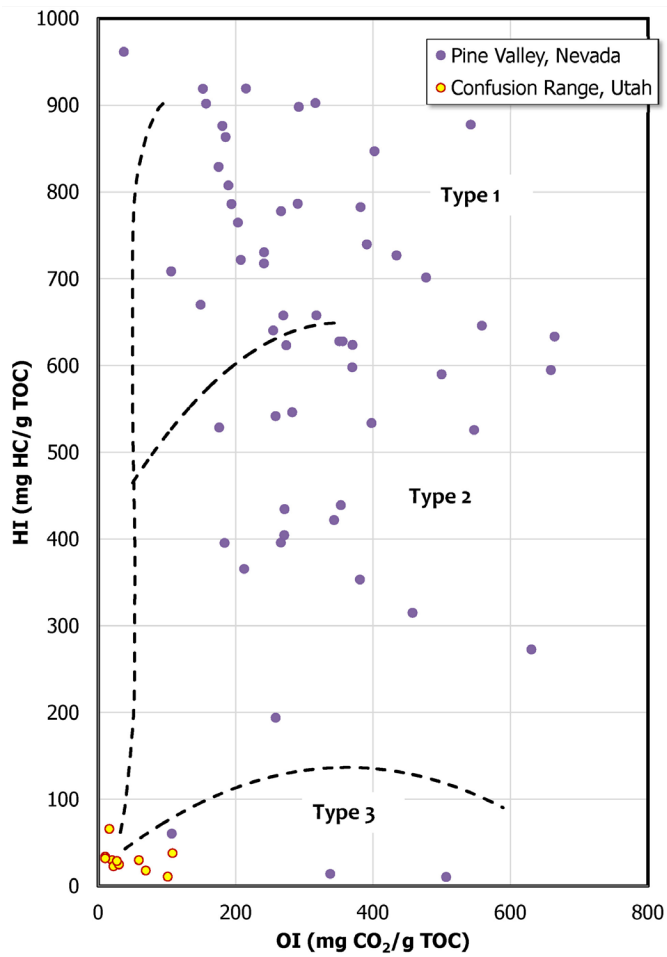

Figure 16. *Van Krevelen diagram showing total organic carbon (TOC) measurements from the samples collected from the Confusion Range in western Utah (yellow circles) and legacy data from Aminoil No. 1-23 Land Co. well, Pine Valley, Nevada (from Poole and Claypool, 1984).*

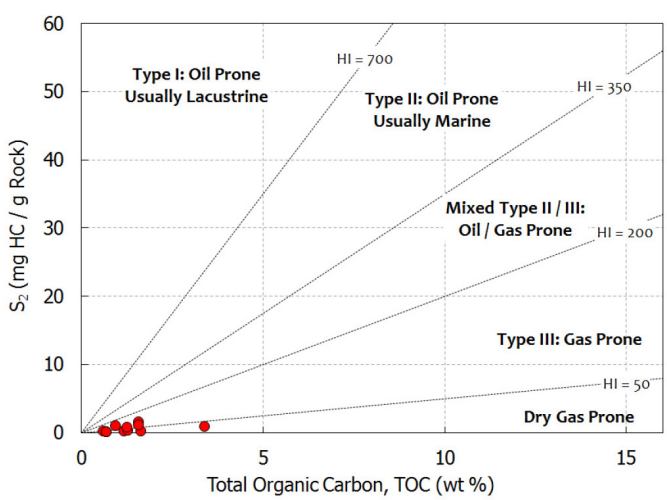

Figure 17. *Hydrocarbon generation (S2) versus TOC plot suggests that the kerogen is gas to dry-gas prone.*

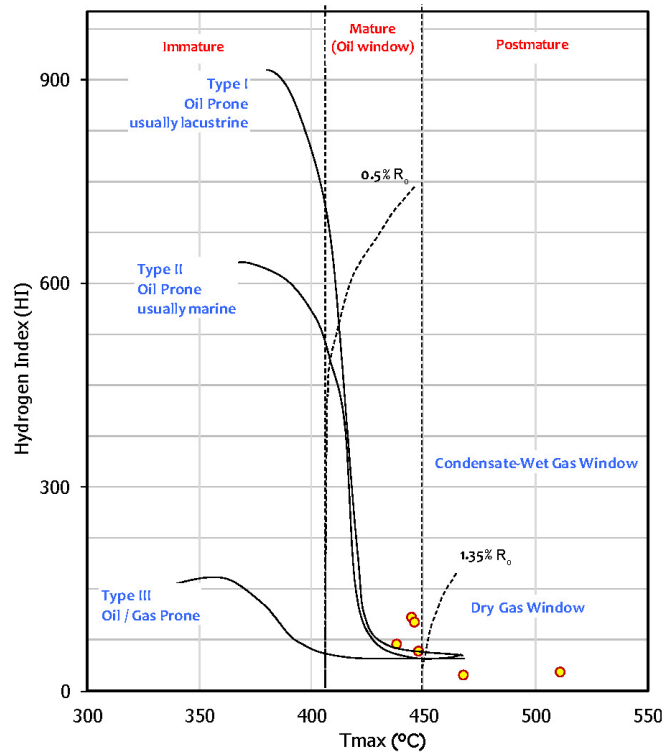

Figure 18. *This plot of hydrogen index (HI) versus Tmax suggests the possibility of oil as well as dry gas.*

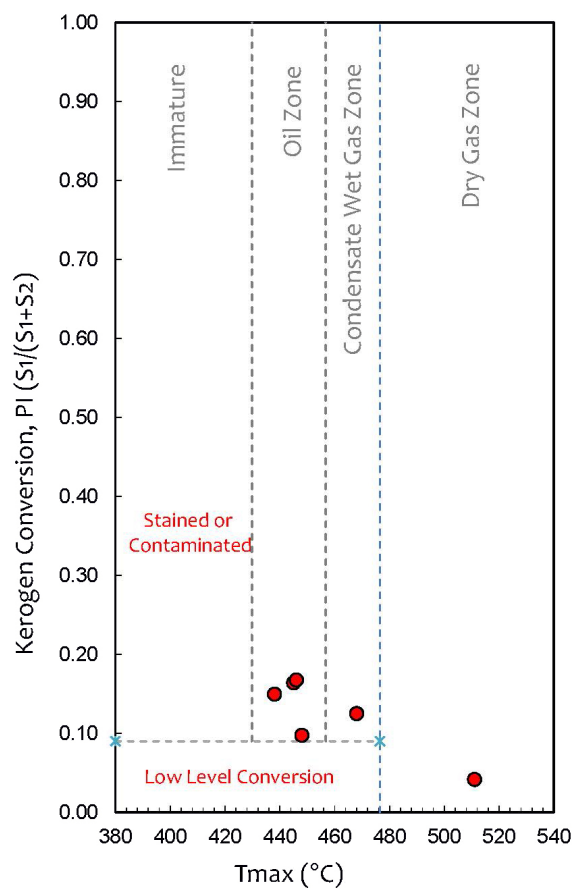

Figure 19. *This plot of the production index (PI) versus Tmax, as in figure 18, suggests dry gas, wet gas, and oil are possibilities in the Chainman Shale.*

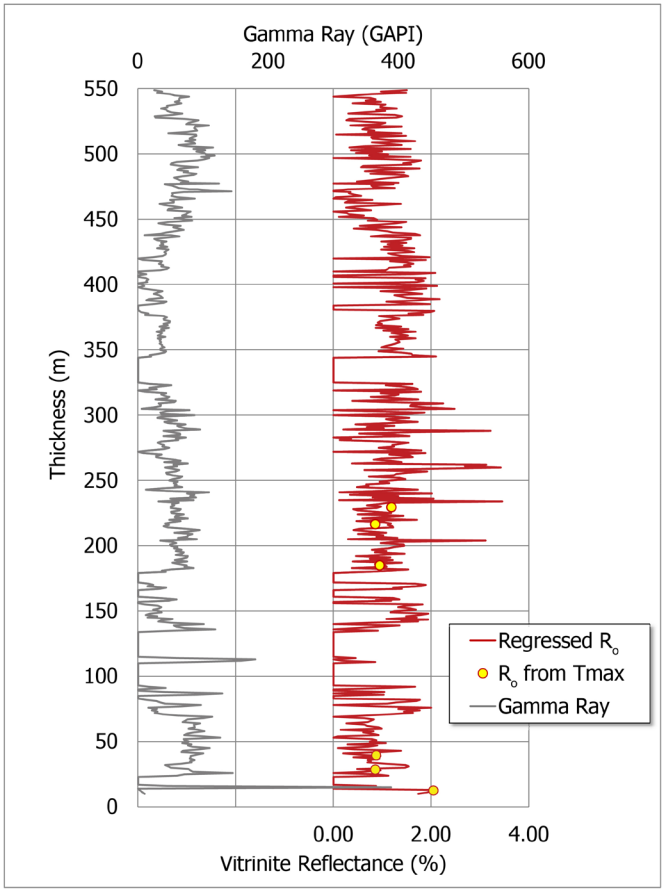

Figure 20. *The total gamma-ray track from hand-held scintillometer measurements and the laboratory measured values for vitrinite reflectance (calculated from Tmax) are shown. The multivariate regressed curve was based on the discrete measurements and the spectral gamma-ray data and should be considered as approximate.*

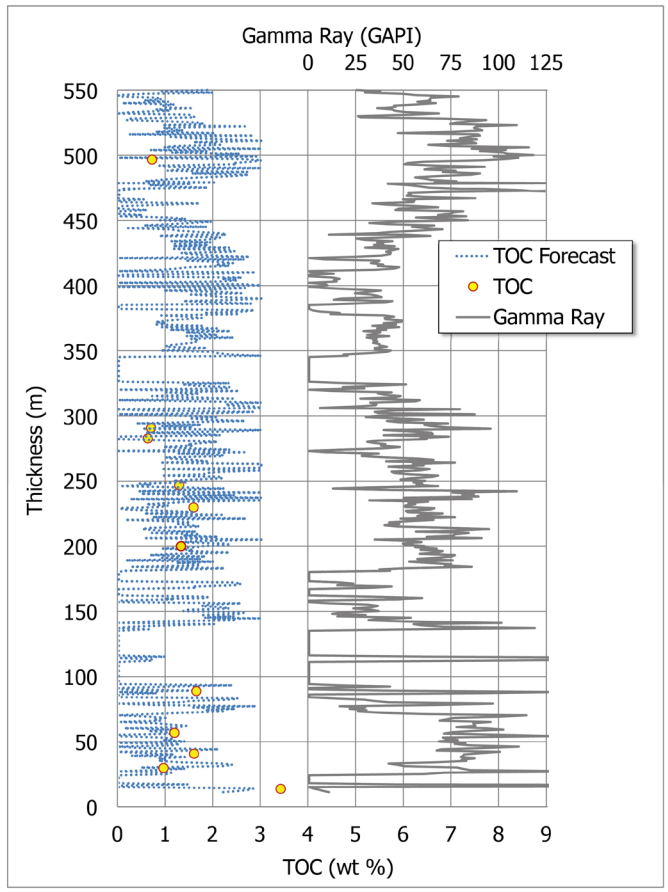

Figure 21. *The total gamma-ray track from hand-held scintillometer measurements and the laboratory measured values for TOC are shown. The multivariate regressed curve was based on the discrete measurements and the spectral gamma-ray data and should be considered as approximate.*

shown on figure 24. Potentially productive zones were picked on the basis of lithology—concentrated in the lower part of the section (figure 22). Porosity was measured on laboratory samples and regressed against the hand-held gamma-ray data. This used multivariate linear regression with the hand-held gamma-ray data (spectral and total) as the independent variable. Porosity is the primary parameter—only compressible storage was considered (figure 23).

The resource calculations incorporated the following conditions and assumptions (also see equations 3 and 4).

1. Depth was specified as 1524 meters true vertical depth. The top of the Skunk Spring Limestone Member of the Chainman Shale was set at this depth.
2. Reservoir pressure was assumed to be hydrostatic (~10.4 kpa/m [0.45 psi/ft]).
3. Reservoir pressure for oil was assumed to be above the bubble point.
4. A temperature gradient was assumed to be 2.5°C/100 m (1.38°F/100 ft) (Blackett, 2004).
5. Oil gravity was assumed to be 32°API. Gas gravity was taken as 0.65 and presumed methane only.
6. Separator pressure was assumed at 1 MPa (145 psi), and Standing's relationship was used to calculate the oil formation volume factor (Standing, 1977).
7. Water saturation was assumed to be 20% on average.
8. Compressible storage only was assumed. This is conservative since some adsorption could be anticipated.
9. For gas production, methane only was assumed. In this reservoir, there is the possibility of some heavier components also being present.
10. The following criteria were required:
    a. TOC must be greater than 0.5% with finite porosity,
    b. for oil production the vitrinite reflectance must be between 0.6 and 1.1%, and
    c. for gas production the vitrinite reflectance must be greater than 1.1%.
11. Initial in-situ volumes were estimated per hectare.

Figure 24 shows potentially recoverable cumulative oil and gas with depth. This plot presumes a 20% recovery factor over a twenty-year well life. This suggested cumulative production, on the order of 270,000 barrels of oil (BO) and 1.5 billion cubic feet of gas (BCFG), might be recovered from a vertical, fully penetrating well on an 80-acre spacing. Volumetric resource estimates relied strictly on the estimates for porosity and whether the sample was in the oil or gas window. These relationships were simply based on summation of oil or gas stored by compressibility in the effective porosity.

For oil:

$$OOIP = \zeta A \int \frac{\phi(1 - S_{wi})}{B_{oi}} dh \quad (3)$$

For gas:

$$OGIP = \zeta A \int \frac{\phi(1 - S_{wi})}{B_{gi}} dh \quad (4)$$

where:

$OOIP$ = original oil in place (STm^3, STB).

$OGIP$ = original gas in place (sm^3, scf).

A = drainage area (acres, hectares, section, …).

ϕ = dimensionless.

S_{wi} = initial water saturation (dimensionless).

B_{oi} = initial oil formation volume factor (ft^3/scf, m^3/sm^3, …).

B_{gi} = initial gas formation volume factor (bbl/STB, m^3/STm^3, …).

ζ = conversion factor for consistent units.

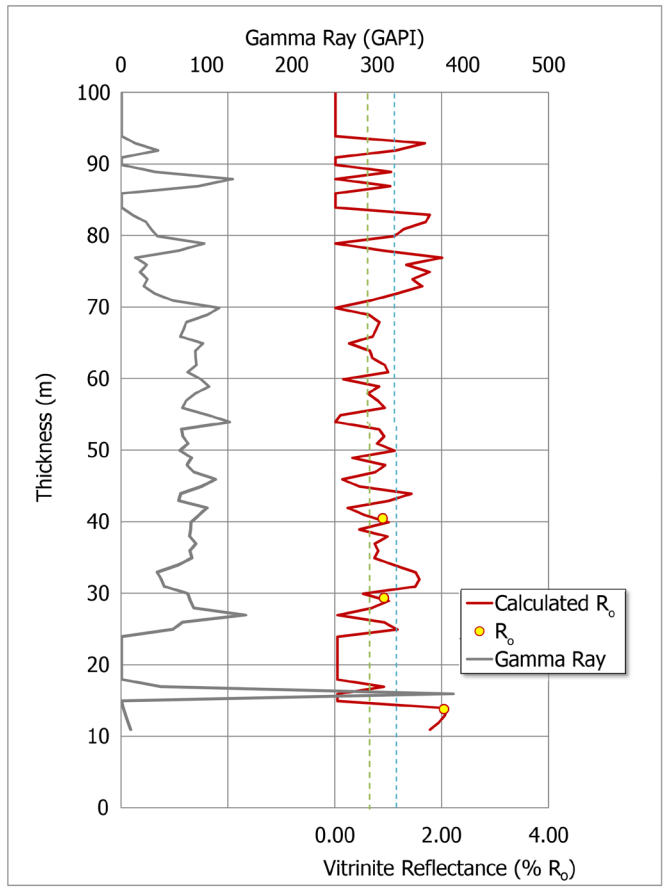

Figure 22. *An inferred vitrinite curve is shown for the lower members of the Chainman Shale (Delle Phosphatic Member through the lower section of the Camp Canyon Member). Two maturity thresholds are shown as dashed lines—a 0.6% R_o green dashed line indicating the oil window and 1.1% R_o blue dashed line demarcating a dry gas window.*

CONCLUSIONS

- Three organic-rich shale facies measured in the central Confusion Range section of the Mississippian Chainman Shale exhibit hydrocarbon potential: (1) a stratigraphically pervasive calcareous mudrock, (2) a siliceous-calcareous facies, and (3) a noncalcareous argillaceous facies. These facies are found in the Delle Phosphatic, uppermost Needle Siltstone, and lower Camp Canyon Members.
- Nonshale facies that also possess hydrocarbon potential include a dolomitic siltstone near the base of the formation, and the Delle Phosphatic Member (phosphorite deposits) that rests directly upon the Joana Limestone.
- The phosphatic zones are commonly present at or near the bases of TSTs. We firmly believe that an erosional disconformity exists on top of the Willow Gap Member that developed after the succession shallowed upward.
- The mineralogy and whole-rock chemistry of the members of the Chainman Shale show ancient erosional patterns from the Antler orogenic highlands, and possibly the volcanic arc systems, by the type and amount of siliciclastic and carbonate sediment deposited into the foredeep basin. Three siliciclastic, apatitic layers identified in the Chainman at the Camp Canyon section indicate repeated deep-water (with upwelling currents), organic-rich, reducing environments during the early depositional phase from the Delle Phosphatic Member through the upper part of the Camp Canyon Member and into the lower Jensen Member. The whole-rock chemistry CIW values from bottom to top of the Chainman show select episodic pulses in the sediment source from more continential, micaeous sediments to more weathered, clay-bearing terrains. Higher CIW index values in most samples indicate that soil-bearing terrains were eroded and clay minerals (montmorillonite and kaolinite) and silicates were transported to the basin. The variable amounts of authigenic carbonate and allogenic silicates show variations in the distance to the fluvial system providing minerals to the basin.

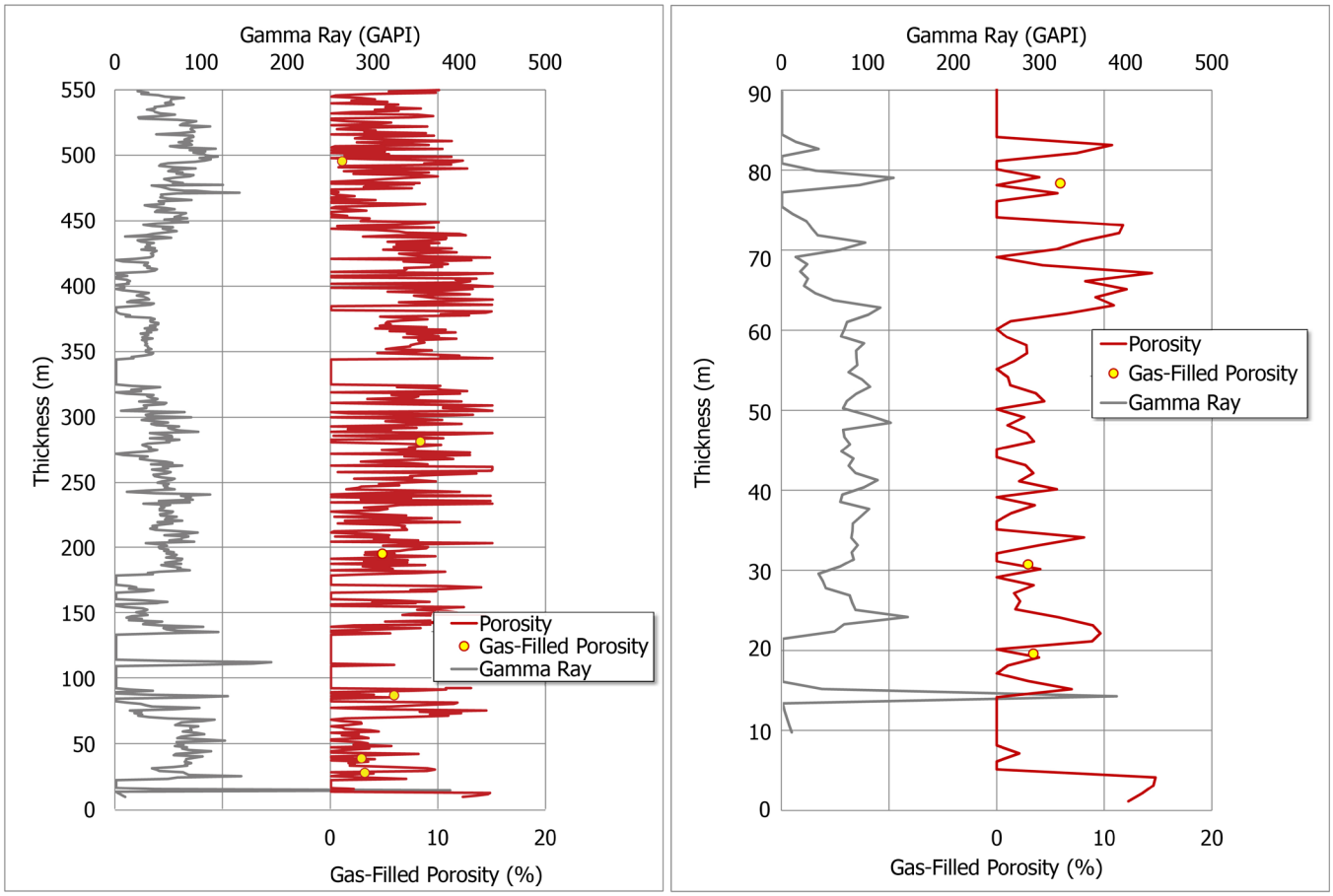

Figure 23. *Gas-filled porosity of the Chainman Shale section is shown in the left-hand panel. Inferred porosity over the hypothesized hydrocarbon-bearing zones is shown in the right-hand panel. The porosity could be gas- or oil-filled.*

High-carbonate, low-silicate concentrations indicate a sediment source to the east, whereas low-carbonate and high-silicate mineral concentrations imply a depositional source from the Antler highlands.

- Geochemical work indicates that the Chainman contains acceptable TOC values to be considered a viable hydrocarbon source, but these surface sample numbers (~1 to 2 wt.%) are modest. The Tmax values fall in the oil window and perhaps in the oil-wet gas category. Mobile oil was found in one of the collected surface samples.
- Other TOC contributors may include nonanalyzed dark, micritic limestone beds found interbedded with the mudrocks in the lower portion (Delle Phosphatic Member through the lower section of the Camp Canyon Member) of the central Confusion Range Chainman Shale section (see figures 2, 6, and 7).
- Mudrock porosities are acceptable for hydrocarbon production potential as compared to other shale gas or shale oil reservoirs. The siliceous-calcareous facies showed ~9.5% effective porosity, although all permeability measurements (TRA) scarcely attain 100 nD, an empirically pre-determined value perhaps mini-

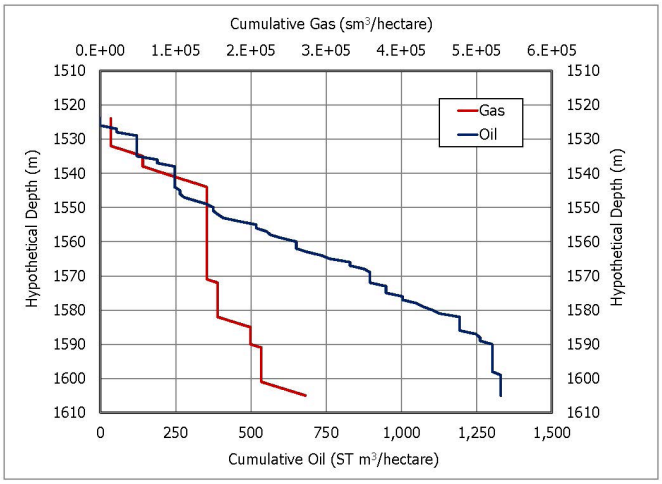

Figure 24. *Possible cumulative volumes (recoverable estimate) of oil (blue line) and gas (red line) for a hypothetical Chainman completion. Recoverable oil and gas was estimated as 20% of the estimated oil and gas in place. The estimates suggests that prospective oil and gas production in the Chainman Shale is a possibility. Permeabilities are low but economic recovery is feasible if the assumptions made are reasonably realistic. The assumptions for these estimates are summarized in the text. For purposes of conversion, 1 m³/hectare is equal to 15.5 barrels/acre and 100,000 m³/hectare = 8.73 MMscf/acre.*

mally essential for economic recoveries. Again, surface weathering effects may also have occurred here.

- The surface gamma-ray log generated for this study might prove an invaluable analog for any well logs penetrating the Chainman Shale in this vicinity. The Outlaw Federal No. 1 well in White Pine County, Nevada, was selected as a type well for the Chainman. The GR, DT, and SPHI curves were used to generate the DLOGR, RLOGR, and TOC curves for the type well. Similar trends between high and low GR zones were correlated between the Camp Canyon section and the Outlaw type well. The correlations between geophysical curves at the Outlaw type well were used to generate synthetic RHOB, RLOGR, and TOC curves for the Camp Canyon section. The RLOGR curves from the Outlaw type well and the Camp Canyon section have areas of separation starting in the middle to lower part of the Camp Canyon Member down through the lower Needle Siltstone Member. The Delle Phosphatic Member has concentrations of organic matter but the curves are skewed due to high concentrations of uranium in the phosphate. The TOC curves generated from the RLOGR curves show an average concentration of approximately 1 to 1.5% TOC. High TOC areas of approximately 3% are found in the Delle Phosphatic Member and small zones in the Needle Siltstone and the Camp Canyon Members. SPHS and DPHS sandstone porosities range from 0 to 30% and average between 5 and 10% through the Chainman.
- Hypothetical oil-in-place measurements and estimated hydrocarbon recoveries are also encouraging. Recoverable hydrocarbons on 80-acre spacing is estimated at 270,000 BO and 1.5 BCFG per well.

No wells currently produce from the Chainman Shale in Utah or Nevada. However, in 2007, Plains Exploration & Production Company drilled the Pluto No. 27-1 well (SW1/4NE1/4SE1/4 section 27, T. 18 N., R. 61 E., White Pine County, Nevada) about 23 kilometers west of Ely, and encountered a significant gas show (377,000 ppm of methane) in a 20-meter-thick sandstone in the upper Chaiman along the steeply dipping east flank of a large anticline (Davis and Namson, 2014). Oil staining and yellow-gold fluorescence were also observed in the cuttings. Although the Pluto well was non-commercial, it demonstrated that hydrocarbons are present in the Chainman of the eastern Basin and Range Province and adds support for the untested potential determined from our study.

ACKNOWLEDGMENTS

This research was funded through the Utah Geological Survey (UGS), Contract # 112610, under the "Characterization of Utah's Hydrocarbon Reservoirs, Metals, and Industrial Minerals Program." Additional funding was provided by Bereskin and Associates, Inc., Craig Poole (Fresno City College), Tom Oesleby (consultant), and Dave Taff (consultant) measured sections, and collected and cataloged samples. We thank Craig Morgan, Steve Herbst, and Tom Dempster of the UGS for conducting gamma-ray field measurements and assisting with field sample collection. Geochemical analysis, SEM, and TRA were provided by TerraTek, a Schlumberger Company. Tarn Bereskin (Bereskin and Associates, Inc.) conducted geologic reconnaissance to identify a specific section of Chainman Shale suited for detailed study and produced graphs of the measured section. Cheryl Gustin and Jay Hill of the UGS assisted with figure preparation. We thank David E. Tabet, Douglas A. Sprinkel, Robert Ressetar, and Stephanie Carney of the UGS for their careful reviews and constructive criticisms of the manuscript.

REFERENCES

Anna, L.O., Roberts, L.N.R., and Potter, C.J., 2007, Chapter 2—geologic assessment of undiscovered oil and gas resources in Paleozoic-Tertiary composite total petroleum system of the eastern Great Basin, Nevada and Utah, *in* Geologic assessment of undiscovered oil and gas of the eastern Great Basin province, Nevada, Utah, Idaho, and Arizona: U.S. Geological Survey Digital Data Series DDS-69-L, 50 p.

Armstrong, R.L., 1968, Sevier orogenic belt in Nevada and Utah: Geological Society of America Bulletin, v. 79, p. 429–458.

Blackett, R.E., 2004, Geothermal gradient data for Utah: Geothermal Resources Council Transactions, v. 28, p. 3–6.

Blakey, R., and Ranney, W., 2008, Ancient landscapes of the Colorado Plateau: Grand Canyon, Grand Canyon Association, 156 p.

Cook, H.E., and Corboy, J.J., 2004, Great Basin Paleozoic carbonate platform—facies, facies transitions, depositional models, platform architecture, sequence stratigraphy and predictive mineral host models: U.S. Geological Survey Open-File Report 2004-1078, 129 p.

Craig, L.C., and Varnes, K.L., 1979, History of the Mississippian System—an interpretive summary: U.S. Geological Survey Professional Paper 1010, p. 371–406.

Davis, T.L., and Namson, J., 2014, Nevada's Chainman Shale shows exploration potential: Oil & Gas Journal, v. 112, no. 6, p. 42.

Davydov, V., Wardlaw, B.R., and Gradstein, F.M., 2004, The Carboniferous Period, *in* Gradstein, F.M., Ogg, J.G., and Smith, A.G., editors, A geologic time scale: Cambridge University Press, p. 222–248.

Dickinson, W.R., 2006, Geotectonic evolution of the Great Basin: Geosphere, v. 2, no. 7, p. 353–368.

Gordon, M., Jr., and Yochelson, E.L., 1987, Late Mississippian gastropods of the Chainman Shale, west-central Utah: U.S. Geological Survey Professional Paper 1368, 122 p, 9 plates.

Greene, D.C., 2014, The Confusion Range, west-central Utah; fold-thrust deformation and a western Utah thrust belt in the Sevier hinterland: Geosphere, Pre-Issue Publication doi:http://dx.doi.org/10.1130/GES00972.1.

Greene, D.C., and Herring, D.M., 2013, Structural architecture of the Confusion Range, west-central Utah: a Sevier fold-thrust belt and frontier petroleum province: Utah Geological Survey Open-File Report 613, 22 p., 6 plates.

Gutschick, R.C., Sandberg, C.A., and Sando, W.J., 1980, Mississippian shelf margin and carbonate platform from Montana to Nevada, *in* Fouch, T.D., and Magathan, E.R., editors, Paleozoic paleogeography of the west-central United States, Rocky Mountain paleogeography symposium 1: Society of Economic Paleontologists and Mineralogists, p. 111–128.

Gutschick, R.C., and Sandberg, C.A., 1983, Mississippian continental margins of the conterminous U.S.: Society of Economic Paleontologists and Mineralogists Special Publication 33, p. 79–96.

Harnois, L., 1988, The CIW index: a new chemical index of weathering: Sedimentary Geology, v. 55, p. 319–322.

Hintze, L.F., 1974, Preliminary geologic map of the Conger Mountain quadrangle, Millard County, Utah, and Lincoln and White Pine Counties, Nevada: U.S. Geological Survey Miscellaneous Field Studies Map MF-634, 2 plates, scale 1:48,000.

Hintze, L.F., 1986, Geologic map of Mormon Gap and Tweedy Wash quadrangles, Millard County, Utah, and Lincoln and White Pine Counties, Nevada: U.S. Geological Survey Miscellaneous Field Studies Map MF-1872, 1 plate, scale 1:24,000.

Hintze, L.F., 1997, Interim geologic map of the Big Jensen Pass quadrangle, Millard County, Utah: Utah Geological Survey Open-File Report 357, 2 plates, scale 1:24,000.

Hintze, L.F., and Davis, F.D., 2002, Geologic map of Tule Valley 30′ x 60′ quadrangle and parts of the Ely, Fish Springs, and Kern Mountains 30′ x 60′ quadrangles, northwest Millard County, Utah: Utah Geological Survey Map 186, 2 plates, scale 1:100,000.

Hintze, L.F., and Davis, F.D., 2003, Geology of Millard County, Utah: Utah Geological Survey Bulletin 133, 305 p.

Hintze, L.F., and Kowallis, B.J., 2009, Geologic history of Utah: Brigham Young University Geology Studies Special Publication 9, 225 p.

Hood, A., Gutjahr, C.C.M., and Heacock, R.L., 1975, Organic metamorphism and the generation of petroleum: American Association of Petroleum Geologists Bulletin, v. 59, p. 986–996.

Horton, B., 2012, Variability of the Mancos Shale: developing preliminary depositional and sequence stratigraphic models of a developing shale gas play: Utah: Salt Lake City, University of Utah, M.S. thesis, p. 413.

Hose, R.K., 1963a, Geologic map and section of Cowboy Pass NE quadrangle, Confusion Range, Millard County, Utah: U.S. Geological Survey Miscellaneous Investigations Series Map I-377, 1 plate, scale 1:24,000.

Hose, R.K., 1963b, Geologic map and sections of Cowboy Pass SE quadrangle, Confusion Range, Millard County, Utah: U.S. Geological Survey Miscellaneous Investigations Series Map I-391, 1 plate, scale 1:24,000.

Hose, R.K., 1965a, Geologic map and sections of the Conger Range SE quadrangle and adjacent area, Confusion Range, Millard County, Utah: U.S. Geological Survey Miscellaneous Investigations Series Map I-435, 1 plate, scale 1:24,000.

Hose, R.K., 1965b, Geologic map and sections of the Conger Range NE quadrangle and adjacent area, Confusion Range, Millard County, Utah: U.S. Geological Survey Miscellaneous Investigations Series Map I-436, 1 plate, scale 1:24,000.

Hose, R.K., 1977, Structural geology of the Confusion Range, west-central Utah: U.S. Geological Survey Professional Paper 971, 9 p.

Hose, R.K., and Repenning, C.A., 1964, Geologic map and sections of Cowboy Pass SW quadrangle, Confusion Range, Millard County, Utah: U.S. Geological Survey Miscellaneous Investigations Series Map I-390, 1 plate, scale 1:24,000.

Hose, R.K., and Ziony, J.I., 1964, Geologic map and sections of Gandy SE quadrangle, Confusion Range, Millard County, Utah: U.S. Geological Survey Miscellaneous Investigations Series Map I-393, 1 plate, scale 1:24,000.

Karklins, O.L., 1986, Chersterian (Late Mississippian) bryozoans from the upper Chainman Shale and the lowermost Ely Limestone of western Utah: Paleontological Society Memoir 17, 48 p.

Machel, H.G., and Mountjoy, E.W., 1986, Chemistry and environments of dolomitization—a reappraisal: Earth Science Reviews, v. 23, no. 3, p. 175–222.

McLennan, S.M., 1993, Weathering and global denudation: The Journal of Geology, v. 101, no. 2, p. 295–303.

Meissner, F.F., 1995, Pattern of maturity in source rocks of the Chainman Formation, central Railroad Valley, Nye County, Nevada and its relation to oil migration and accumulation, *in* Hansen, M.W., Walker, J.P., and Trexler, J.H., Jr., editors, Mississippian source rocks of the Antler Basin of Nevada and associated structural and stratigraphic traps: Field Trip Guidebook, Nevada Petroleum Society, p. 74–95.

Meissner, F.F., Woodward, J., and Clayton, J.L., 1984, Stratigraphic relationships and distribution of source rocks in the greater Rocky Mountain region, *in* Woodward, J., Meissner, F.F., and Clayton, J.L., editors, Hydrocarbon source rocks of the greater Rocky Mountain region: Rocky Mountain Association of Geologists Guidebook, p. 1–34.

Nesbitt, H.W., and Young, G.M., 1982, Early Proterozoic climates and plate motions inferred from major element chemistry of lutites: Nature, v. 299, p. 715–717.

Passey, Q.R., Creaney, S., Kulla, J.B., Moretti, F.J., and Stroud, J.D., 1990, A practical model for organic richness from porosity and resistivity logs: American Association of Petroleum Geologists Bulletin, v. 74, p. 1777–1794.

Poole, F.G., and Claypool, G.E., 1984, Petroleum source-rock potential and crude-oil correlation in the Great Basin, *in* Woodward, J., Meissner, F.F., and Clayton, J.L., editors, Hydrocarbon source rocks of the greater Rocky Mountain region: Rocky Mountain Association of Geologists Guidebook, p. 179–229.

Price, J.R., and Velbel, M.A., 2003, Chemical weathering indices applied to weathering profiles developed on heterogeneous felsic metamorphic parent rocks: Chemical Geology, v. 202, p. 397–416.

Sadlick, W., 1965, Biostratigraphy of the Chainman Formation, eastern Nevada and western Utah: Salt Lake City, University of Utah, Ph.D. dissertation, 227 p.

Sageman, B.B., and Lyons, T.W., 2003, Geochemistry of fine-grained sediments and sedimentary rocks, *in* MacKenzie, F., editor, Sediments, diagenesis, and sedimentary rocks: Elsevier, Treatise on Geochemistry, v. 7, p. 115–158.

Sandberg, C.A., and Gutschick, R.C., 1980, Sedimentation and biostratigraphy of Osagean and Meramecian starved basin and foreslope, western United States, *in* Fouch, T.D., and Magathan, E.R., editors, Paleozoic paleogeography of the west-central United States, Rocky Mountain paleogeography symposium 1: Denver, Rocky Mountain Section, Society of Economic Paleontologists and Mineralogists, p. 129–147.

Sandberg, C.A., and Gutschick, R.C., 1984, Distribution, microfauna, and source-rock potential of Mississippian Delle Phosphatic Member of Woodman Formation and equivalents, Utah and adjacent states, *in* Woodward, J., Meissner, F.F., and Clayton, J.L., editors, Hydrocarbon source rocks of the greater Rocky Mountain region: Rocky Mountain Association of Geologists, p. 135–178.

Sandberg, C.A., Poole, F.G., and Gutschick, R.C., 1980, Devonian and Mississippian stratigraphy and conodont zonation of Pilot and Chainman Shales, Confusion Range, Utah, *in* Fouch, T.D., and Magathan, E.R., editors, Paleozoic paleogeography of the west-central United States: Denver, Rocky Mountain Section, Society of Economic Paleontologists and Mineralogists, p. 71–79.

Sandberg, C.A., Gutschick, R.C., Johnson, J.G., Poole, F.G., and Sando, W.J., 1982, Middle Devonian to Late Mississippian geologic history of the overthrust belt region, western United States, *in* Powers, R.B., editors, Geologic studies of the Cordilleran thrust belt, v. II: Rocky Mountain Association of Geologists, p. 691–719.

Sheldon, R.P., Cressman, E.R., Cheney, T.M., and McKelvey, V.E., 1967, Permian—Middle Rocky Mountains and northeastern Great Basin: U.S. Geological Survey Professional Paper 515, p. 157-174.

Skipp, B., 1979, Mississippian—Great Basin region: U.S. Geological Survey Professional Paper 1010, p. 273–328.

Spencer, A.C., 1917, Geology and ore deposits of Ely, Nevada: U.S. Geological Survey Professional Paper 96, 189 p.

Standing, M.B., 1977, Volumetric and phase behavior of oil field hrdrocarbon systems: Dallas, Texas, Society of Petroleum Engineers, 150 p.

Stokes, W.L. 1986, Geology of Utah, chapter 9—the Mississippian period: Utah Museum and Natural History and the Utah Geological and Mineral Survey, Occasional Paper No. 6, p. 77–84.

Taylor, S.R., and McLennan, S.M, 1985, The continental crust—its composition and evolution, an examination of the geochemical record preserved in sedimentary rocks: Oxford, United Kingdom, Blackwell Scientific Publication, 312 p.

Webster, G.D., Gordon, M., Jr., Langenheim, R.L., and Henry, T.W., 1984, Road logs for the Mississippian-Pennsylvanian boundary in the eastern Great Basin, *in* Lintz, J., Jr., editor, Western geological excursions, sponsored by the Geological Society of America and the Department of Geosciences, University of Nevada-Reno: Reno, Department of Geosciences, University of Nevada-Reno, v. 1, p. 1–86.

Welsh, J.E., and Bissell, H.J., 1979, The Mississippian and Pennsylvanian (Carboniferous) Systems in the United States: U.S. Geological Survey Professional Paper 1110-Y, 35 p.

Wernicke, B.P., 1992, Cenozoic extensional tectonics of the U.S. Cordillera, *in* Burchfield, B.C., Lipman, P.W., and Zoback, M.L., editors, The Cordilleran orogen—conterminous U.S.: Geological Society of America, The Geology of North America, v. G-3, p. 553–581.

Appendix A - Measured Section

Part 1

Section: Chainman Shale, Camp Canyon

Location: Confusion Range, Utah Interval Thickness: 254-0 meters

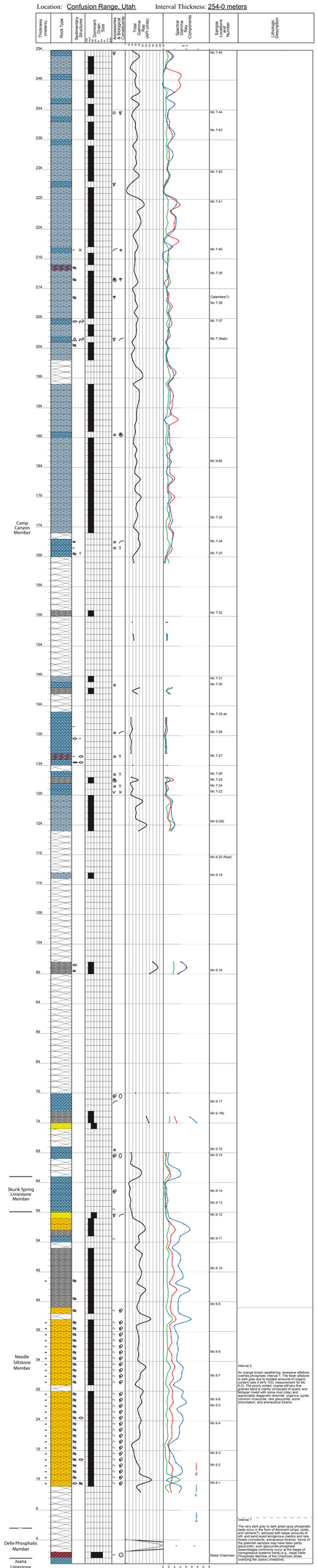

Part 2

Section: Chainman Shale, Camp Canyon

Location: Confusion Range, Utah Interval Thickness: 508-254 meters

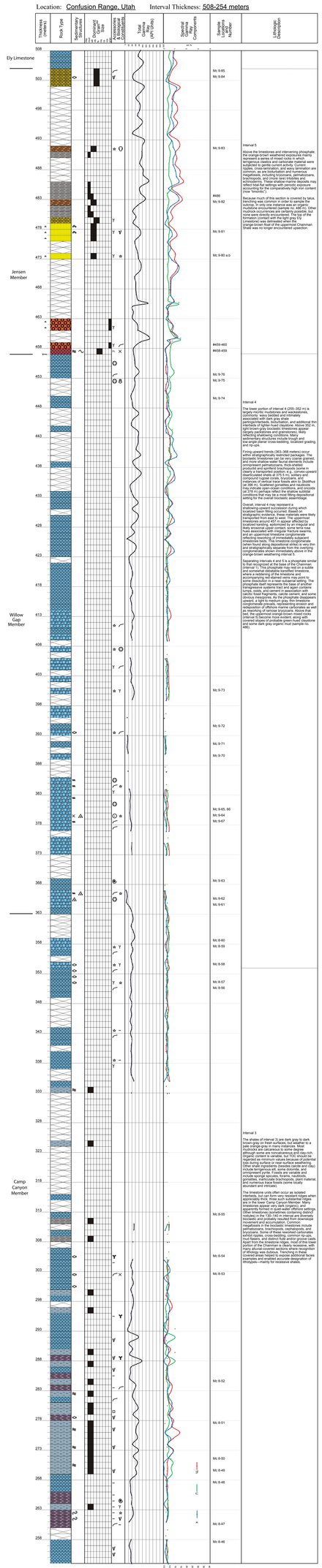

Explanation

- Limestone Conglomerate
- Limestone
- Covered Interval
- Muddy Limestone
- Packstone
- Sandstone
- Sandy Limestone
- Shale or Mudstone - Calcareous
- Shale or Mudstone - Poorly Calcareous
- Siliceous or Layered Phosphate
- Siltstone
- Silty Limestone

- Bioturbated
- Bryozoan
- Calcitic
- Carbonaceous
- Cephalopod
- Cross-Lamination or Bedding
- Erosion Surface
- Flaser Bedding
- Gastropod
- Grading
- Loading
- Microfossil
- Mottled
- Muddy Remnant
- Nodular

- Oolitic
- Ostracod
- Pelmatozoan
- Peloid
- Ph Phosphatic
- Planar Lamination
- Py Pyritic
- Rippled
- Rip-Up or Breccia Clast
- Rugose Coral
- Shell Fragment
- Soft-Sediment Deformation
- Sponge Spicule
- Stylolitic
- Tribolite
- Wavy Lamination

Most strata in this outcrop section belong to five distinguishable lithostratigraphic intervals:

1) The lowest interval resting on the Joana Limestone is a dark gray layered phosphate (Delle Phosphatic Member); however, much of this material is not exposed.
2) A dark gray, poorly sorted, muddy siltstone forms the lower part of the Needle Siltstone Member.
3) Interbedded dark gray to black, organic, calcareous to noncalcareous mudstone and fine-grained, muddy, organic limestones make up most of the section to the upper Camp Canyon Member. The mudstone comprises most of the potential "shale" pay. The limestones likely reflect offshore marine, both quiet-water and current-swept environments.
4) Very thick and resistant, light brown-gray to medium dark gray, muddy to distinctly bioclastic limestones represent the upper Camp Canyon and Willow Gap Members. Capping this interval is layered phosphate at 458–459 m.
5) Recessive beds of orange-brown weathered siltysandy limestones, calcareous sandstones/siltstones, and minor amounts of recognizable shales or claystones constitute the Jensen Member.

Appendix B - Plate 1. Camp Canyon Measured Section Geophysical Log

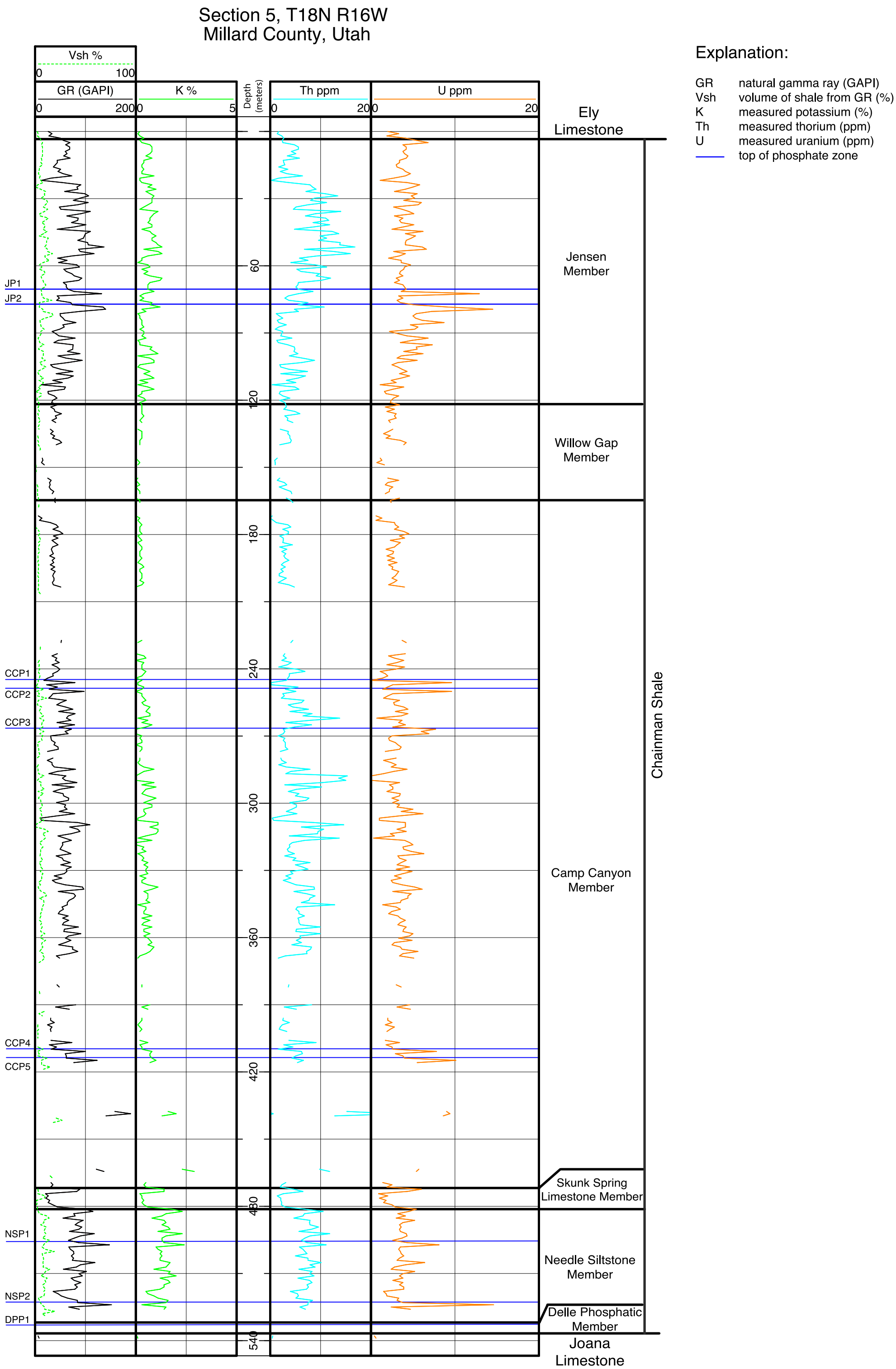

Appendix B - Plate 2. Geophysical and Petrophysical Log Cross Section Between the Outlaw Federal No. 1 Well and Camp Canyon Section

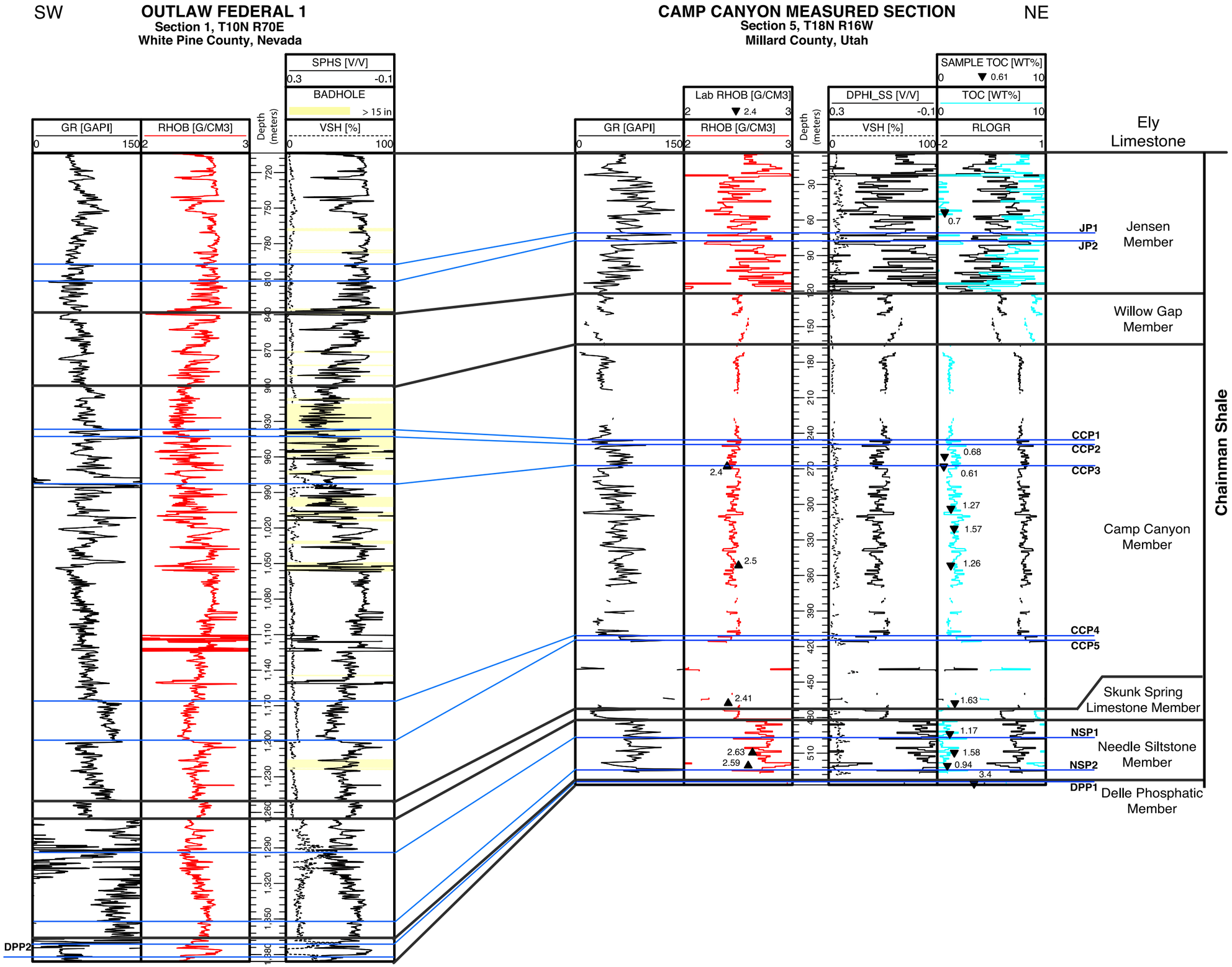

Explanation:

GR	natural gamma ray (GAPI)
Vsh	volume of shale from GR (%)
DT	compressional wave time (µs/ft)
SPHI	sonic porosity (V/V)
RHOBDT	bulk density (g/cm³) calculated from DT
LLD	laterolog deep resistivity (OHMM)
TOC	total organic carbon (wt%)
DPHI_SS	density porosity sandstone
RLOGR	RHOB - LOG RES
BADHOLE	borehole diameter greater than 15 inches
——	top of phosphate zone

▲ 2.41

Lab RHOB are "As Received" bulk density from table 1. Lab measurements plotted on the sample scale as the calculated bulk density RHOB curve for the Camp Canyon measured section.

▼ 1.63

Sample TOC are laboratory measurments from table 1. Values plotted on the sample scale as the calculated bulk density RHOB curve for the Camp Canyon measured section.

Appendix B - Plate 3. Outlaw Federal No. 1 Chainman Shale Type Well Geophysical and Petrophysical Log

OUTLAW FEDERAL 1

Section 1, T10N R70E
White Pine County, Nevada

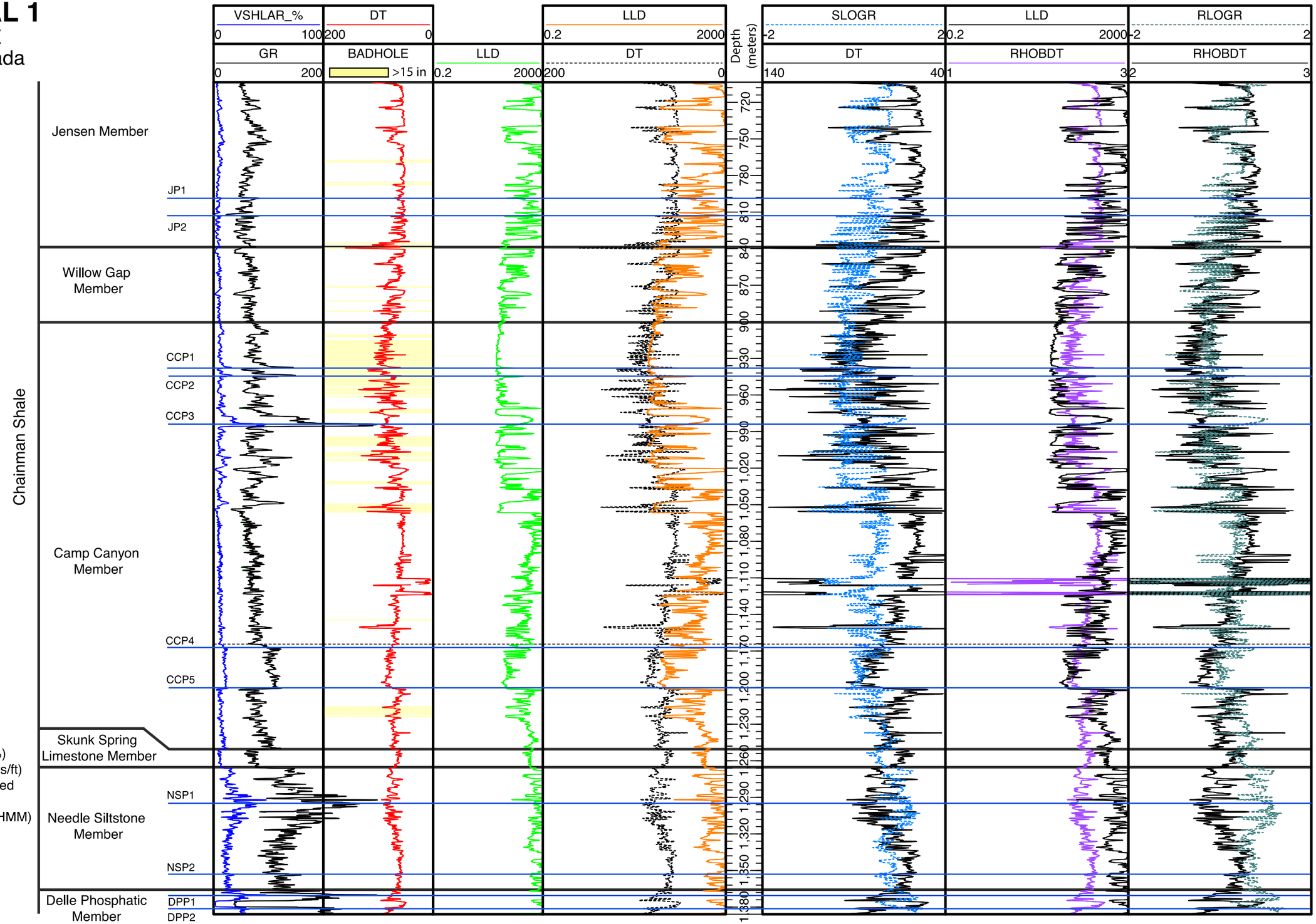

Explanation:

GR	natural gamma ray (GAPI)
Vsh	volume of shale from GR (%)
DT	compressional wave time (µs/ft)
RHOBDT	bulk density (g/cm³) calculated from DT
LLD	laterolog deep resistivity (OHMM)
TOC	total organic carbon (wt%)
RLOGR	RHOB - LOG RES
BADHOLE	borehole diameter greater than 15 inches
——	top of phosphate zone

Plate I

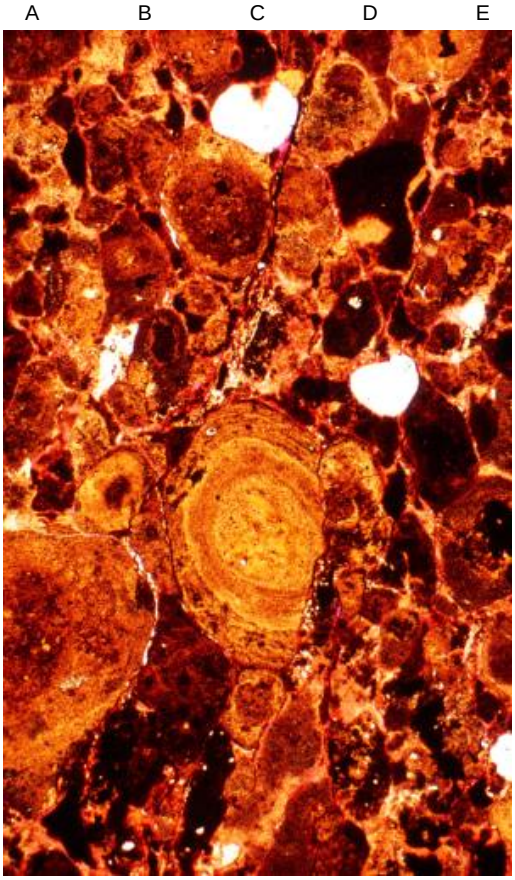

A.

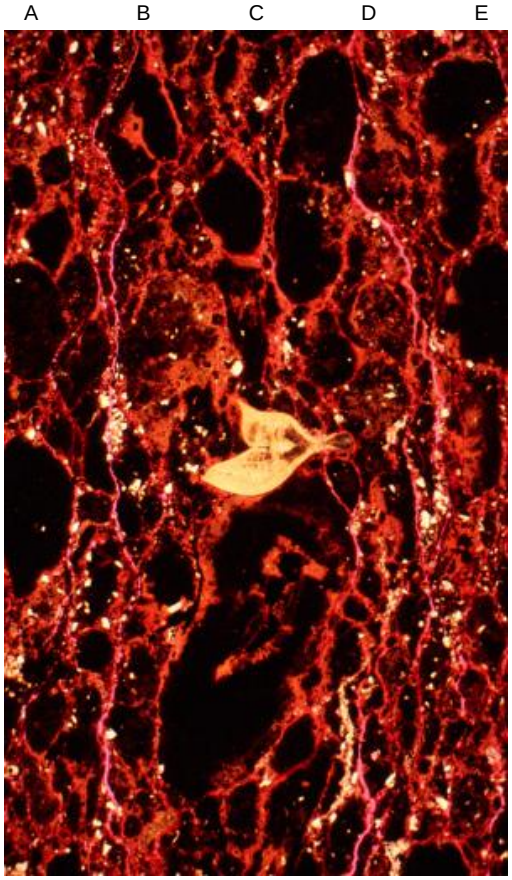

B.

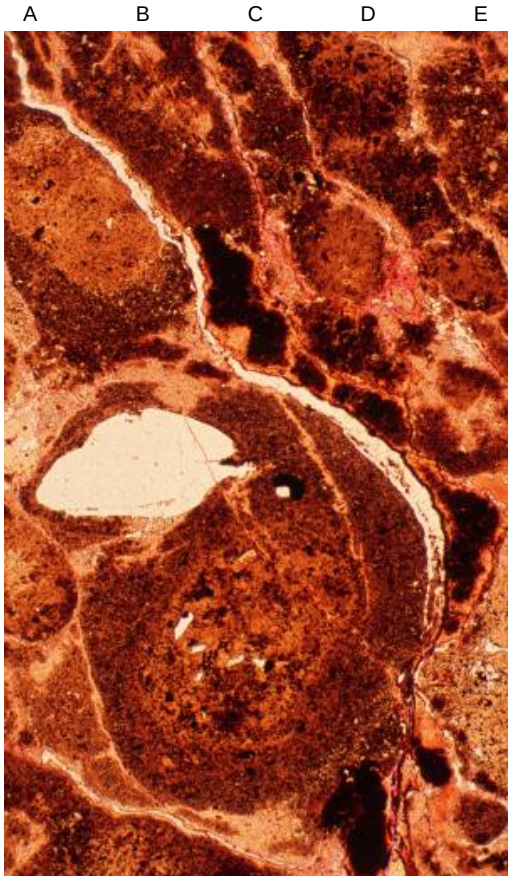

C.

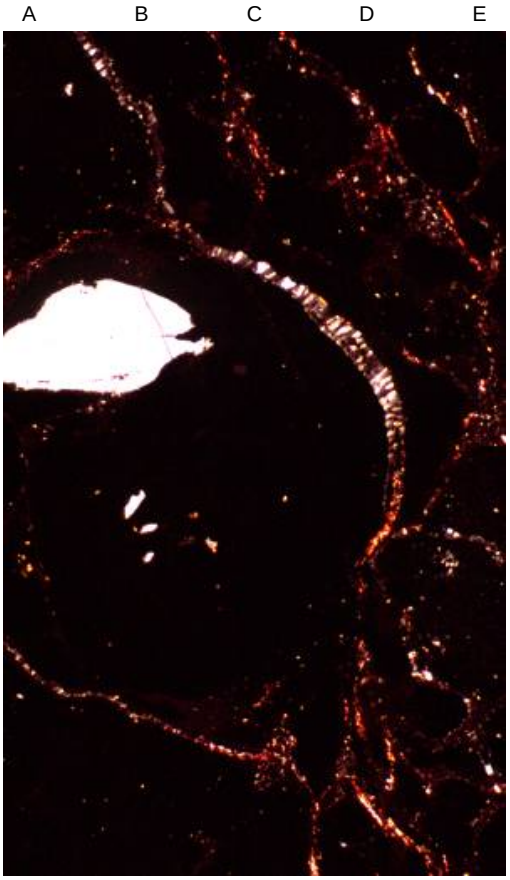

D.

Plate I Descriptions

A. **Confusion Range: Sample--Basal Beds (Delle Phosphatic Member).** Base of formation is represented by a dense phosphate accumulation common to lower portions of a transgressive systems tract. Phosphate is in the form of lumps, ooids, and cements--all admixed with a small percentage of terrigenous clastics (white grains). Very dark material is likely a combination of organic material and replacive pyrite. Plane polarized light (40x)

B. **Confusion Range: Sample--Basal Beds (Delle Phosphatic Member).** Under cross polarization, the phosphatic material is predictably isotropic (black); a rare conodont is seen at the center along with scattered detrital silt (white). The magenta epoxy running subparallel to bedding filled in induced fractures--cracks related to outcrop-related desiccation and/or to stress release. Crossed-nicols (40x)

C. **Confusion Range: Sample--Basal Beds (Delle Phosphatic Member).** Detailed view of phosphatic cement (lighter brown hues) material in layered phosphate. The white material extending from upper left to lower right is diagenetic silica further cementing the rock. Most of the siliceous mixture is composed of silt and rounded siltstone grains, but some larger grains are detrital quartz (B-4). Plane polarized light (100x)

D. **Confusion Range: Sample--Basal Beds (Delle Phosphatic Member).** Cross polarized view reveals the isotropic outlines of the phosphatic material as well as siliceous material in the form of dispersed silt (small white dots), irregularly shaped quartz sand (with overgrowth), and arcuate quartz-lining cement (seen best at C-3 to D-4). Crossed-nicols (100x)

Plate II

A B C D E

A.

A B C D E

B.

1
2
3
4
5
6
7
8

A B C D E

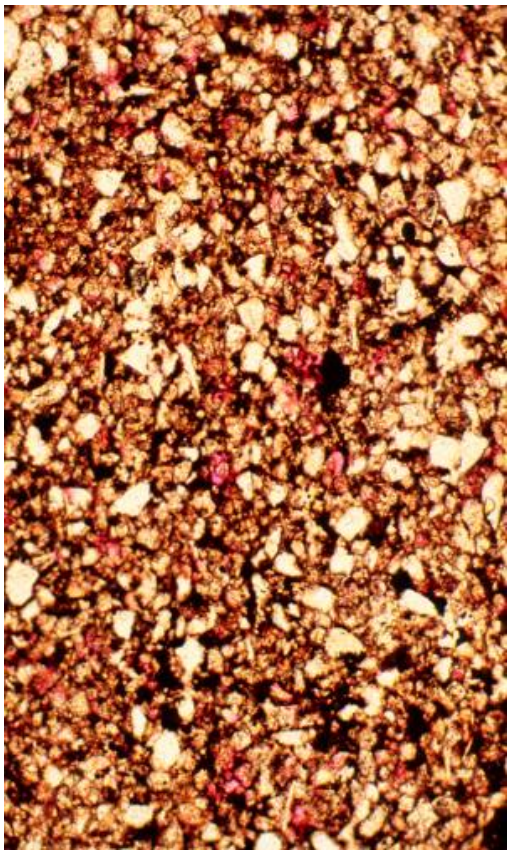

C.

A B C D E

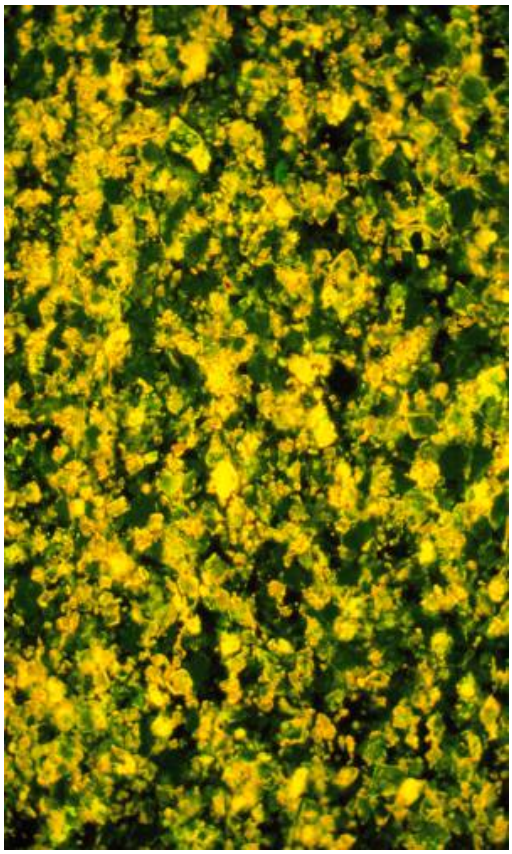

D.

Plate II Descriptions

A. Confusion Range: Sample--Mc 6-2 (Needle Siltstone Member). Although the lower portion of the formation is severely obscured by alluvium, a somewhat continuous dolomitic siltstone overlies the phosphatic materials. The quartz, feldspar, and muscovite materials are only moderately sorted in this view, and the bronze dolomite and illitic clay incorporate organic material and/or pyrite of some significant percentage--causing a decided darkish gray hue on a fresh surface. The irregular distribution of coarser clastics as seen in the upper right corner may be related to bioturbation. Clearer examples of trace fossil activity are seen best in weathered orange-gray field exposures. Plane polarized light (40x)

B. Confusion Range: Sample--Mc 6-2. (Needle Siltstone Member). Same view as view A under cross-polarized light shows mixed birefringence of quartz, feldspar in white to gray shades, and of dolomite and illite in typical bronze. The dark grays are reflective of pyrite and organics. In terms of recognizable biotics, arenaceous forams are the most common fossil type, seen in a later photomicrograph (plate III, view A). Crossed-nicols (40x)

C. Confusion Range: Sample--Mc 6-2 (Needle Siltstone Member). High magnification view of the dolomitic siltstone demonstrates the poor sorting of the white terrigenous material as well as its pronounced angularity. Most of the brownish material is authigenic dolomite. The black material is reflective of pyrite/organics, and the magenta hues indicate the presence of some porosity (approximating 3%). Plane polarized light (100x)

D. Confusion Range: Sample--Mc 6-2 (Needle Siltstone Member). Reflected light example of the previous view demonstrates opacity of grains in the green to black hues, mineral fluorescence from dolomite appears yellow, and void space is qualitatively revealed in subtle shades of orange. Reflected ultra-violet light with blue-violet filter (100x)

Plate III

A B C D E

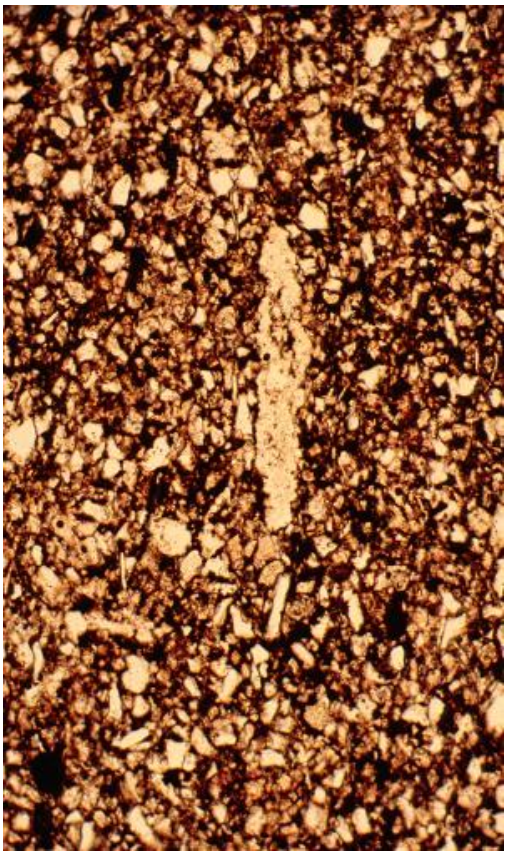

A.

A B C D E

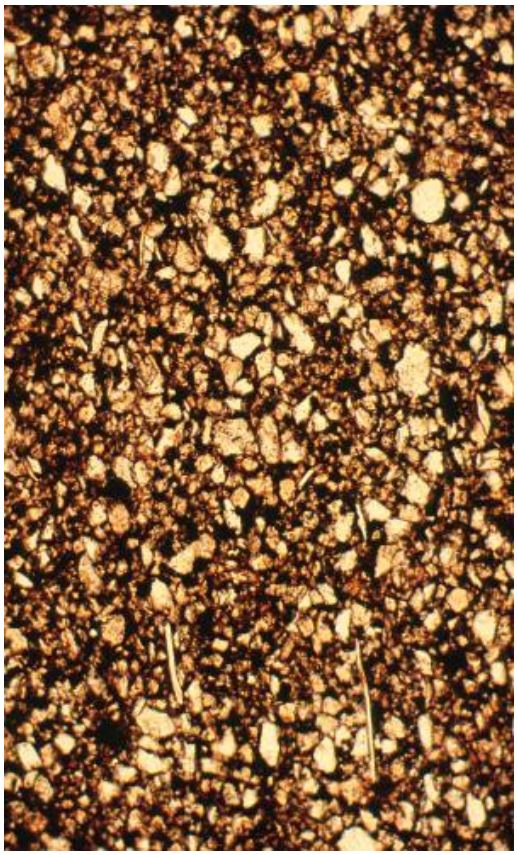

B.

1
2
3
4
5
6
7
8

A B C D E

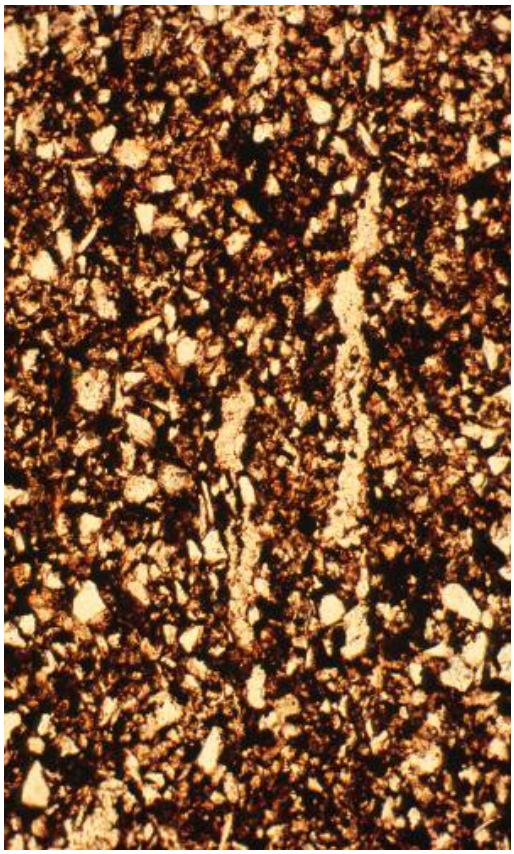

C.

A B C D E

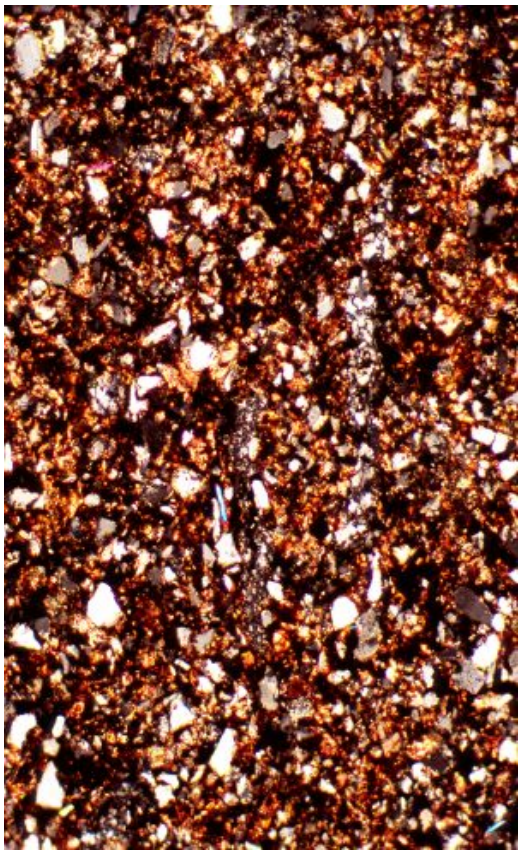

D.

Plate III Descriptions

A. Confusion Range: Sample--Mc 6-2 (Needle Siltstone Member). One additional view of this sample indicates the presence of compacted arenaceous or agglutinated Foraminifera, relatively common to this siltstone facies. Also quite striking in this example is the amount of dark material, much of which is organic carbon. Total organic carbon values in this interval range from 0.94 to 1.58 wt.%, and this somewhat porous siltstone facies should be considered part of the potential Chainman pay in any engineering or geochemical calculation. Plane polarized light (100x)

B. Confusion Range: Sample--Mc 6-6 (Needle Siltstone Member). This sample from the dolomitic siltstone interval occurs 10 meters above the previous example, and contains many of the same constituents and textural characteristics. In this view, very fine grained sand is more common as are numerous elongate muscovite flakes seen best along columns B and D, row 7. Dark organic hues continue to prevail, and subtle shades of the magenta epoxy (pores) can also be discerned. Very importantly, this particular sample contains a substantial percentage of mobile oil (7.72%), a high value especially derived from a surface sample. Plane polarized light (100x)

C. Confusion Range: Sample--Mc 6-9 (Needle Siltstone Member). Approximately 15 meters above sample Mc 6-6, this sample shows two crushed and compacted arenaceous forams. Although this silty interval is not really a mudrock, such clastically diluted muds(?) may be important from a potential hydrocarbon perspective because of the facies appreciable thickness (see appendix A, measured section, part 1). Plane polarized light (100x)

D. Confusion Range: Sample--Mc 6-9 (Needle Siltstone Member). Cross-polarized view of the view C accentuates the linear quartz birefringence particularly along column D, the bronze birefringence of the associated dolomite, and finally, the very small, highly birefringent muscovite flake at C-5. Crossed-nicols (100x)

Plate IV

A B C D E

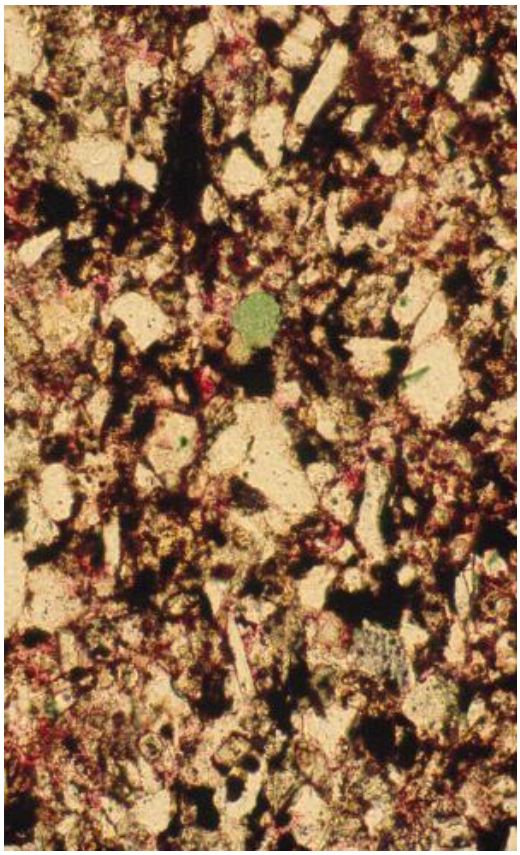

A.

A B C D E

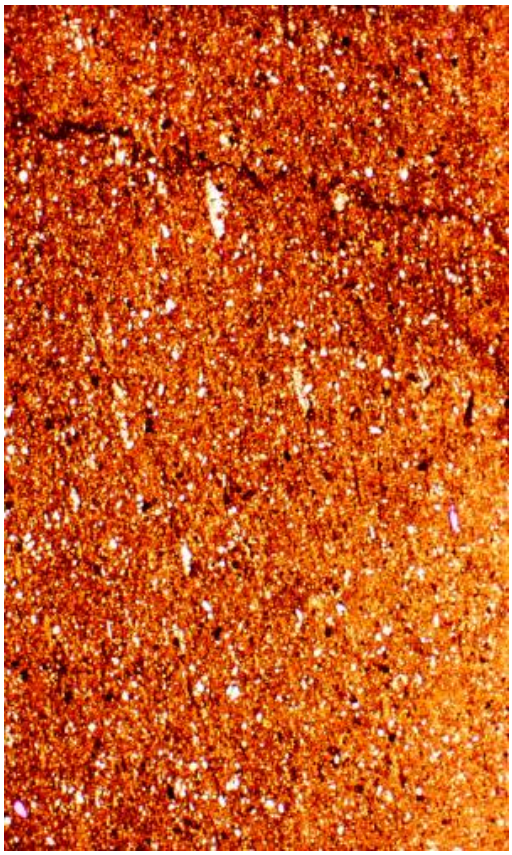

B.

A B C D E

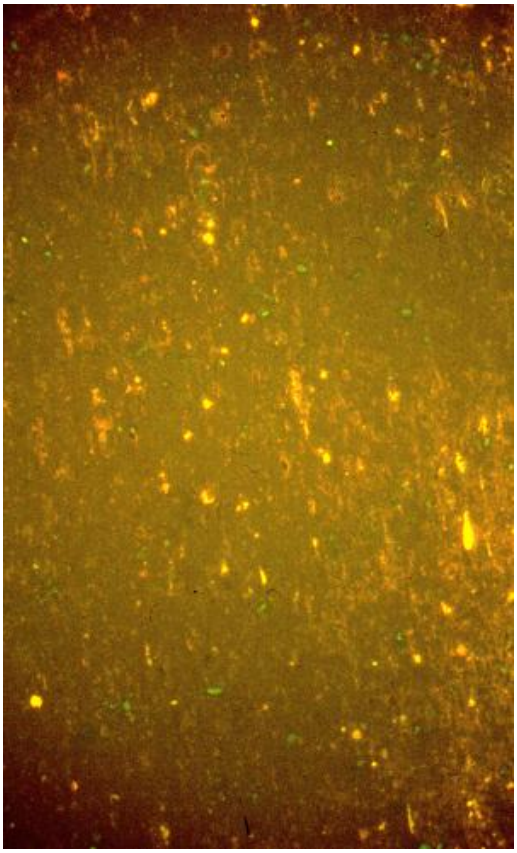

C.

A B C D E

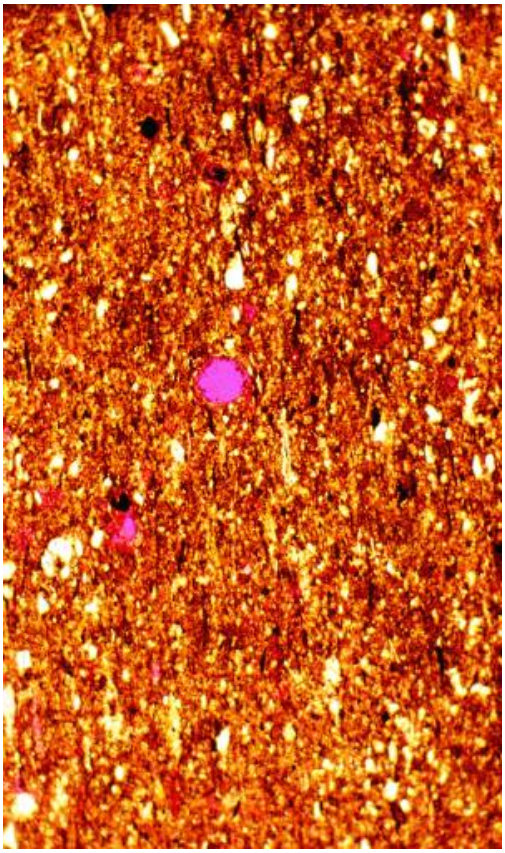

D.

1 2 3 4 5 6 7 8

Plate IV Descriptions

A. Confusion Range: Sample--Mc 6-9 (Needle Siltstone Member). Very high magnification of the dolomitic siltstone dramatically reveals the poor sorting, variable rounding, small amounts of pore space (magenta), and significant amounts of dark or dirty pyrite and organics. The green grain is glauconite, and its occurrence along with presence of arenaceous forams likely indicates deposition in a marine setting. Specifically, the textural details may point to a variable sedimentary source area shedding continuous clastic debris into an offshore basin--perhaps related to erosion of the Antler highlands located farther to the west and/or perhaps to the north. Plane polarized light (200x)

B. Confusion Range: Sample--Mc 6-16b (Camp Canyon Member). This sample is representative of a very thick (40 meters), dark gray, noncalcareous mudrock, rich in clay and modestly silty (see appendix A, measured section, part 1). White grains in this view represent the fairly common presence of arenaceous forams. Organic content is also significant, at least 1.63%, and the porosity is comparatively high for siltstones, due perhaps to the presence of leached fossils and to the probable weathered state of the sample. Plane polarized light (40x)

C. Confusion Range: Sample--Mc 6-16b (Camp Canyon Member). Porosity-only image of the previous image indicates two void types in this noncalcareous mudrock. The yellow color is indicative of leached microfossils (see subsequent image and additional example of plate V, view A), and the orange hues represent smaller and tighter micropores from the dominant clay matrix. Green, again, is opaque material. Reflected ultra-violet light with blue-violet filter (40x)

D. Confusion Range: Sample--Mc 6-16b (Camp Canyon Member). A leached radiolarian (circular magenta feature) is recognized at C-4 as well as another possible example at B-5, 6. Dark material of pyrite and organics is also readily recognizable. The white grains are mainly dispersed silt in addition to the elongate and compacted arenaceous foram at C, D-5. Plane polarized light (100x)

Plate V

A B C D E

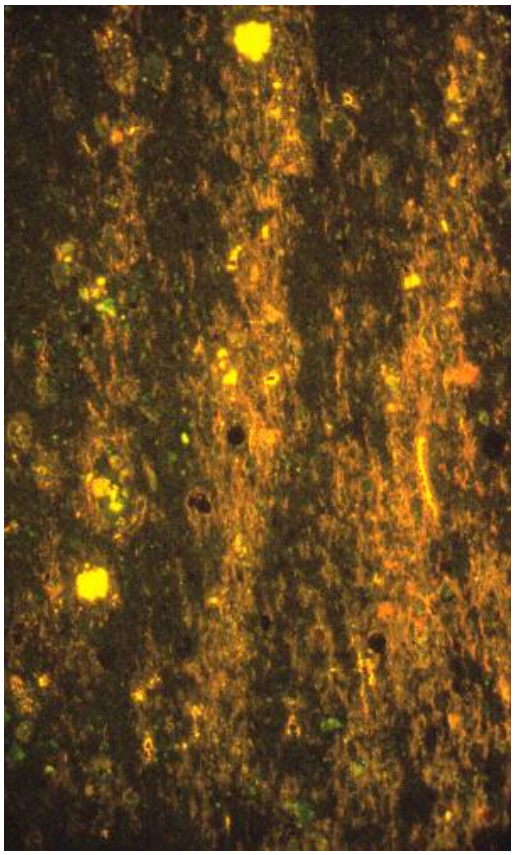

A.

A B C D E

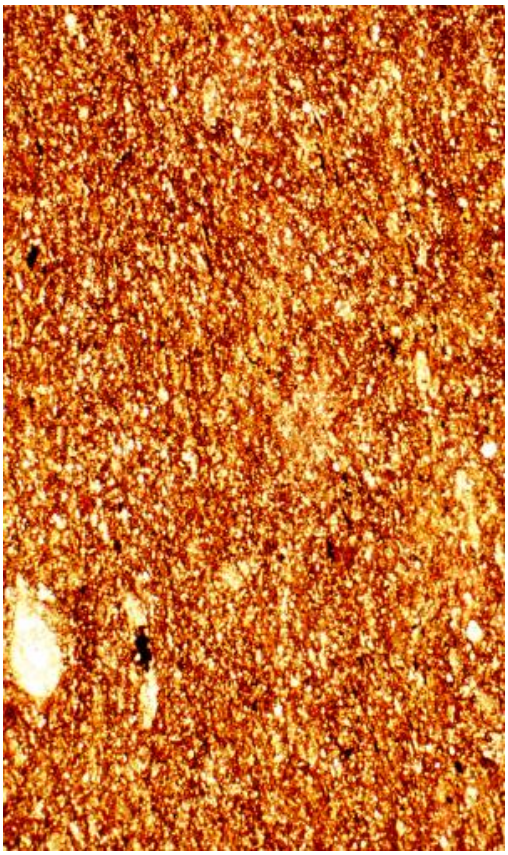

B.

1
2
3
4
5
6
7
8

A B C D E

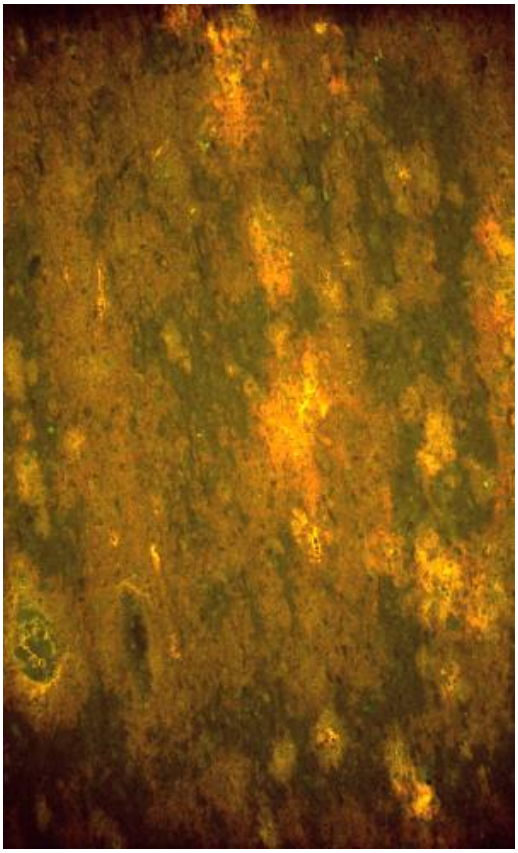

C.

A B C D E

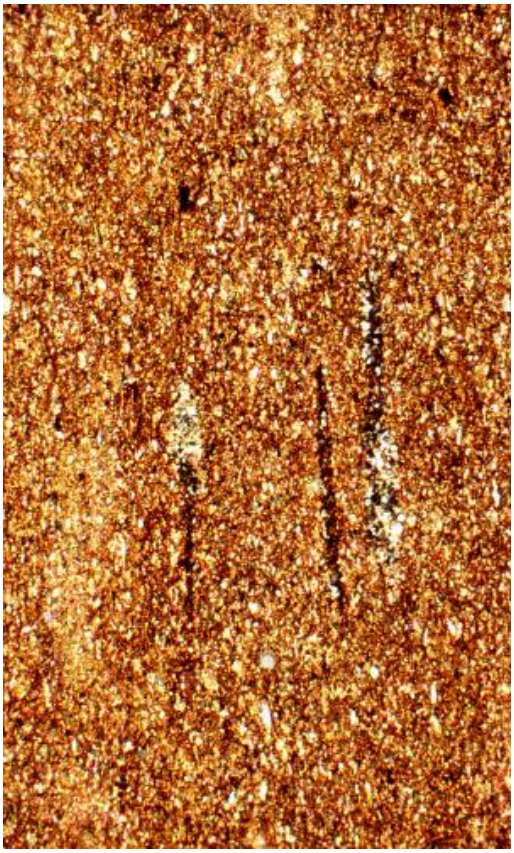

D.

Plate V Descriptions

A. Confusion Range: Sample--Mc 6-16b (Camp Canyon Member). Reflected light view of the noncalcareous mudstone facies demonstrates in detail the leached grains (yellow) and the bedding-parallel streaks or microporosity (orange). The dark green to black shades, are opaque to near-opaque (nonporous) materials. Admittedly, one cannot be sure that all such revealed void space will be present in unweathered samples from the deep subsurface. Reflected ultra-violet light with blue-violet filter (100x)

B. Confusion Range: Sample--Mc 7-42 (Camp Canyon Member). A decidedly calcareous mudrock sequence occurs higher in the section, particularly above the top of a conspicuous limestone at 169 meters, and intimately associated with limestone interbeds thereafter. The red hues represent stained calcite, mostly as cement matrix, and in some cases, as fossil remains. Most fossils occur as fragments: ostracods, brachiopods, and some of unidentifiable origin. Other biotics that are more unaffected by breakage are numerous sponge spicules (E-4) and the omnipresent arenaceous forams (B-7). Other constituents in this thick facies include dispersed silt, pyrite, clay, and some organics perhaps belonging to the carbonaceous category. In some cases, the fabric appears somewhat disrupted, likely resulting from mostly horizontal trace fossil activity. Plane polarized light (40x)

C. Confusion Range: Sample--Mc 7-42 (Camp Canyon Member). Epifluorescent view of view B reveals variably dense "clouds" of microporosity—some areas apparently tighter than adjacent regions. Some microporous regions are more isolated than others (see right hand and bottom margins). In spite of any quantitatively measured pore space, one might suspect that the permeabilities might be very low in terms of comparative mudrock standards. Reflected ultra-violet light with blue-violet filter (40x)

D. Confusion Range: Sample--Mc 7-42 (Camp Canyon Member). An unstained view taken with cross-polarized light indicates the presence of horizontal trace fossil activity. The resulting birefringence streaks occur because of preferential quartz accumulation (D-5) augmented by organic matter concentration. Dispersed quartz and feldspar silt is also readily apparent here. The unit, however, is mostly calcareous. Crossed-nicols (40x)

Plate VI

A B C D E

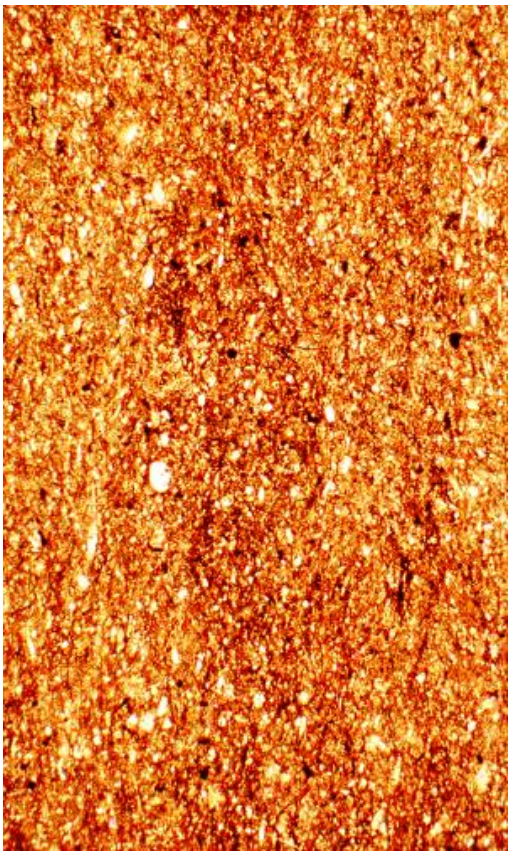

A.

A B C D E

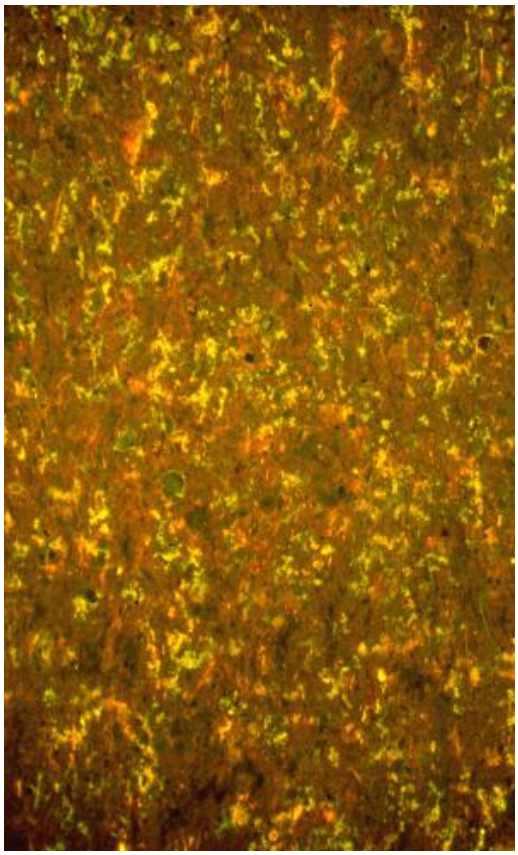

B.

1
2
3
4
5
6
7
8

A B C D E

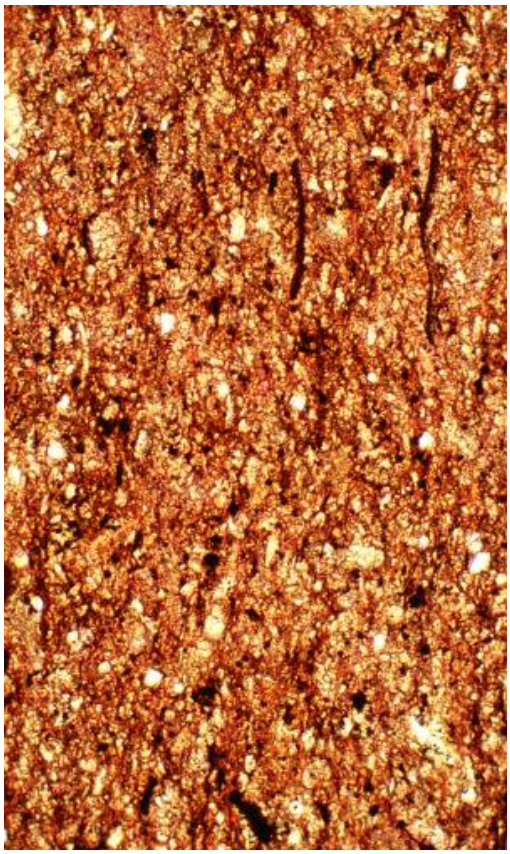

C.

A B C D E

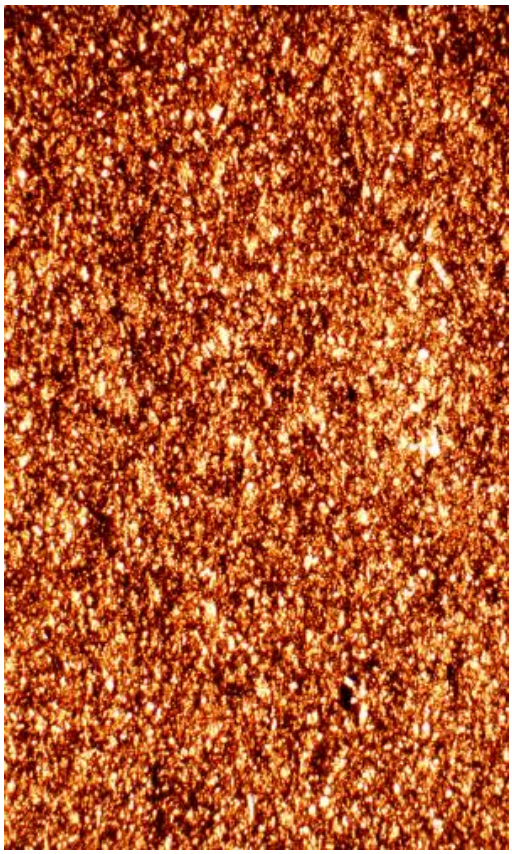

D.

Plate VI Descriptions

A. Confusion Range: Sample--Mc 8-49 (Camp Canyon Member). Apart from some intervening limestones, this calcareous mudstone sample lies approximately 40 meters above the previous sample. Yet, the basic lithology is very similar in terms of a somewhat disrupted (bioturbated) fabric, and calcareous grains and cement associated with dispersed silt and illitic mud. Again, the reddish stain allows identification of the calcitic component, and siliceous sponge spicules are clearly recognized at E-2. Some pyrite and organic matter (dark grains) are also discernible. The fossil fragments are more diverse in this sample: biota now include additional examples of echinoids, endothyroid forams, pelmatozoans, and spherical bodies that likely represent radiolarians in various states of diagenetic alteration (quartzose, calcitic, dolomitic). Plane polarized light (40x)

B. Confusion Range: Sample--Mc 8-49 (Camp Canyon Member). The reflected light view of view A reveals two classes of pore types: (1) the yellow areas are regions commonly leached to varying degrees, and (2) the orange shades are regions of microporosity. Upon close inspection, a gradation exists between the leached and microporous regions, recognizable by the transitions in color in some cases. Porosity is high (11.71%); some pores may be vadose weathering effects. In any case, the connectivity of the pores is poor as indicated by the 50 nD measured permeability. Reflected ultra-violet light with blue-violet filter (40x)

C. Confusion Range: Sample--Mc 8-49 (Camp Canyon Member). Higher magnification of previous sample reveals admixture of calcareous material, detrital silt, illitic clay, pyrite, and organic material. In some samples, the organic material appears as carbonaceous flakes as seen especially along row 2. The Chainman Shale likely contains a mixture of oil-prone (algal) and gas-prone (woody or carbonaceous) kerogens. In Nevada, the Chainman does contain local accumulations of coal flora—ferns, horsetails, and club mosses. Plane polarized light (100x)

D. Confusion Range: Sample--Mc 9-86 (Camp Canyon Member). This specimen represents a "grab" sample taken at approximately 185 meters from the base of the formation. This calcareous mudstone is consistent with other examples of the sandy limestone facies. In spite of the abundance of silica and other insoluble framework grains, a TOC of 1.26% was obtained here. The Tmax clearly indicates a source bed in the oil-generating window. Most TOC numbers are quite modest in this surface study, but given the thickness of this shale section in western Utah, these modest TOC values are quite important. Plane polarized light (40x)

Plate VII

A B C D E

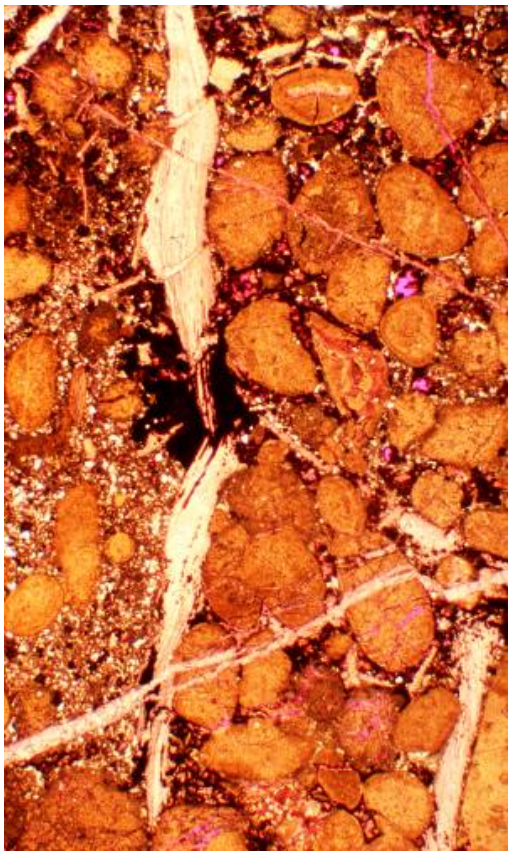

A.

A B C D E

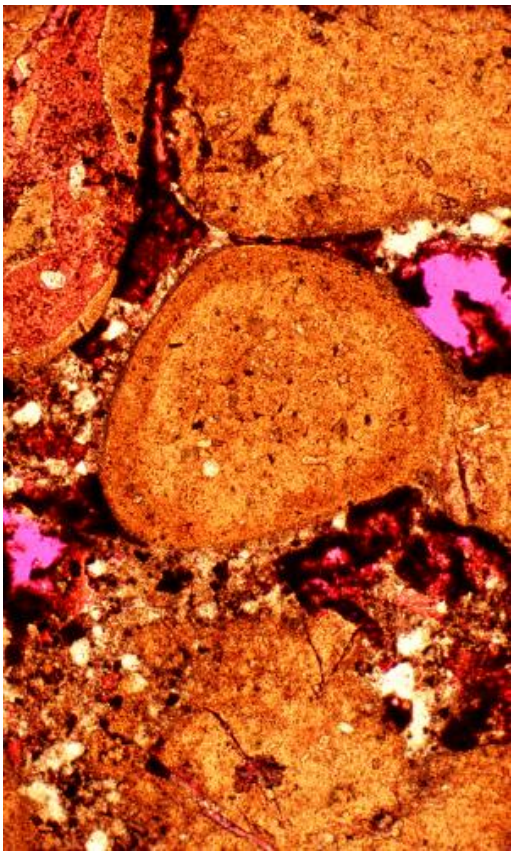

B.

1
2
3
4
5
6
7
8

A B C D E

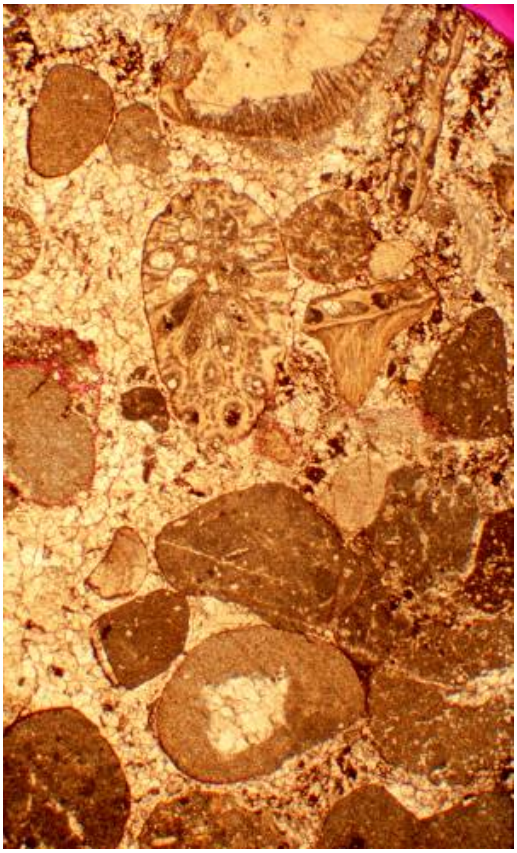

C.

A B C D E

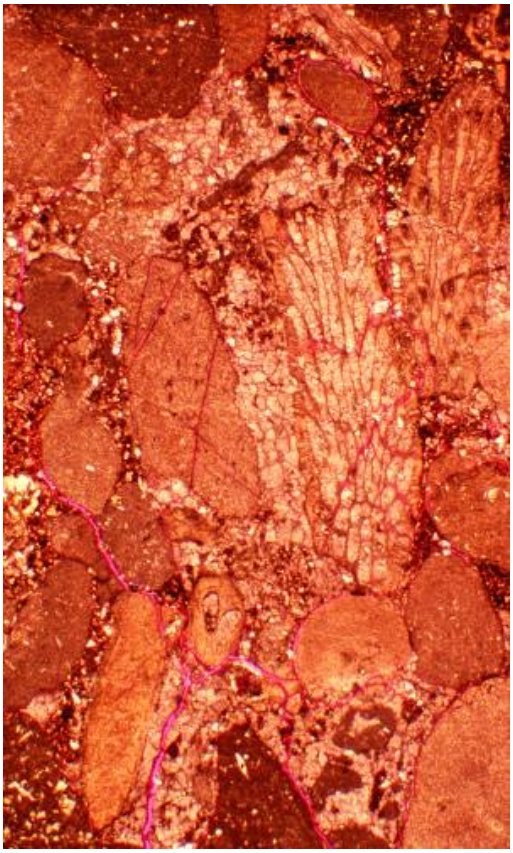

D.

Plate VII Descriptions

A. Confusion Range: Sample--458-459 m (Jensen Member). Sitting directly on top of the thick limestone (topographically resistant) at 458 meters, this layered phosphate marks the base of another transgressive systems tract, which may rest on a modestly karstic surface. In addition to the phosphatic lumps and large clasts, ooids, and cement, dispersed silt/sand is plentiful as well as clearly eroded very fine grained sandstone clasts (A-7, 8). Calcareous material abounds in the form of brachiopod fragments (large elongate grain along column B), calcite cement, and calcite-filled fractures (near base of photomicrograph). Most of the dark material is pyritic although a small amount of organic material additionally occurs. Plane polarized light (20x)

B. Confusion Range: Sample--458-459 m (Jensen Member). Close up of the phosphatic unit reveals not only the presence of dispersed silt, clay, organic matter, and pyrite in the matrix entombing the phosphate itself, but also the presence of some secondary intergranular pores (magenta). Whether these pores are present at depth is pure conjecture at this time. Plane polarized light (100x)

C. Confusion Range: Sample--459-460 m (Jensen Member). The underlying layered phosphate passes upsection into a pebble conglomerate of a limestone composition. Rounded micritic limestone clasts and reworked bryozoans largely comprise make up this conglomeratic grainstone seen under very low magnification. Clearly, some erosive event was present at this moment of Chainman time—perhaps the erosion and reworking of the underlying, thick carbonate sequence undoubtedly found in the stratigraphic "neighborhood." Plane polarized light (20x)

D. Confusion Range: Sample--459-460 m (Jensen Member). This stained version of the pebble conglomerate confirms the overwhelming calcite content (red) along with the basic allochemical ingredients. As is common with most Chainman rocks, dispersed silt is recognized as the white (unstained) material. Above this depth (460 meters), the Chainman does take on a silty/sandy composition in many of the orange-brown weathering strata occurring upwards to the base of the Ely Limestone. Plane polarized light (20x)

SEM PLATE 1
Mc-6-6

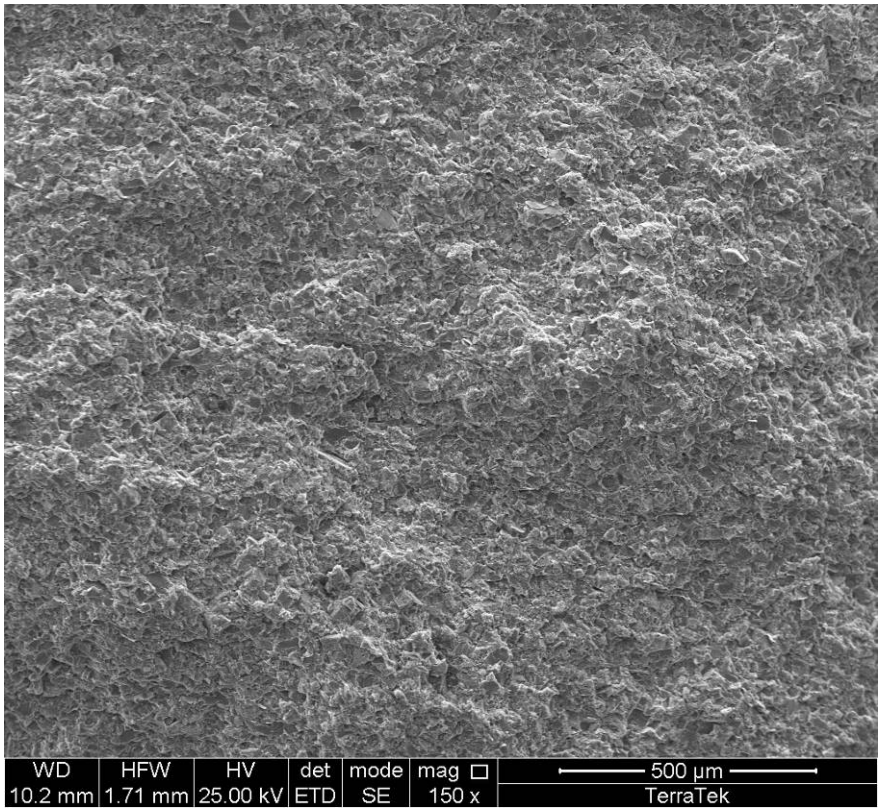

Textural overview of dolomitic siltstone showing the homogeneous character of the mudstone. (Scale bar = 500 microns)

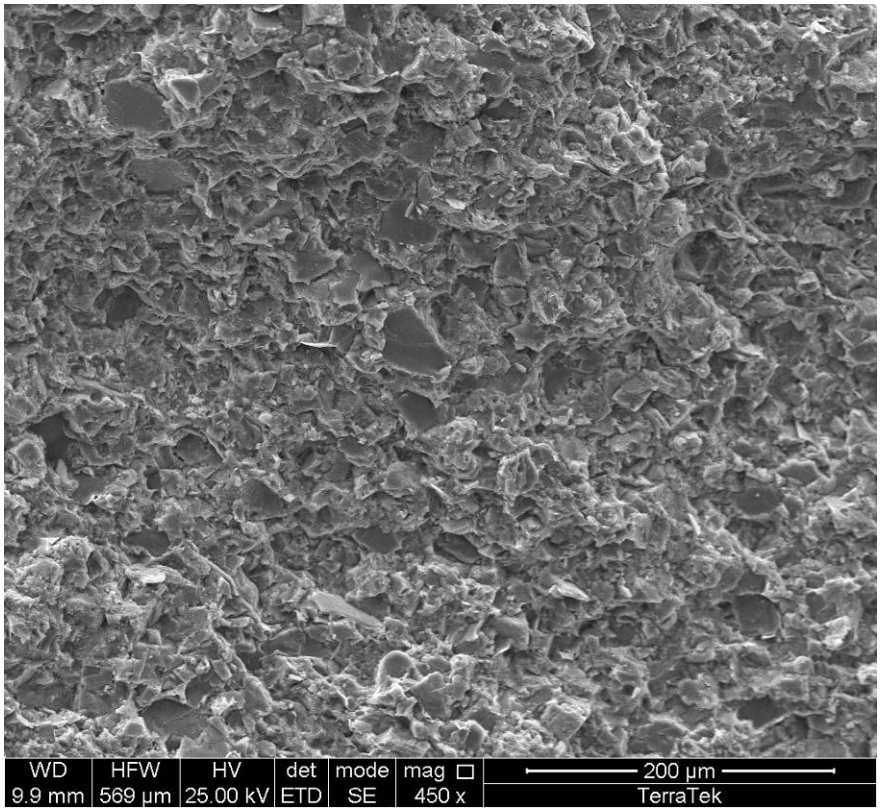

Silt-sized 'grains' are almost entirely composed of dolomite. (Scale bar = 200 microns)

Schlumberger Confidential

TerraTek
A Schlumberger company

1935 S. Fremont Drive • Salt Lake City, Utah 84104
Telephone (801) 584-2400
FAX (801) 584-2406

SEM PLATE 2
Mc-6-6

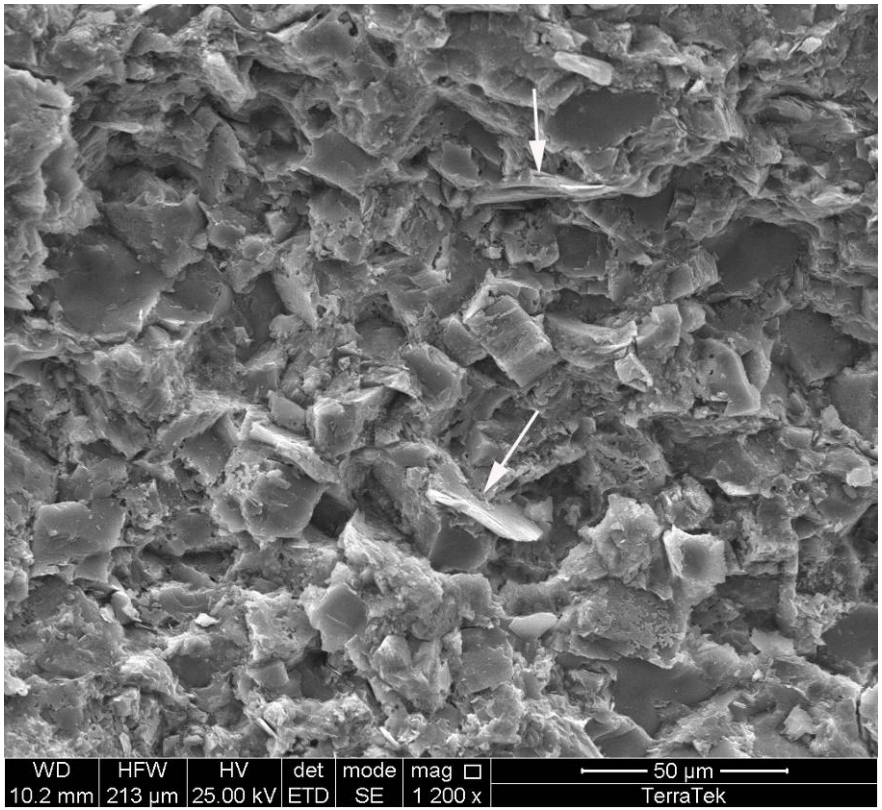

Although there is some matrix material, the mudstone is dominated by sugary microcrystalline dolomite. A few detrital mica plates (arrows) are present in the mudstone. (Scale bar = 50 microns)

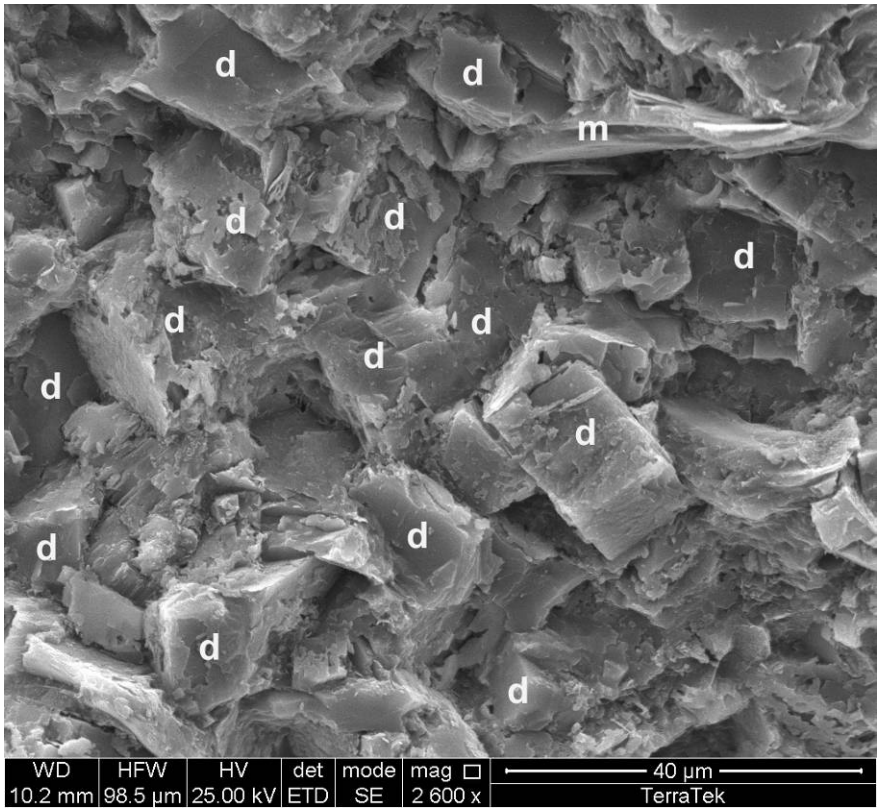

The dolomite is composed of equant dolomite crystals (d), about 20 microns in size. Here, the crystals occur in an interlocking mosaic without much intercrystalline material and very limited porosity. Mica plates (m) are the only detrital material in this view. (Scale bar = 40 microns)

Schlumberger Confidential

TerraTek
A Schlumberger company

1935 S. Fremont Drive • Salt Lake City, Utah 84104
Telephone (801) 584-2400
FAX (801) 584-2406

SEM PLATE 3
Mc-6-6

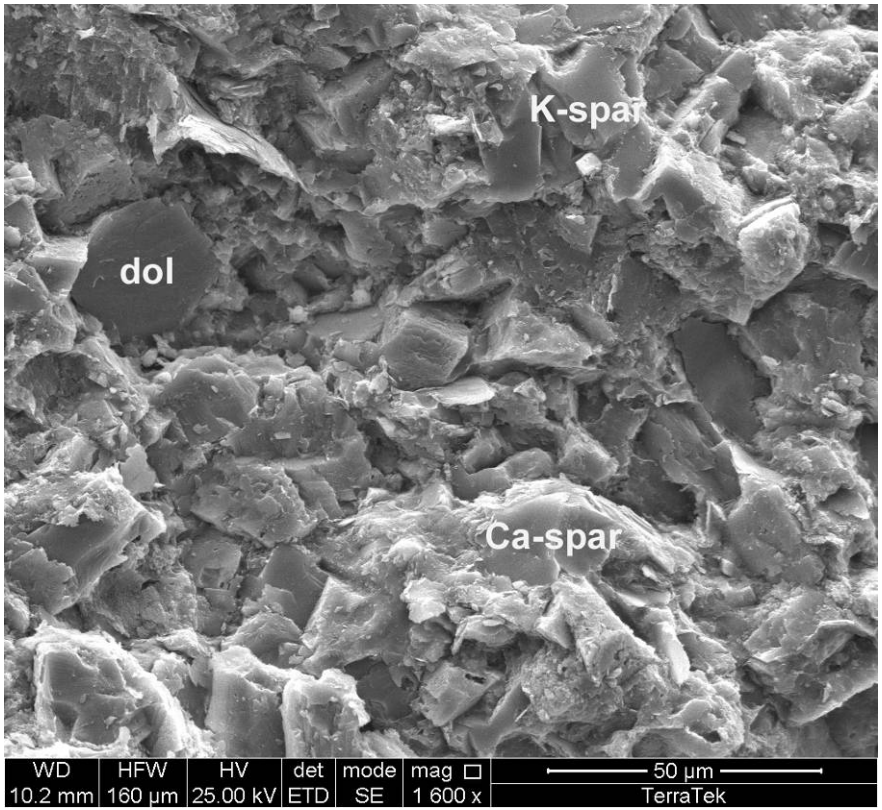

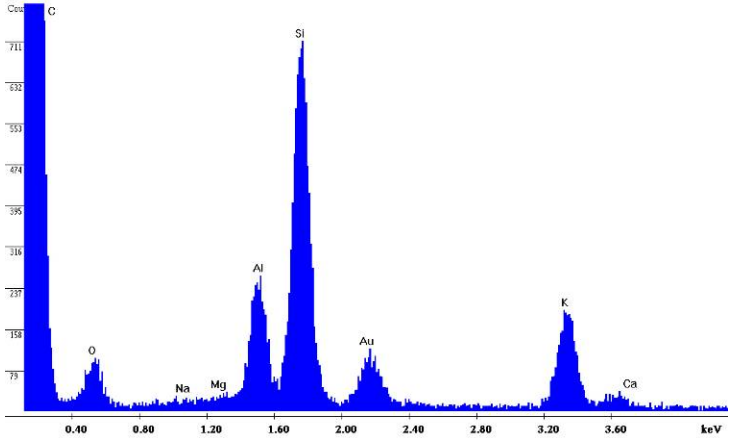

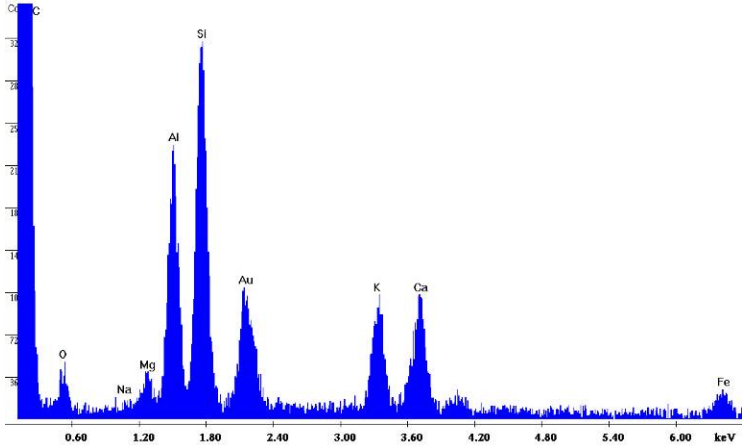

Rare detrital feldspar grains are composed of potassium feldspar (K-spar, upper spectra), and more calcic feldspar, possibly with some iron (Ca-spar, lower spectra). Note authigenic rhombohedral crystal (dol) in upper left. The gold peak represents the conductive coating applied to the sample. (Scale bar = 50 microns)

Schlumberger Confidential

TerraTek
A Schlumberger company

1935 S. Fremont Drive • Salt Lake City, Utah 84104
Telephone (801) 584-2400
FAX (801) 584-2406

SEM PLATE 4
Mc-6-6

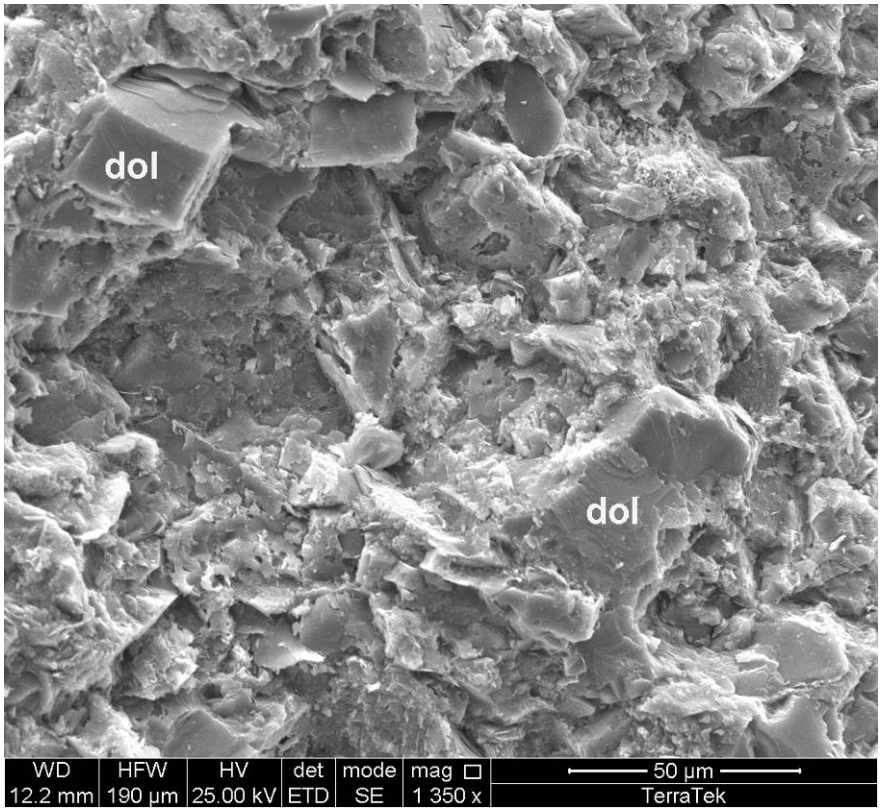

Although most of the dolomite occurs in authigenic rhombohedral crystals (dol, upper left), more irregularly shaped particles (lower right) may represent replaced calcic fossil fragments. (Scale bar = 50 microns)

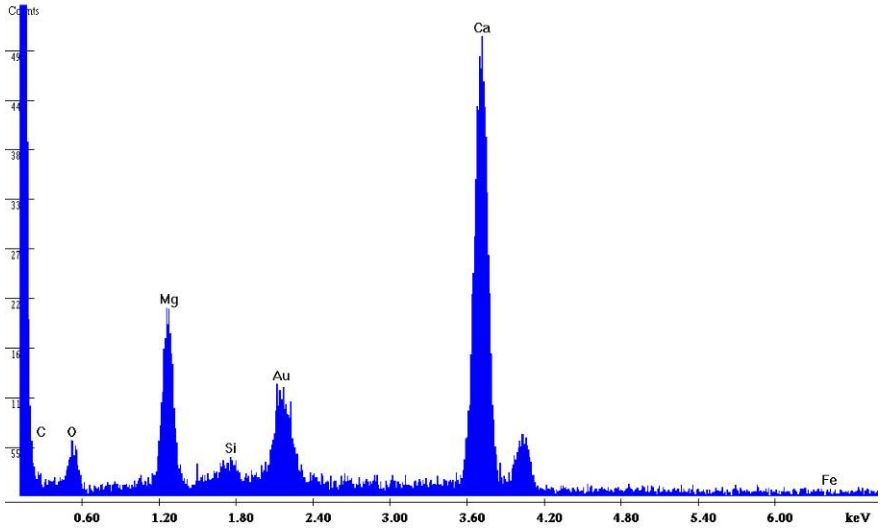

Elemental analysis of the dolomite crystals consistently indicates a pure calcium-magnesium composition, without any iron.

Schlumberger Confidential

TerraTek
A Schlumberger company

1935 S. Fremont Drive • Salt Lake City, Utah 84104
Telephone (801) 584-2400
FAX (801) 584-2406

SEM PLATE 5
Mc-6-6

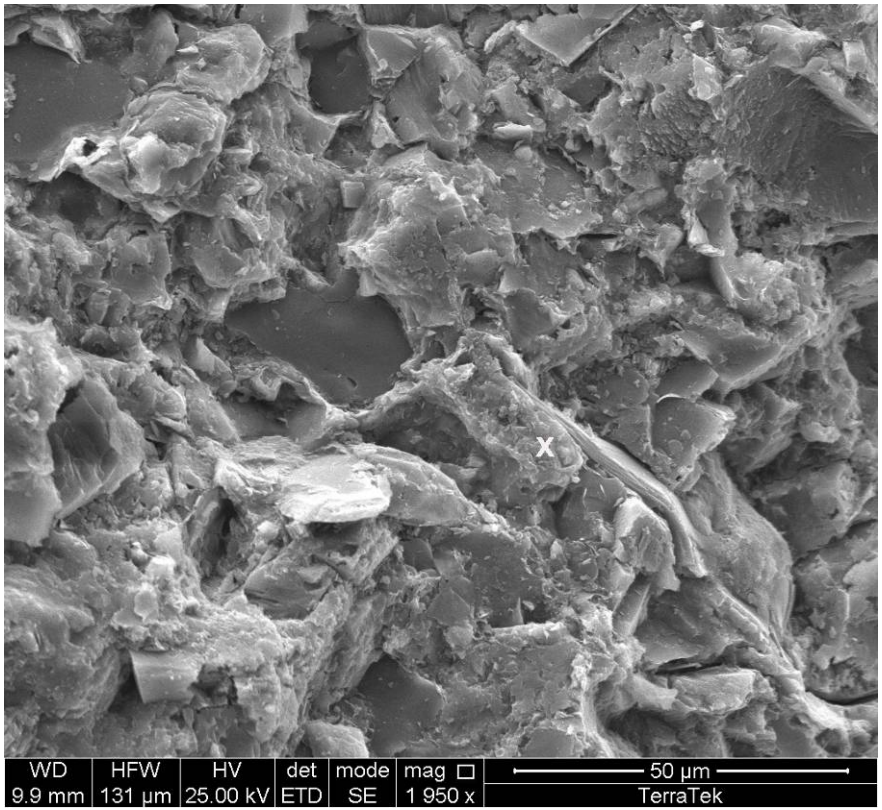

Here, there is dense cement (x) between the dolomite crystals. The intercrystalline material is composed of chert that further cements the dolomite, occluding pores. (Scale bar = 50 microns)

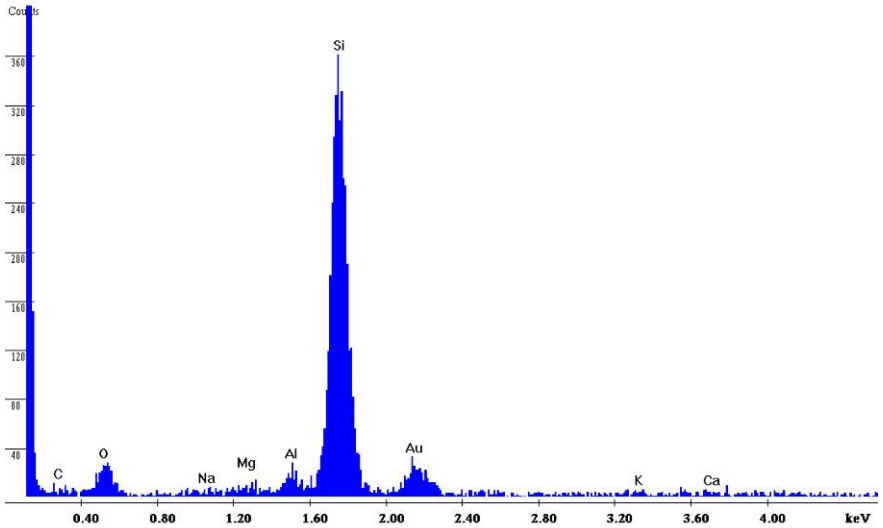

Spot elemental analysis (x) of the intercrystalline cement indicates a pure siliceous composition for the chert.

Schlumberger Confidential

TerraTek
A Schlumberger company

1935 S. Fremont Drive • Salt Lake City, Utah 84104
Telephone (801) 584-2400
FAX (801) 584-2406

SEM PLATE 6
Mc-6-6

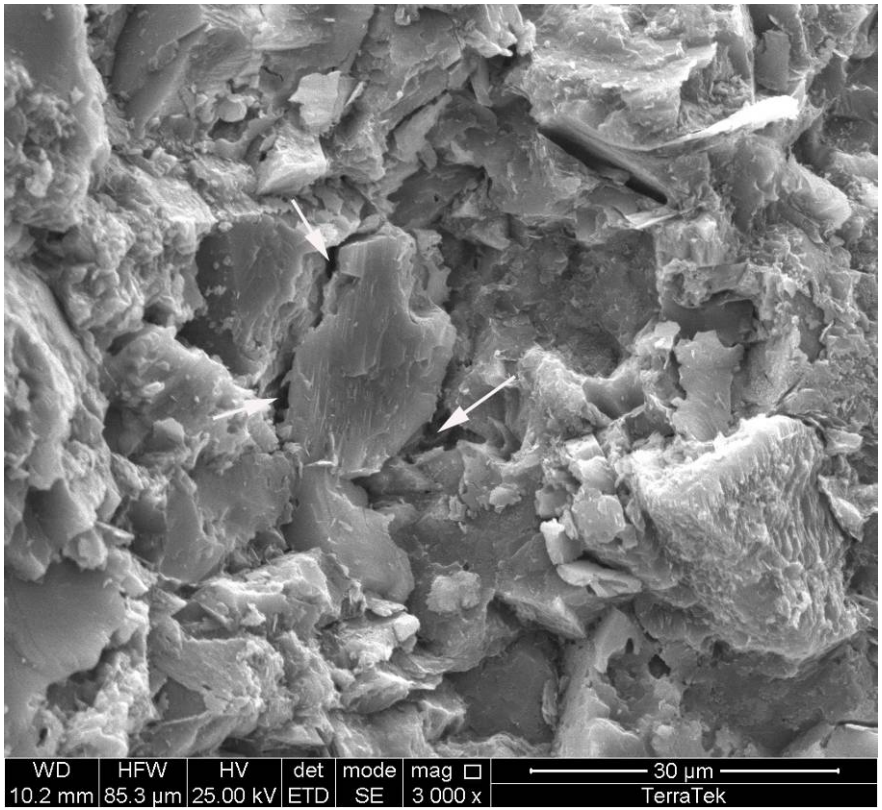

The crystalline dolomite is mostly densely interlocking, but a minor amount of intercrystalline microporosity is found in some areas (arrows). These pores are likely poorly connected, and overall permeability in the mudstone is also likely to be very limited. (Scale bar = 30 microns)

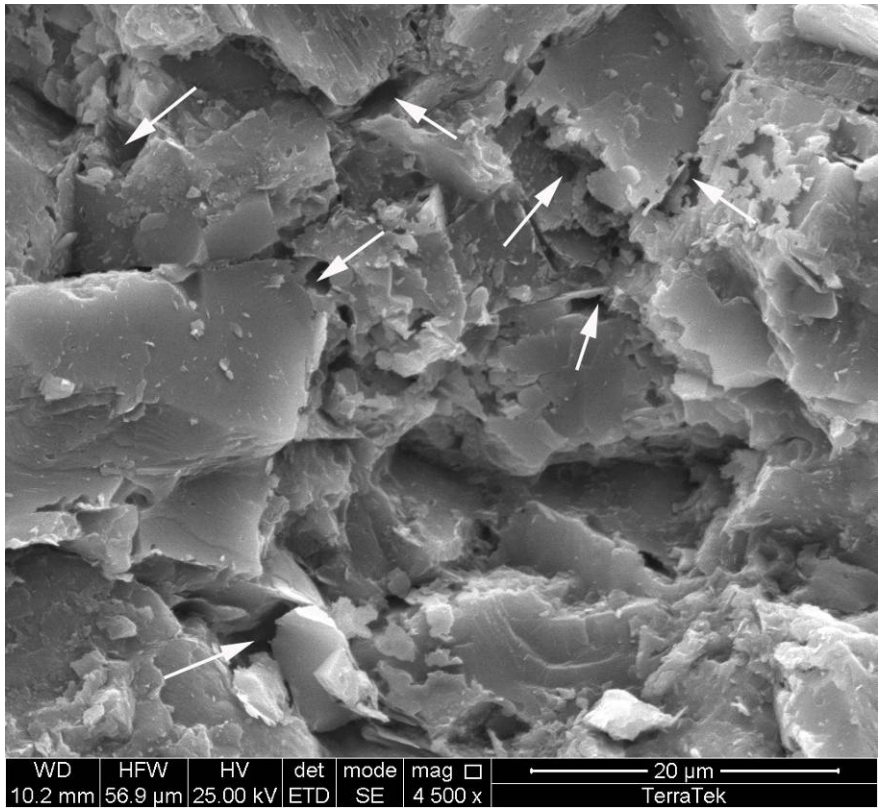

These dolomite crystals appear slightly corroded, and have associated dissolution micropores (arrows). In these outcrop samples, the dissolution may be related to surficial weathering of the sample. (Scale bar = 20 microns)

Schlumberger Confidential

TerraTek
A Schlumberger company

1935 S. Fremont Drive • Salt Lake City, Utah 84104
Telephone (801) 584-2400
FAX (801) 584-2406

SEM PLATE 7
Mc-6-16b

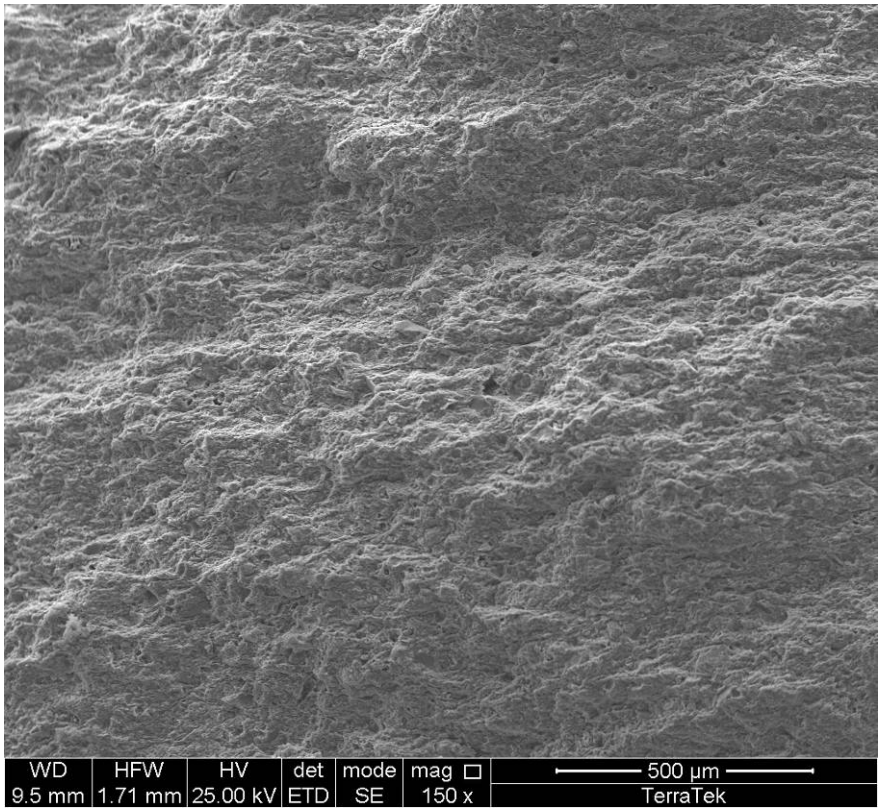

Argillaceous mudstone with vague laminations and subparallel thin veins. (Scale bar = 500 microns)

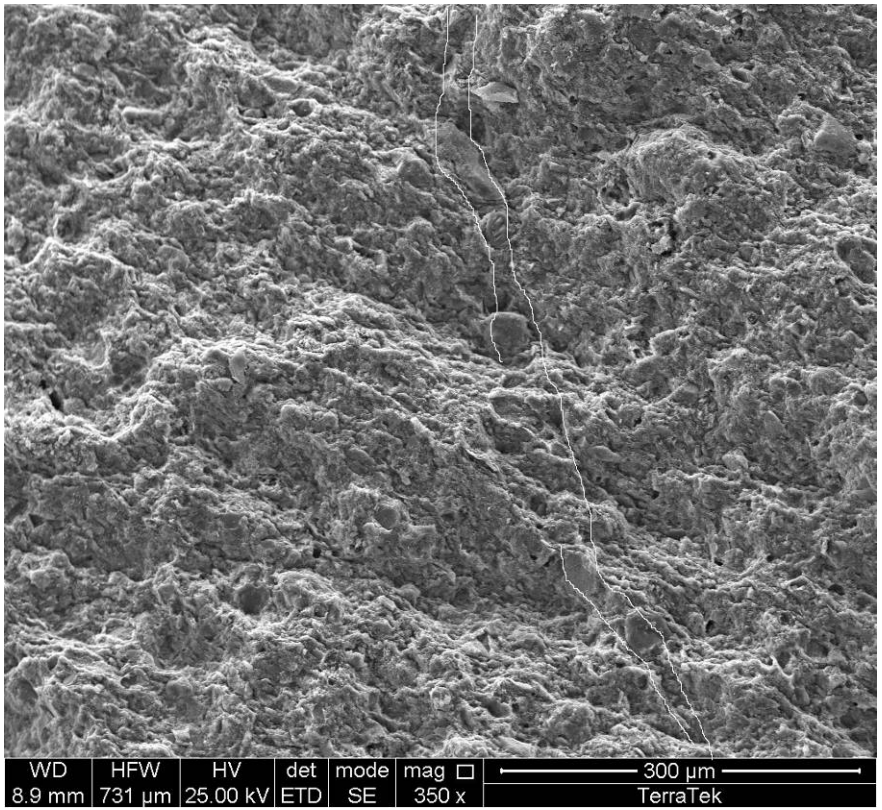

Closer view of one of the high-angle veins (outlined) that cuts across the lamination. (Scale bar = 300 microns)

Schlumberger Confidential

TerraTek
A Schlumberger company

1935 S. Fremont Drive • Salt Lake City, Utah 84104
Telephone (801) 584-2400
FAX (801) 584-2406

SEM PLATE 8
Mc-6-16b

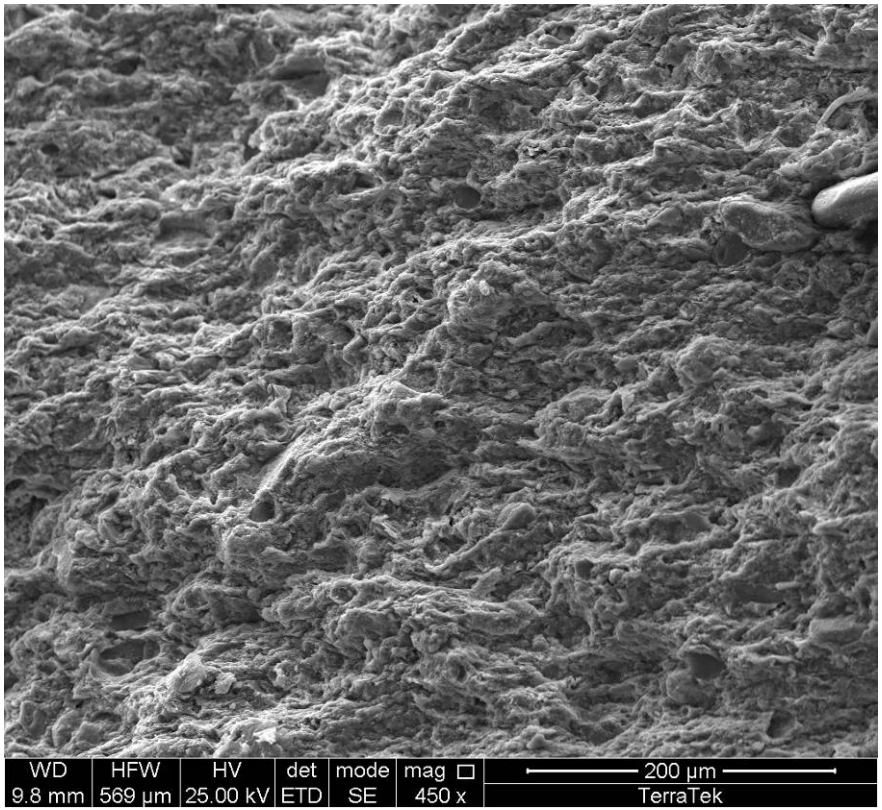

Clay-rich mudstone with very few detrital silt or fossil grains. The mudstone appears tightly compacted with minimal porosity. (Scale bar = 200 microns)

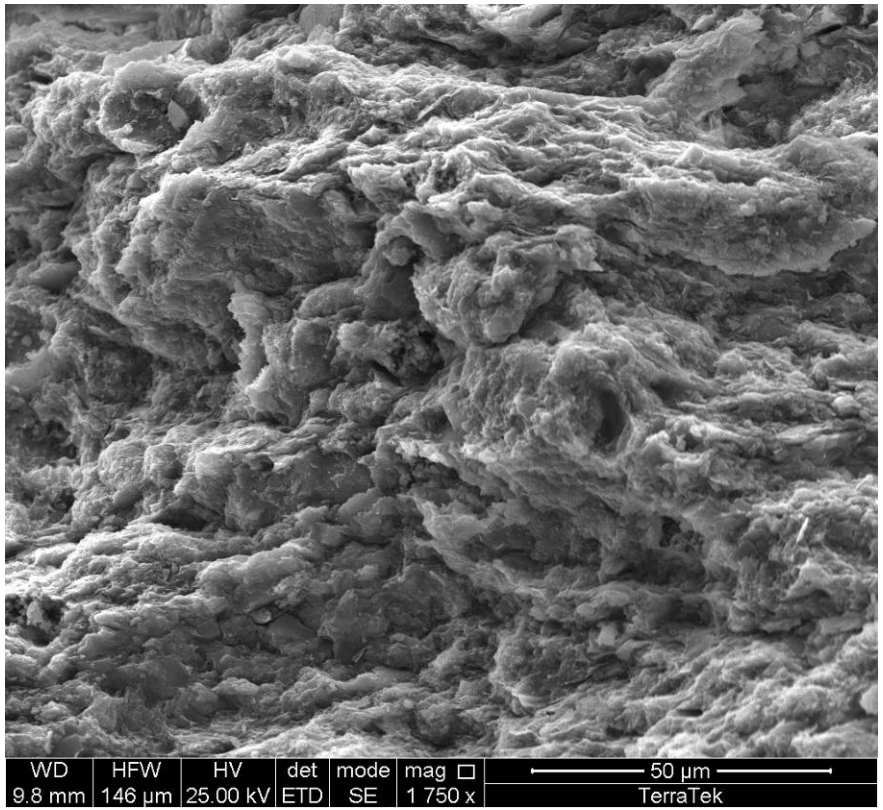

Closer view of gooey-looking clay in the matrix. Individual crystallites cannot be recognized and there is no visible intercrystalline microporosity. (Scale bar = 50 microns)

Schlumberger Confidential

TerraTek
A Schlumberger company

1935 S. Fremont Drive • Salt Lake City, Utah 84104
Telephone (801) 584-2400
FAX (801) 584-2406

SEM PLATE 9
Mc-6-16b

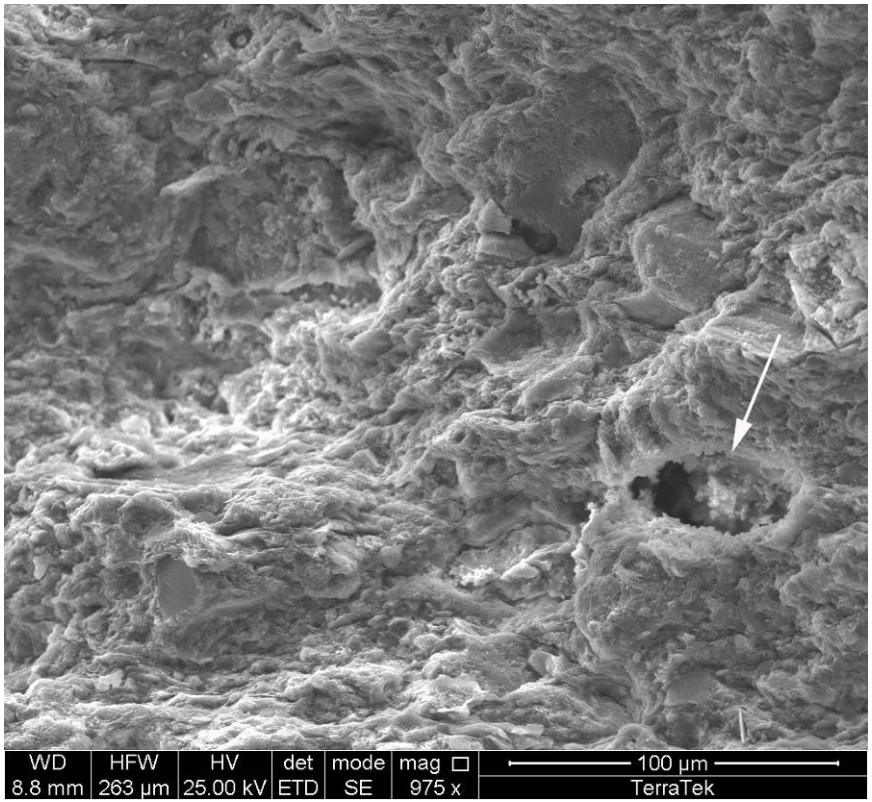

The only obvious porosity in the tight matrix consists of ovoid vuggy pores (arrow), where entire particles have been dissolved or removed. The original particles may have been organic macerals where the original organic material has been converted to oil and gas. (Scale bar = 100 microns)

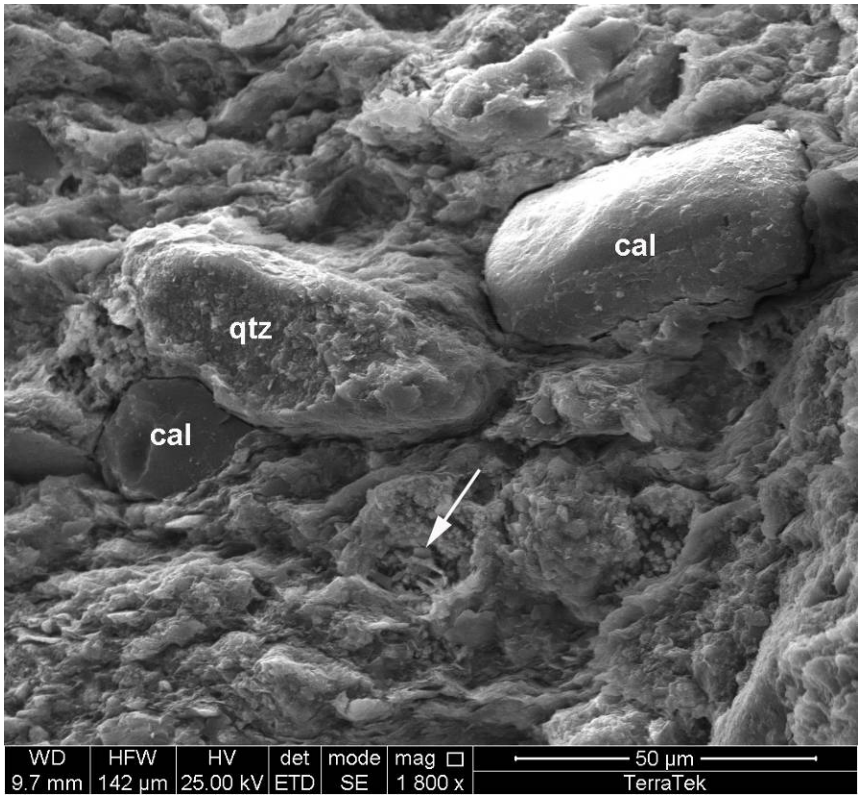

Rare silt-sized detrital grains consist of subrounded calcic fossil fragments (cal) and a few quartz-rich or silicified grains (qtz). Vuggy pores are partially filled with fine iron oxides (arrow). (Scale bar = 50 microns)

Schlumberger Confidential

TerraTek
A Schlumberger company

1935 S. Fremont Drive • Salt Lake City, Utah 84104
Telephone (801) 584-2400
FAX (801) 584-2406

SEM PLATE 10
Mc-6-16b

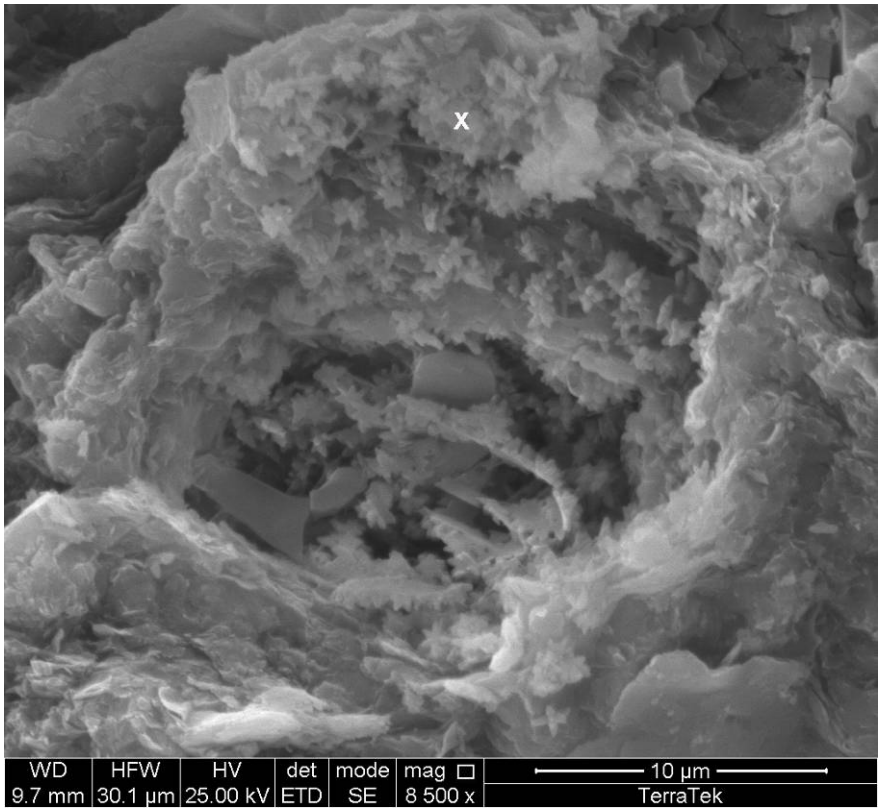

High magnification view of vuggy pore in previous image. Star-shaped crystal aggregates lining the pore are composed of iron oxide, and may represent oxidized pyrite in the outcrop sample. The pyrite would have replaced original organic material in the organic particles/macerals. (Scale bar = 10 microns)

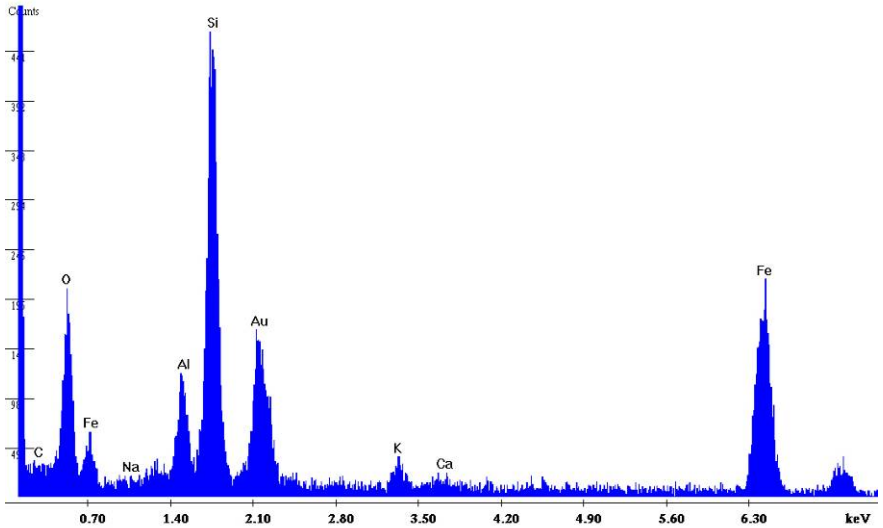

Spot elemental analysis (x) of the fine star-shaped aggregates indicates the presence of illite clay (Si, O, Al, and K), and iron oxide (Fe, O). Based on the radiating crystal morphologies, the iron oxide is probably hematite or goethite.

Schlumberger Confidential

TerraTek
A Schlumberger company

1935 S. Fremont Drive • Salt Lake City, Utah 84104
Telephone (801) 584-2400
FAX (801) 584-2406

SEM PLATE 11
Mc-6-16b

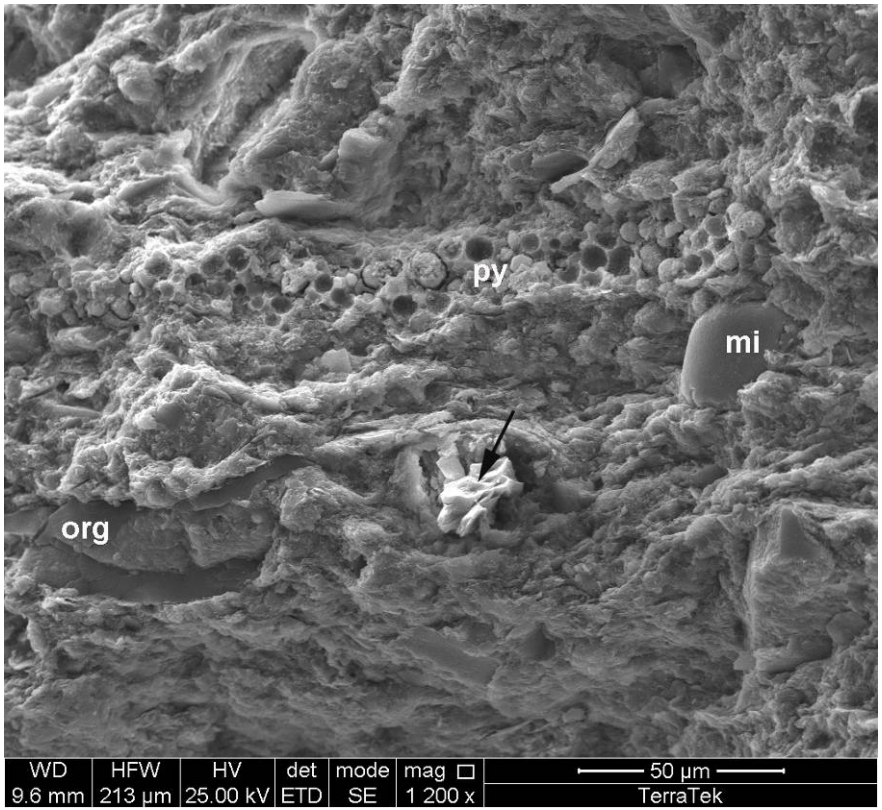

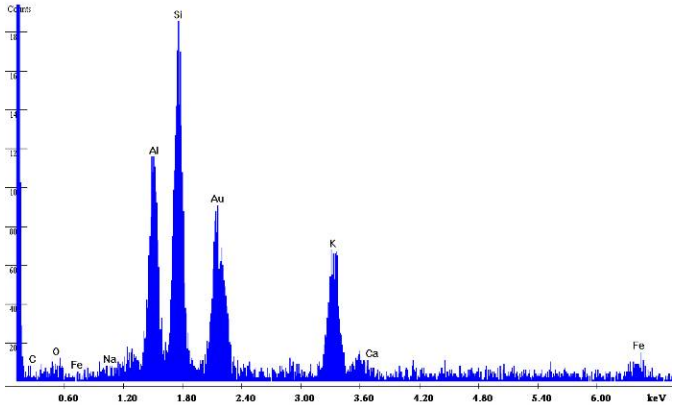

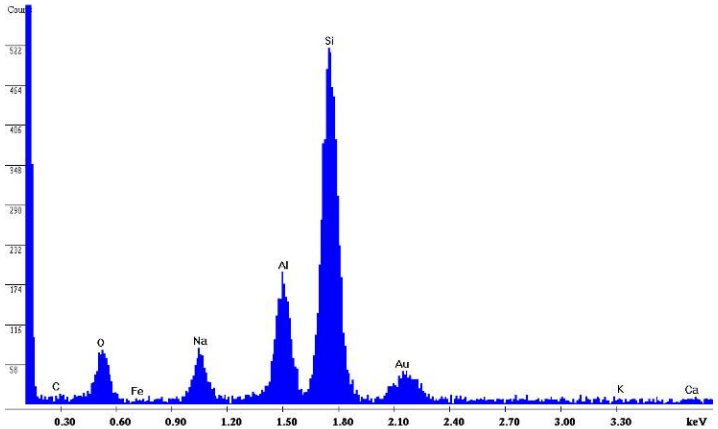

A variety of particles in this view include a long clast replaced by silica and framboidal pyrite (py), an organic maceral aligned with the bedding (org), a bent mica flake (mi, upper elemental spectra), and a fossil grain infilled with authigenic albite (arrow, lower spectra). (Scale bar = 50 microns)

Schlumberger Confidential

TerraTek
A Schlumberger company

1935 S. Fremont Drive • Salt Lake City, Utah 84104
Telephone (801) 584-2400
FAX (801) 584-2406

SEM PLATE 12
Mc-6-16b

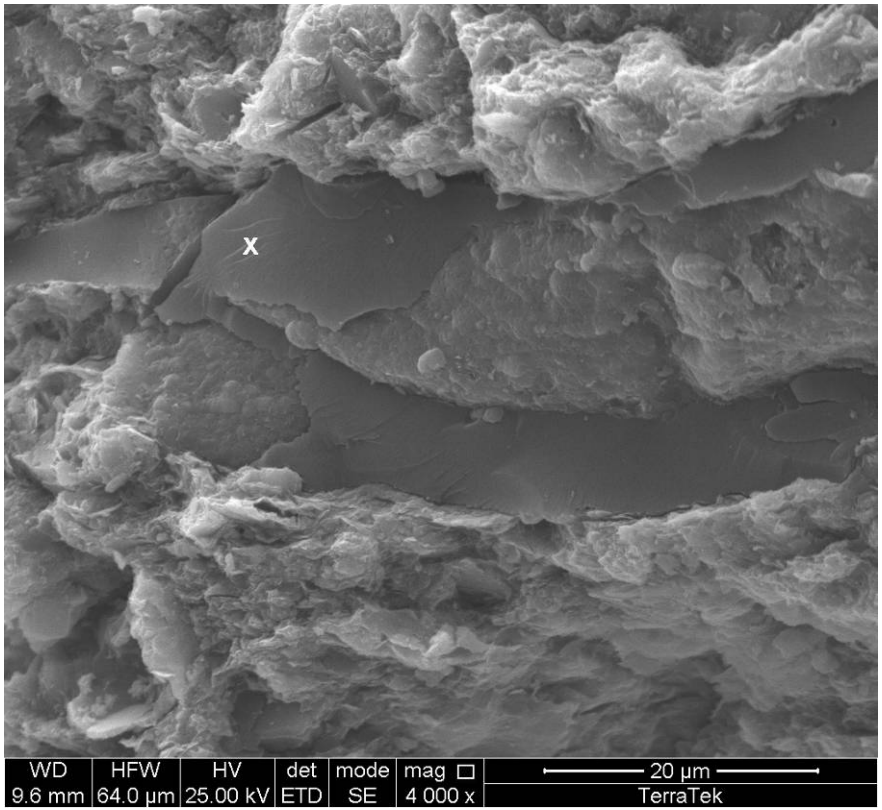

Closer view of partially silica-replaced organic maceral along the bedding plane. (Scale bar = 20 microns)

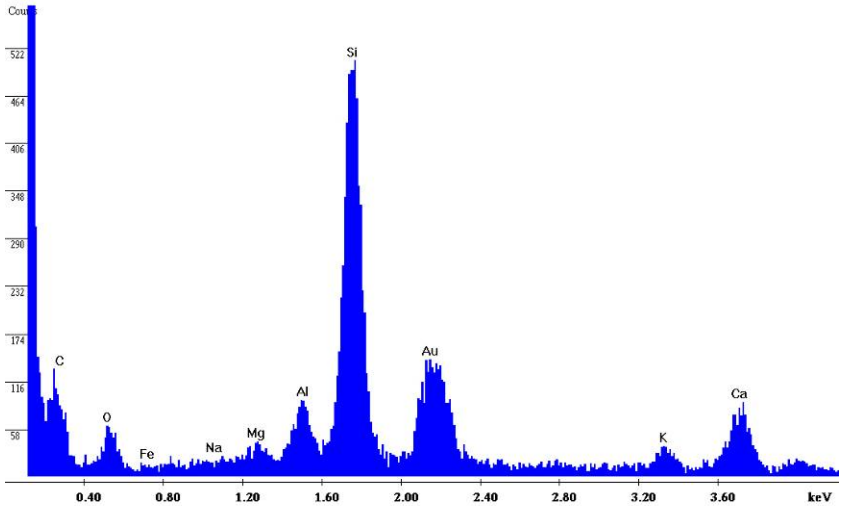

Elemental analysis of the organic particle indicates dominant silicon (replacing the organic material in the particle and from surrounding illite), and minor carbon from remaining organic material in the maceral, and possibly from nearby calcite.

Schlumberger Confidential

TerraTek
A Schlumberger company

1935 S. Fremont Drive • Salt Lake City, Utah 84104
Telephone (801) 584-2400
FAX (801) 584-2406

SEM PLATE 13
Mc-6-16b

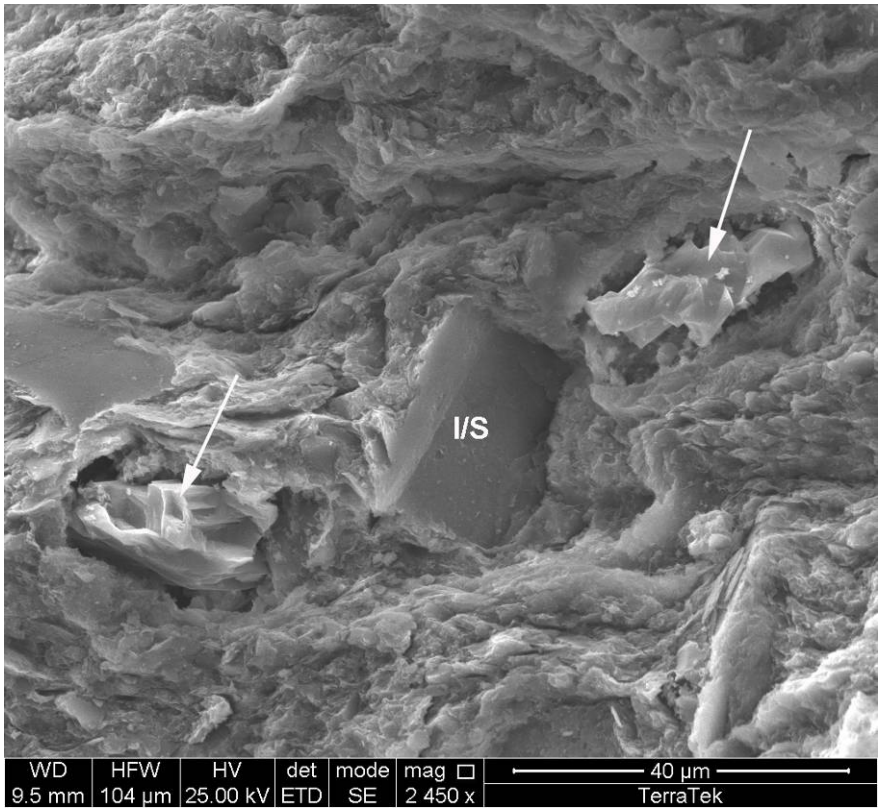

Two more particles that are infilled with authigenic albite crystals (arrows, see composition in next plate). These may have been hollow fossil or organic particles that have been removed by diagenesis and/or converted/infilled with the authigenic feldspar. (Scale bar = 40 microns)

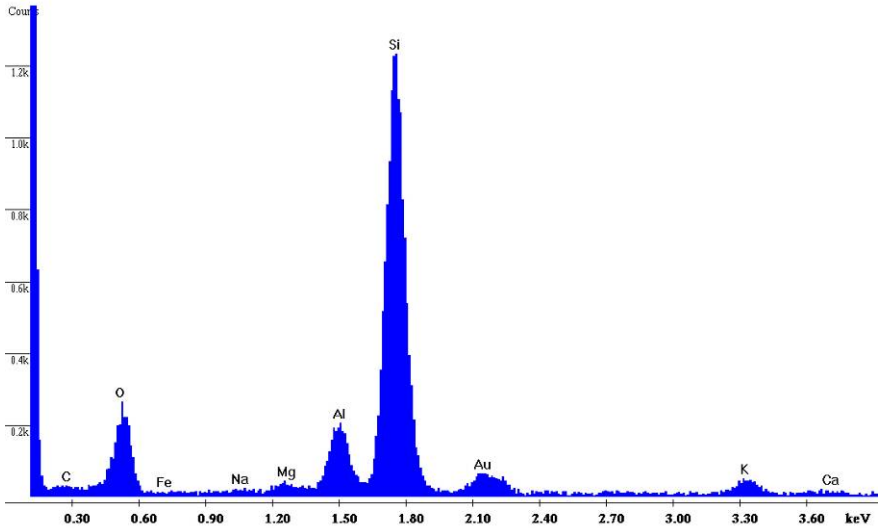

The wallrock of a rectangular grain mold is composed of mixed-layer illite-smectite (I/S). Elemental analysis of the matrix clay indicates silicon, aluminum, oxygen, and potassium from the illite portion of the mixed-layer clay, and trace amounts of magnesium from the small amount of smectite in the I/S structure.

Schlumberger Confidential

TerraTek
A Schlumberger company

1935 S. Fremont Drive • Salt Lake City, Utah 84104
Telephone (801) 584-2400
FAX (801) 584-2406

SEM PLATE 14
Mc-6-16b

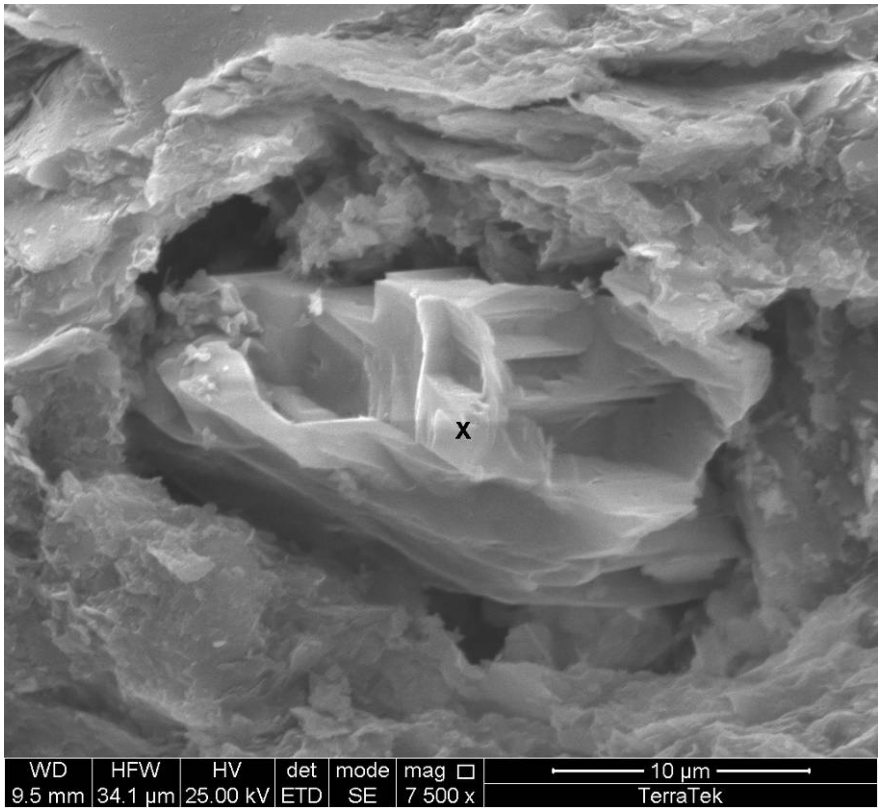

High magnification view of authigenic feldspar crystals in the middle of a dissolved-out particle. (Scale bar = 10 microns)

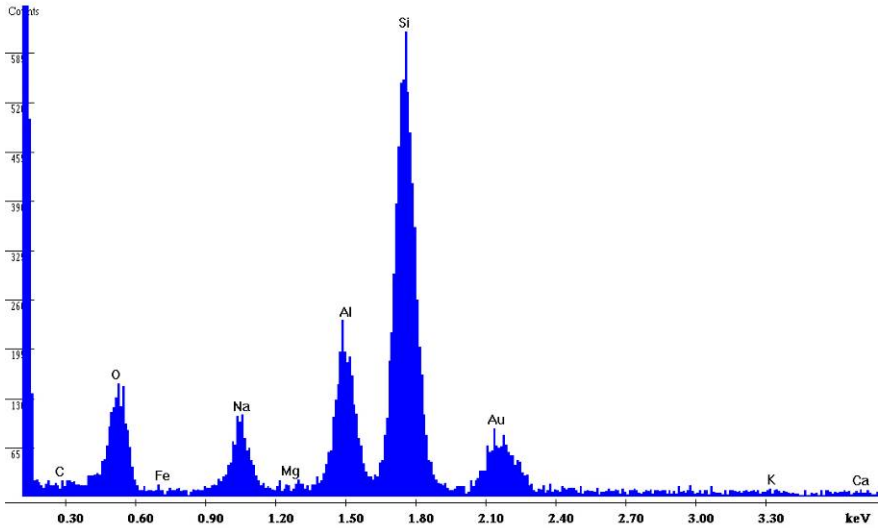

Spot elemental analysis (x) of the authigenic feldspar indicates a pure sodic composition, identifying albite. The sodic composition suggests the presence of saline formation or other fluids in the mudstone.

Schlumberger Confidential

TerraTek
A Schlumberger company

1935 S. Fremont Drive • Salt Lake City, Utah 84104
Telephone (801) 584-2400
FAX (801) 584-2406

SEM PLATE 15
Mc-7-42

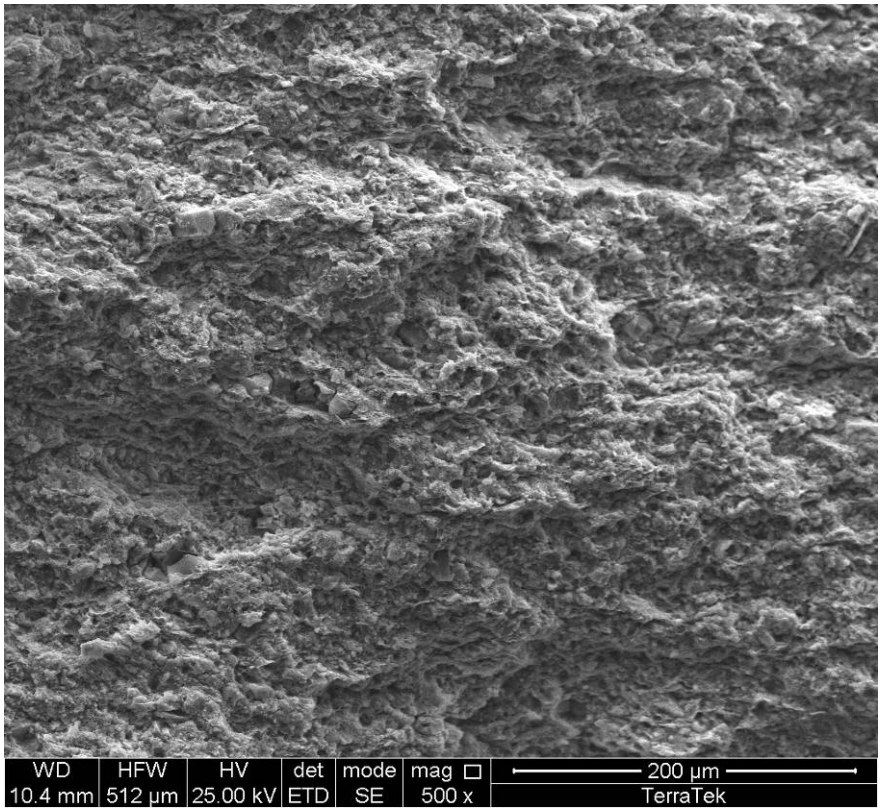

Textural overview of faintly laminated calcareous/argillaceous mudstone. (Scale bar = 200 microns).

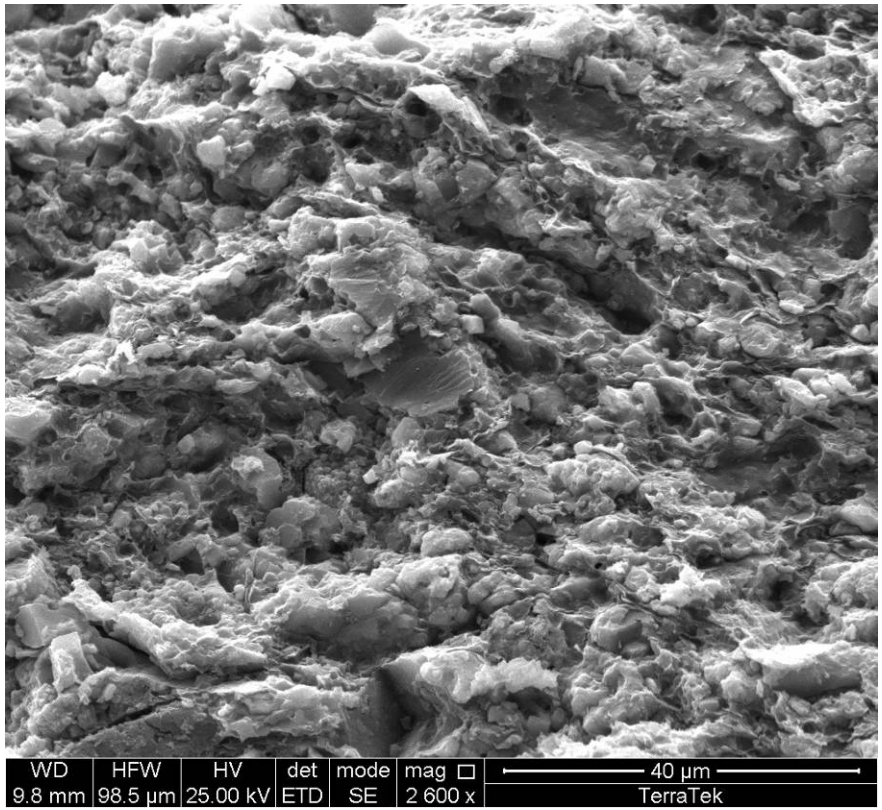

Closer view shows abundant calcic fossil fragments and a microporous matrix. (Scale bar = 40 microns)

Schlumberger Confidential

TerraTek
A Schlumberger company

1935 S. Fremont Drive • Salt Lake City, Utah 84104
Telephone (801) 584-2400
FAX (801) 584-2406

SEM PLATE 16
Mc-7-42

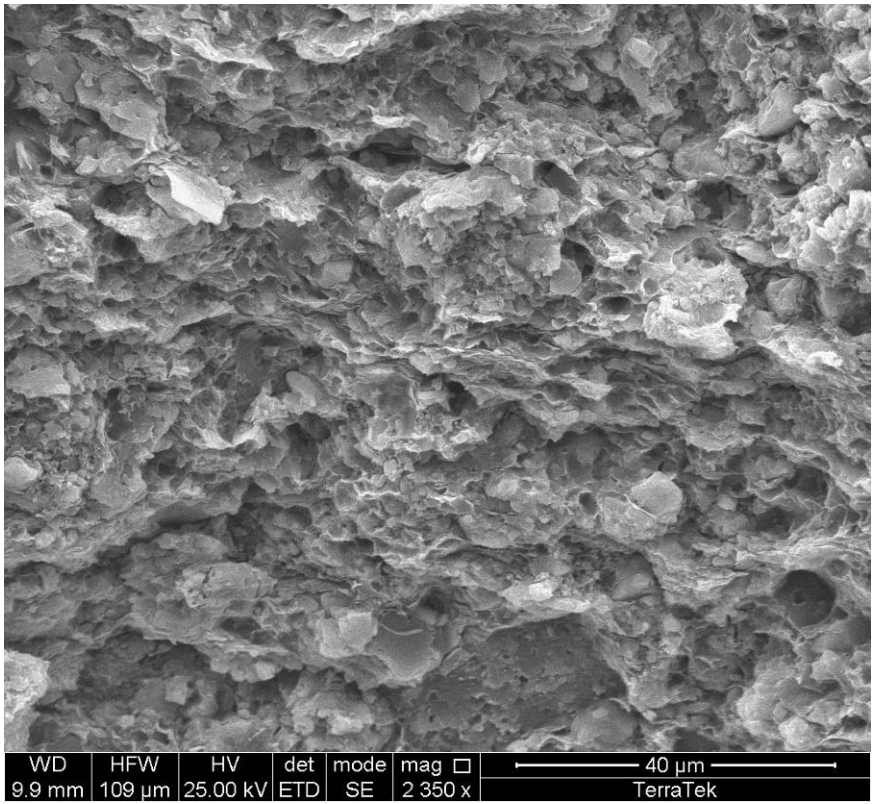

Some laminations within the mudstone are more argillaceous and have foliated flaky illitic clays along the bedding planes. (Scale bar = 40 microns)

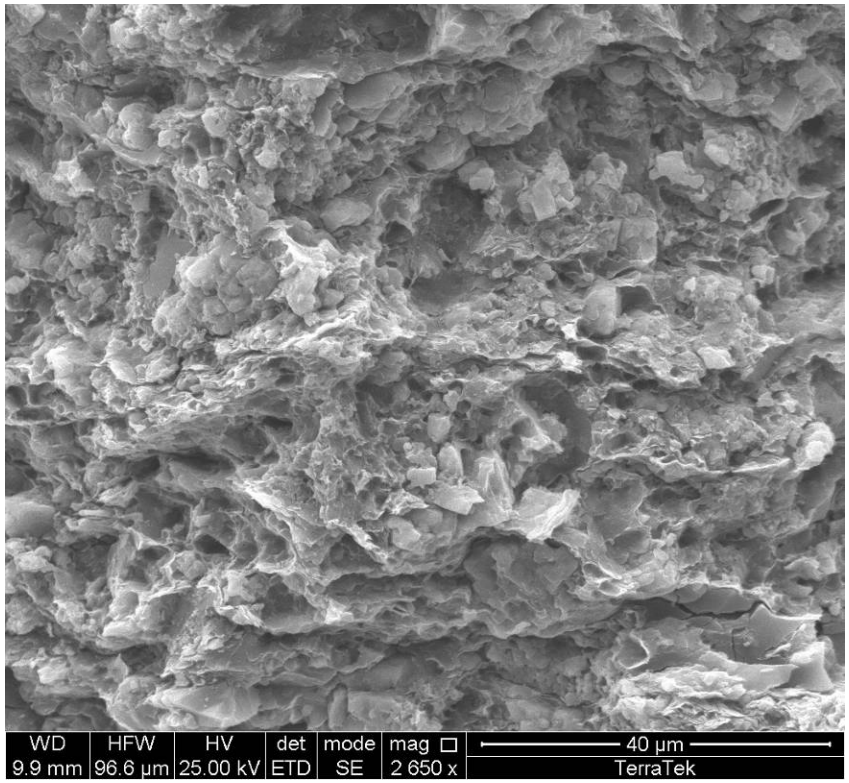

The wavy to flaky morphologies indicate the presence of abundant mixed-layer illite-smectite within the matrix. Although the clays appear to host abundant intercrystalline matrix micropores, depending upon how much interlayered smectite is present, the clays could be susceptible to expansion. (Scale bar = 40 microns)

Schlumberger Confidential

TerraTek
A Schlumberger company

1935 S. Fremont Drive • Salt Lake City, Utah 84104
Telephone (801) 584-2400
FAX (801) 584-2406

SEM PLATE 17
Mc-7-42

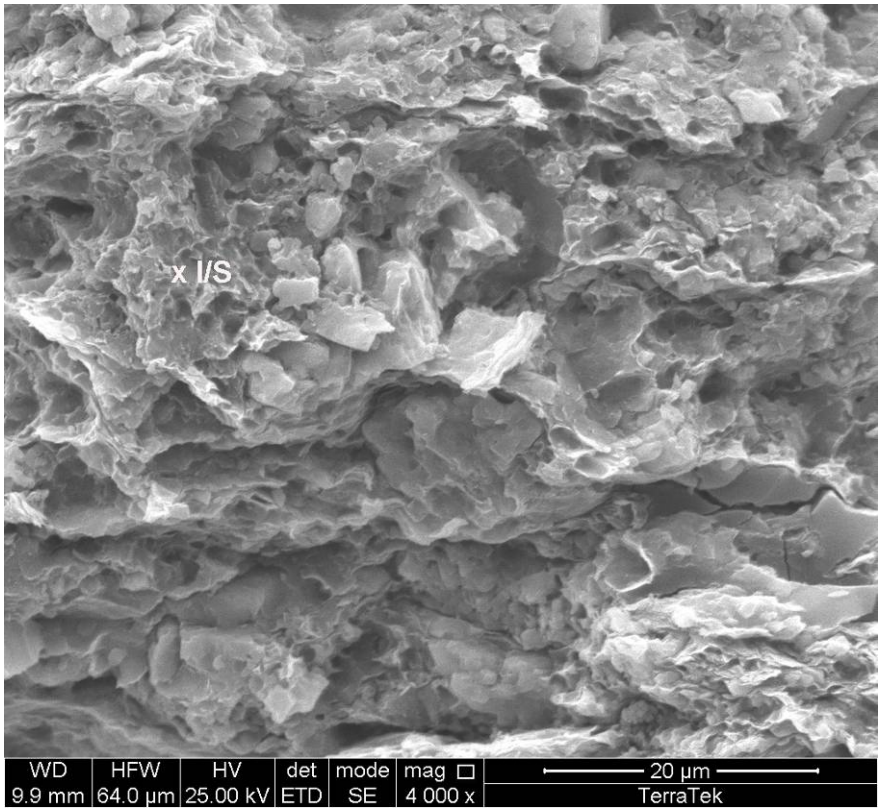

Closer view of delicate webby illite-smectite clay (I/S). (Scale bar = 20 microns)

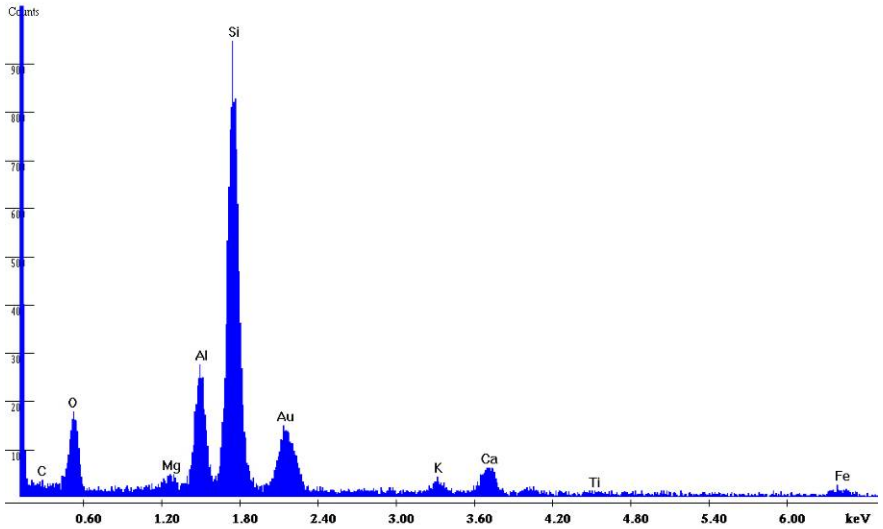

Elemental analysis of the clay (x) indicates more calcium, magnesium, and iron than potassium, suggesting a high proportion of potentially expandable smectite in the mixed-layer clay.

Schlumberger Confidential

TerraTek
A Schlumberger company

1935 S. Fremont Drive • Salt Lake City, Utah 84104
Telephone (801) 584-2400
FAX (801) 584-2406

SEM PLATE 18
Mc-7-42

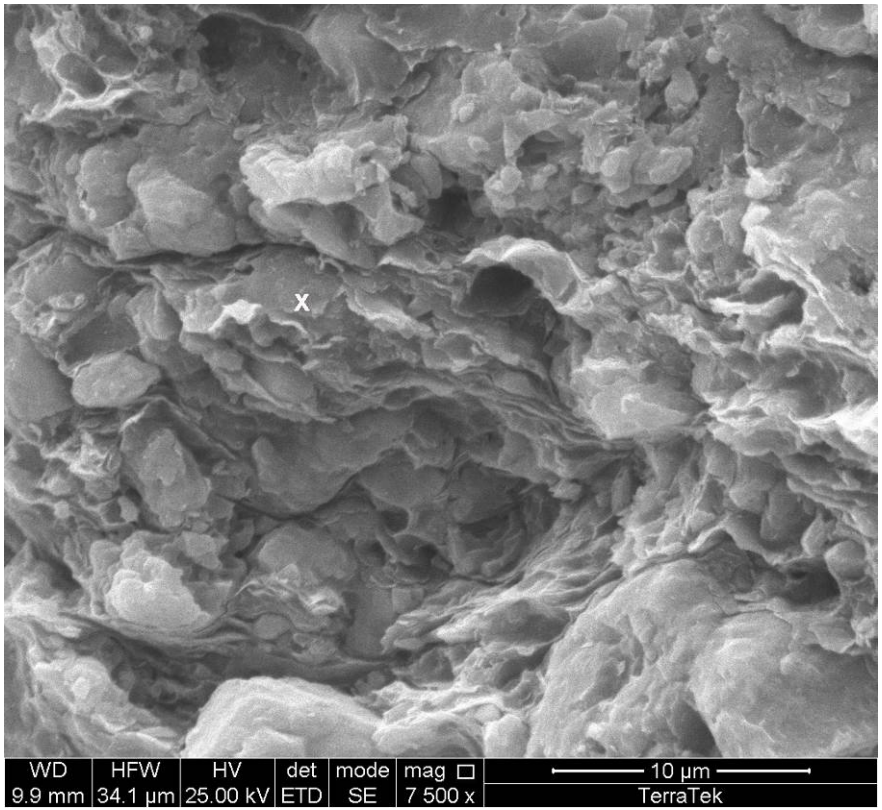

Another area with flaky, wavy clays. (Scale bar = 10 microns)

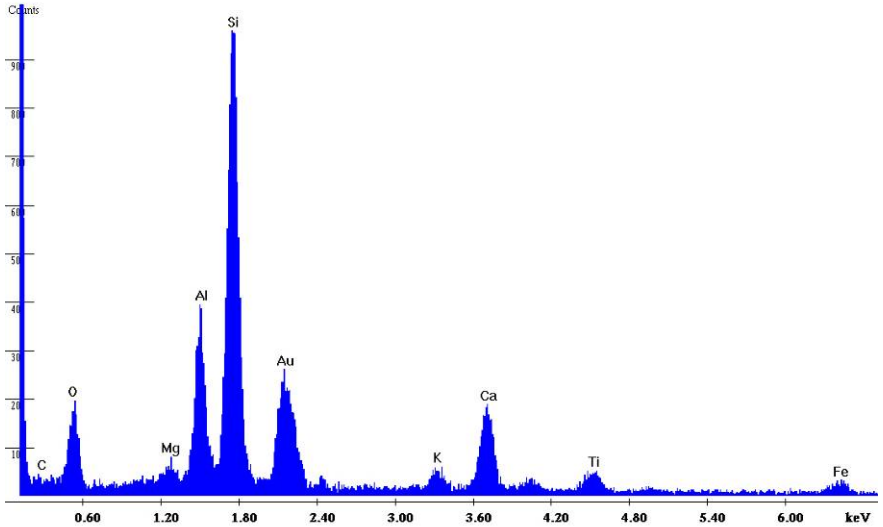

Spot elemental analysis (x) again reveals significant amounts of calcium from the smectite portion of the clay.

Schlumberger Confidential

TerraTek
A Schlumberger company

1935 S. Fremont Drive • Salt Lake City, Utah 84104
Telephone (801) 584-2400
FAX (801) 584-2406

SEM PLATE 19
Mc-7-42

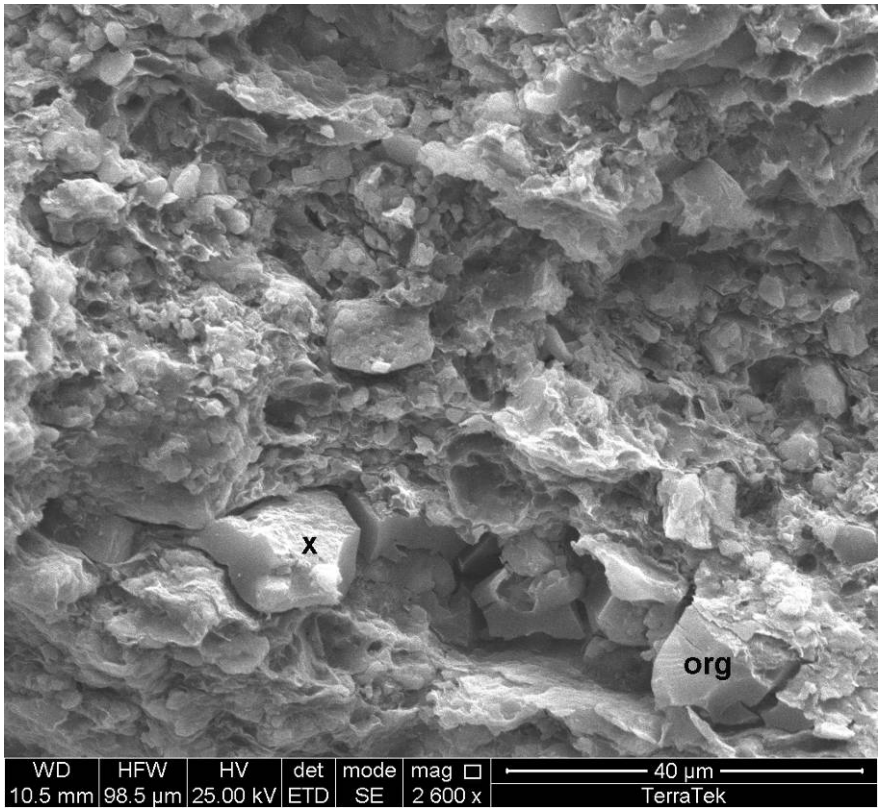

Organic material in the mudstone consists of discrete particles (org), and no disseminated kerogen appears to be present within the argillaceous matrix. (Scale bar = 40 microns)

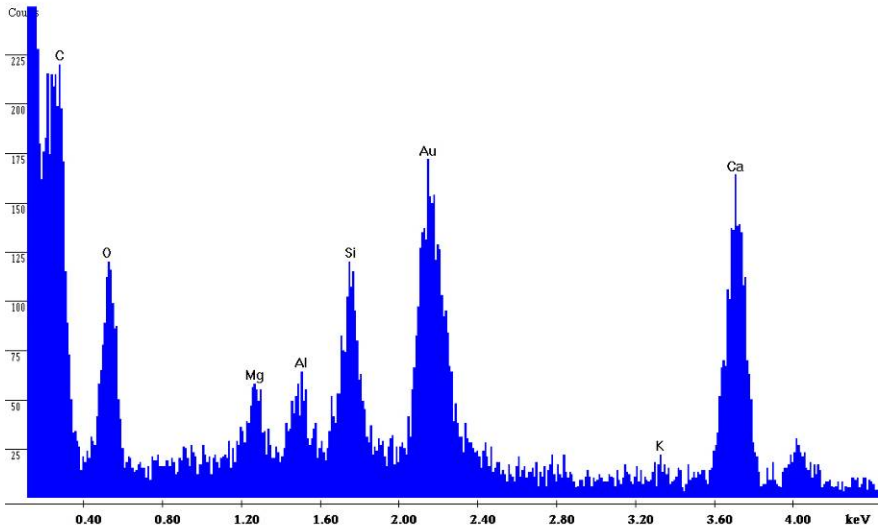

Spot elemental analysis (x) on the organic maceral indicates overall low counts and major peaks only for carbon (C) in the particle and the gold (Au) used to coat the samples. Other elements suggest the presence of nearby illite (Si, Al, K), and calcite or dolomite (Ca, Mg).

Schlumberger Confidential

TerraTek
A Schlumberger company

1935 S. Fremont Drive • Salt Lake City, Utah 84104
Telephone (801) 584-2400
FAX (801) 584-2406

SEM PLATE 20
Mc-7-42

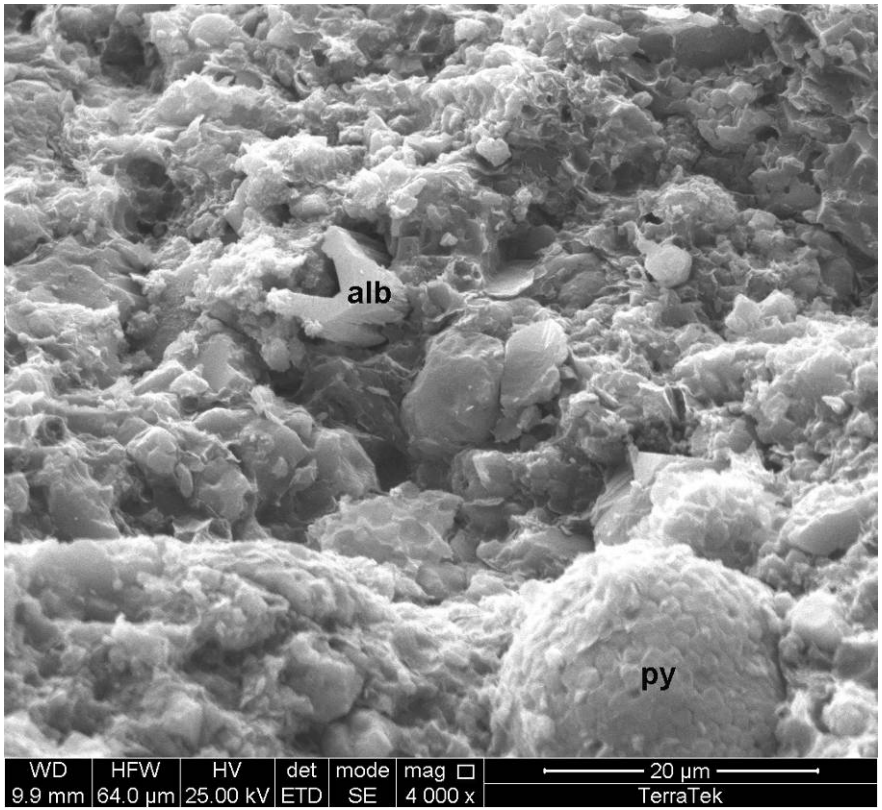

Back into an area with more calcareous fossil debris. Some fossils are replaced or infilled with authigenic albite (alb). Pyrite framboids are also fairly common (py) within the matrix. (Scale bar = 20 microns)

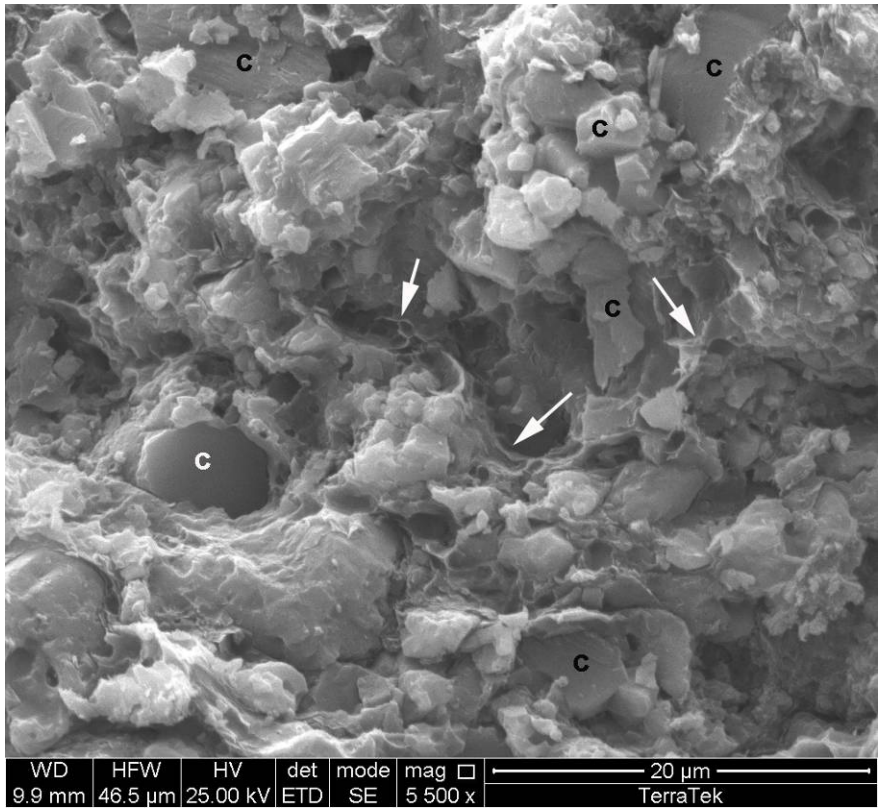

Calcite (c) occurs as fossil hash and as microcrystalline cement in the matrix, occluding matrix micropores. Webby smectite-rich clays coat the fossil grains and occur in intergranular areas (arrows). (Scale bar = 20 microns)

Schlumberger Confidential

TerraTek
A Schlumberger company

1935 S. Fremont Drive • Salt Lake City, Utah 84104
Telephone (801) 584-2400
FAX (801) 584-2406

SEM PLATE 21
Mc-7-42

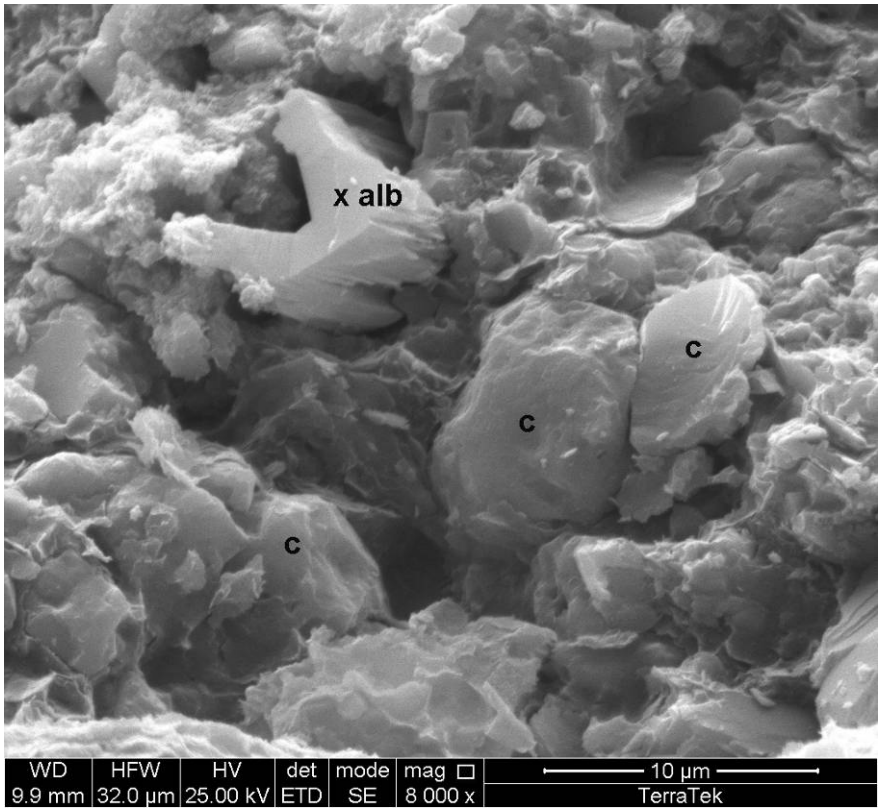

Close up of an authigenic albite crystal (alb) that replaces or infills a fossil fragment. Surrounding calcite grains (c) may represent ground-up or recrystallized fossil material that essentially forms a cement within the mudstone. (Scale bar = 10 microns)

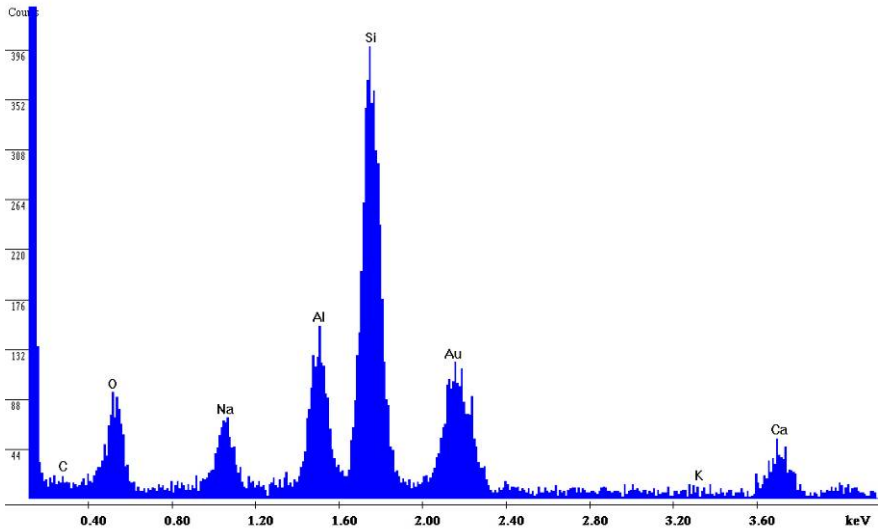

Elemental analysis on the authigenic feldspar (x) indicates a mixed sodium-calcium composition.

Schlumberger Confidential

TerraTek
A Schlumberger company

1935 S. Fremont Drive • Salt Lake City, Utah 84104
Telephone (801) 584-2400
FAX (801) 584-2406

SEM PLATE 22
Mc-9-86

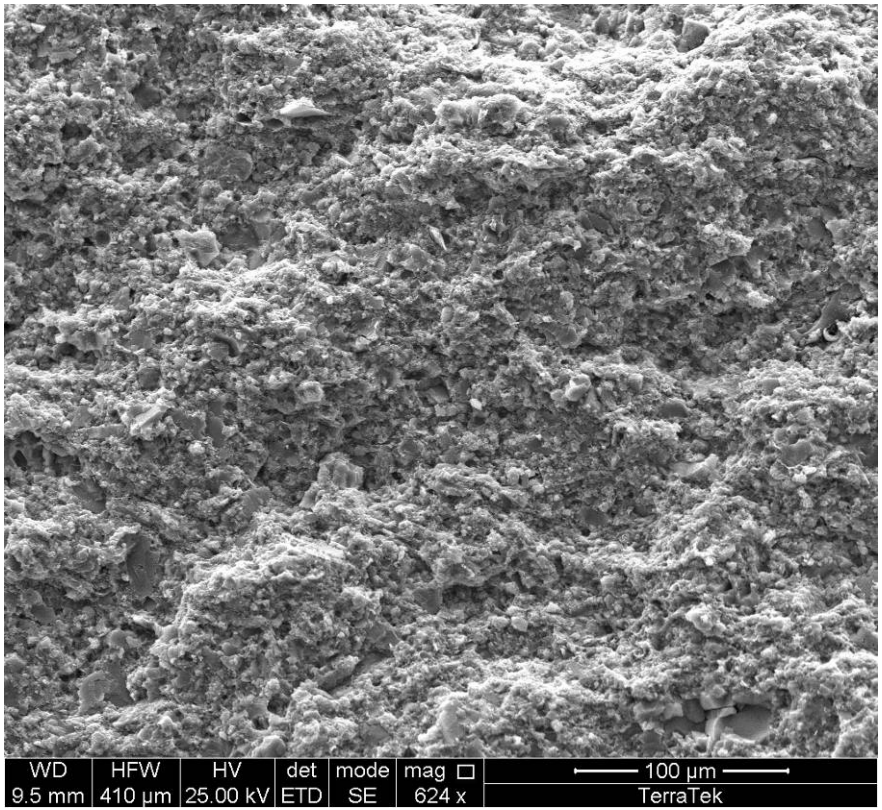

Mixed siliceous-calcareous mudstone that appears to host abundant matrix micropores. (Scale bar = 100 microns)

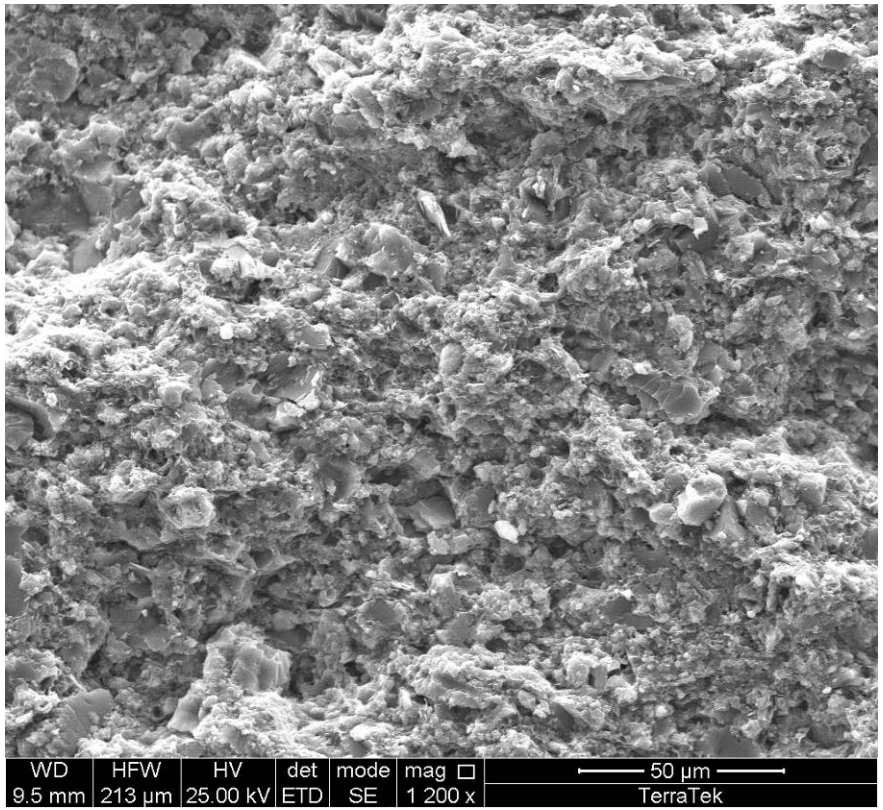

The granular microtexture is characteristic of a siliceous matrix. (Scale bar = 50 microns)

Schlumberger Confidential

TerraTek
A Schlumberger company

1935 S. Fremont Drive • Salt Lake City, Utah 84104
Telephone (801) 584-2400
FAX (801) 584-2406

SEM PLATE 23
Mc-9-86

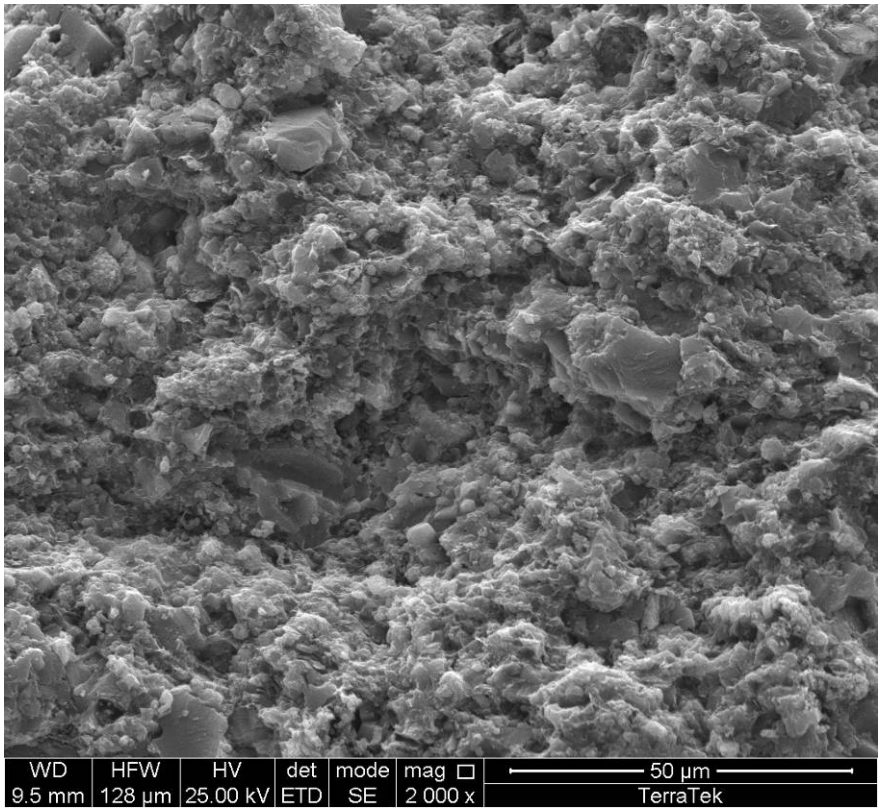

Another characteristic of a siliceous matrix is the microtopography; silica-cemented areas stand out in relief. (Scale bar = 50 microns)

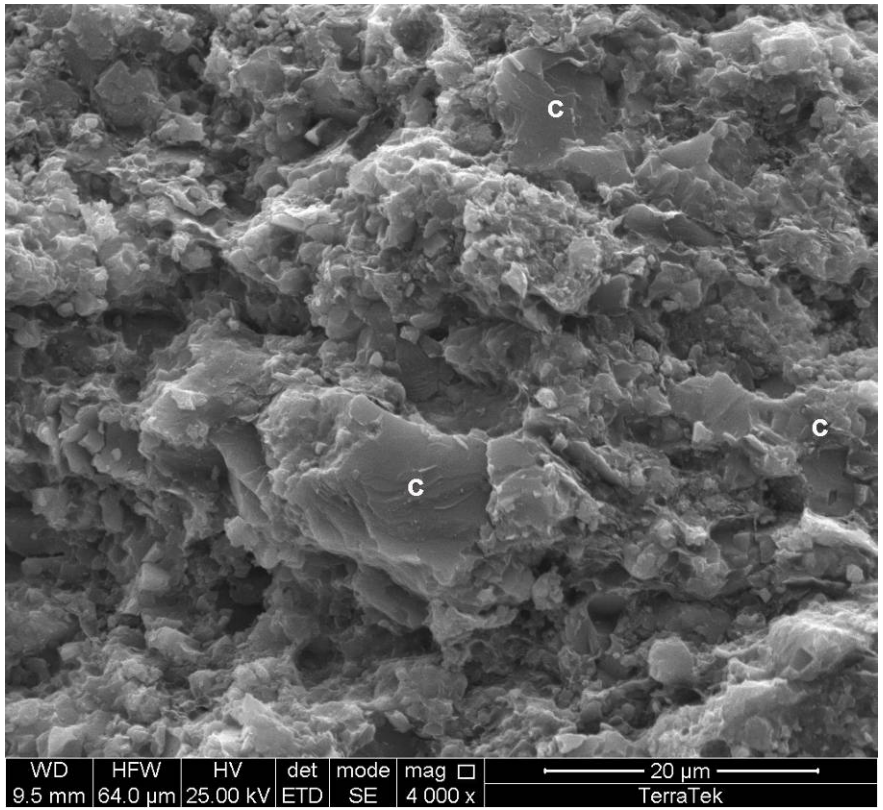

Detail of adjacent image showing the calcareous fossil fragments (c) in the siliceous matrix. The silica-cemented matrix supports the mudstone against compaction, preserving matrix microporosity. (Scale bar = 20 microns)

Schlumberger Confidential

TerraTek
A Schlumberger company

1935 S. Fremont Drive • Salt Lake City, Utah 84104
Telephone (801) 584-2400
FAX (801) 584-2406

SEM PLATE 24
Mc-9-86

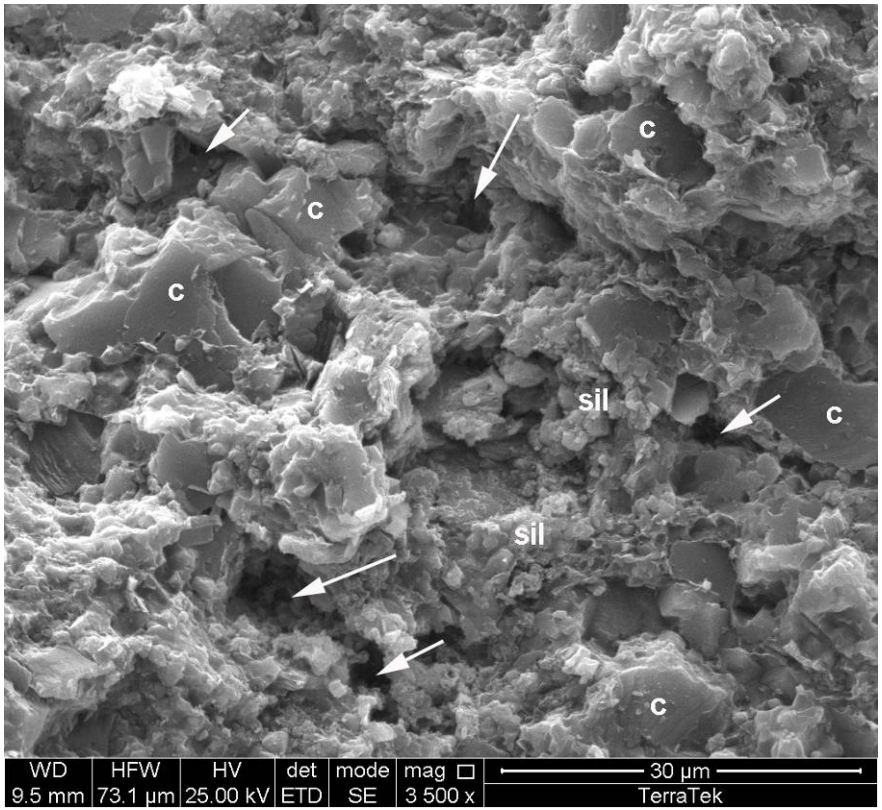

Another view of silt-sized calcic fossil fragments (c) and the porous siliceous matrix (sil). The largest pores are 5-10 microns across (arrows), and appear to be well-connected in a permeable network of matrix micropores. (Scale bar = 30 microns)

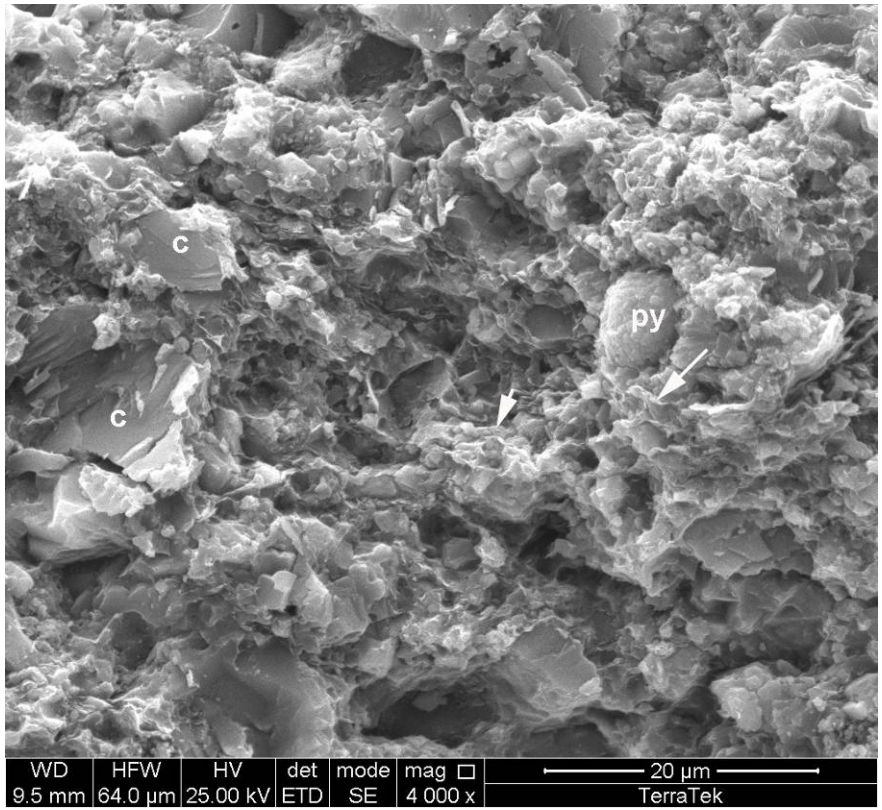

Although there are some flaky clays in the matrix (arrows), the dominant matrix constituent is microcrystalline quartz. Some pyrite framboids (py) are also present. (Scale bar = 20 microns)

Schlumberger Confidential

TerraTek
A Schlumberger company

1935 S. Fremont Drive • Salt Lake City, Utah 84104
Telephone (801) 584-2400
FAX (801) 584-2406

SEM PLATE 25
Mc-9-86

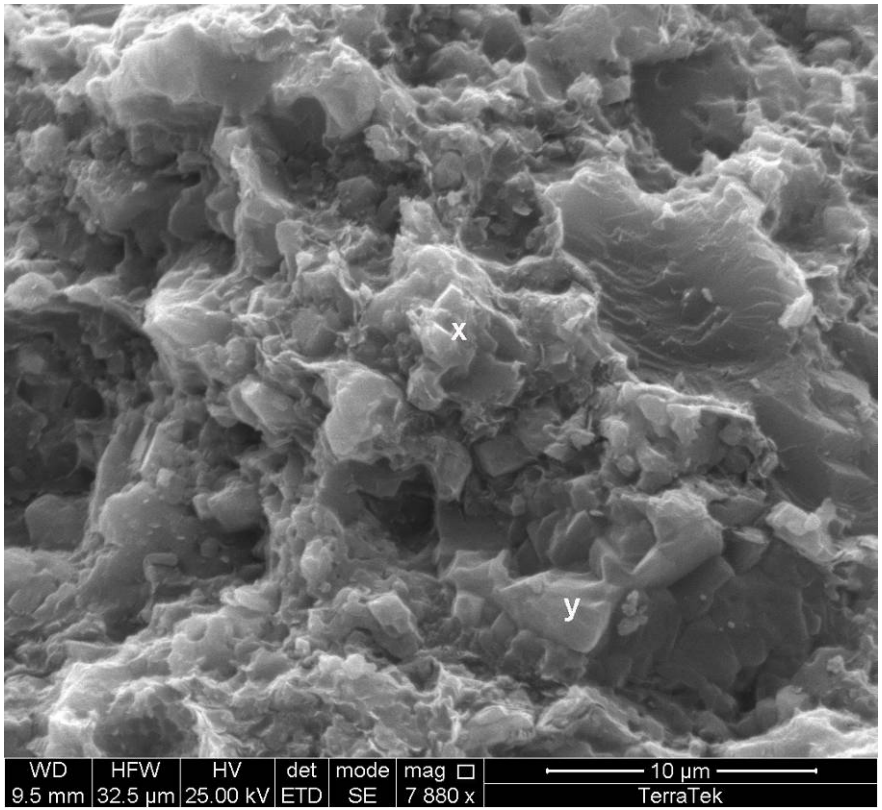

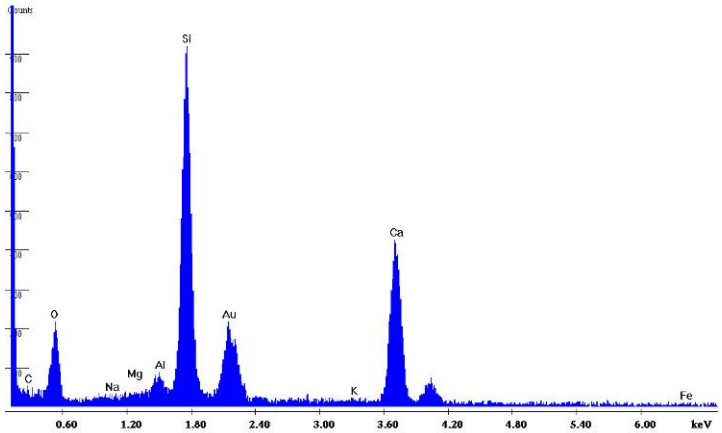

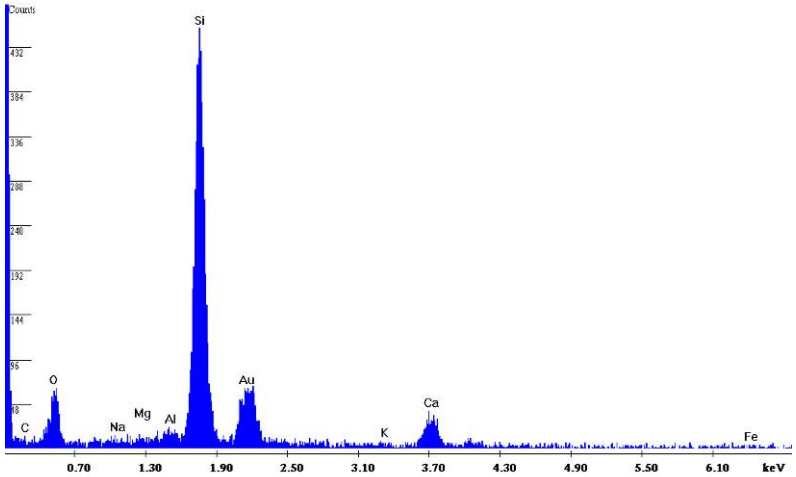

High magnification of an area of the microcrystalline matrix. Area x (upper spectra) is composed of both quartz and calcite cements, and area y (lower spectra) is composed only of quartz. (Scale bar = 10 microns)

Schlumberger Confidential

TerraTek
A Schlumberger company

1935 S. Fremont Drive • Salt Lake City, Utah 84104
Telephone (801) 584-2400
FAX (801) 584-2406

SEM PLATE 26
Mc-9-86

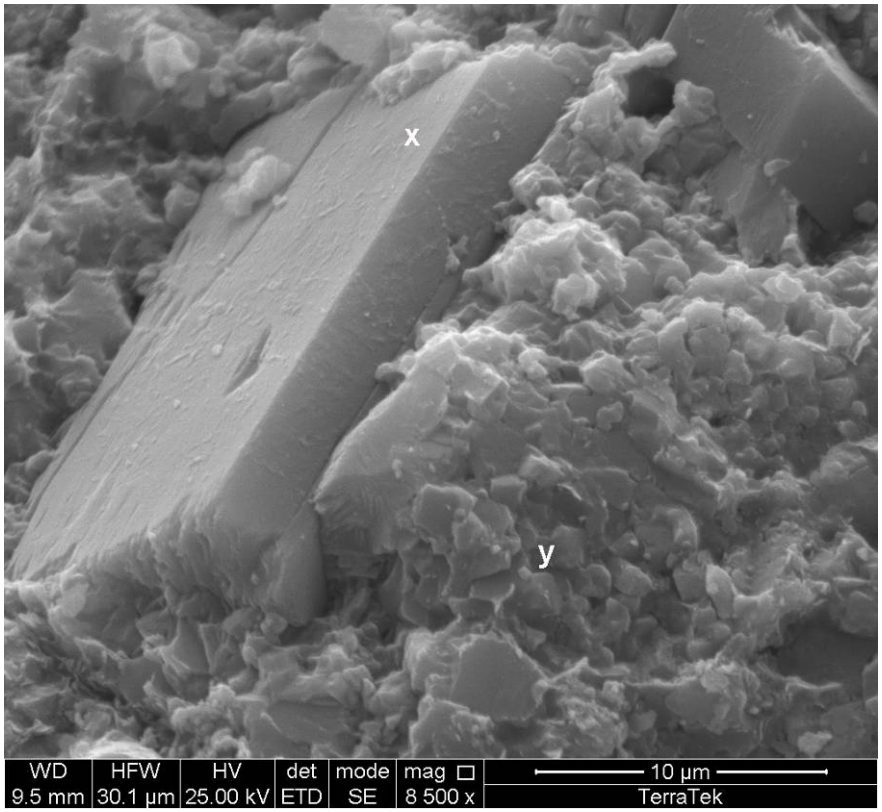

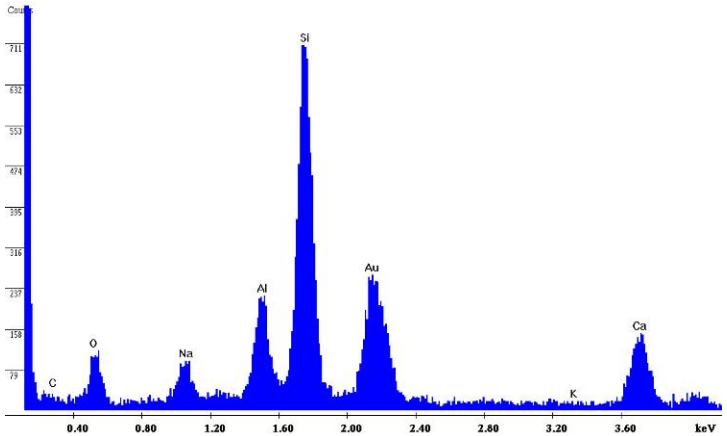

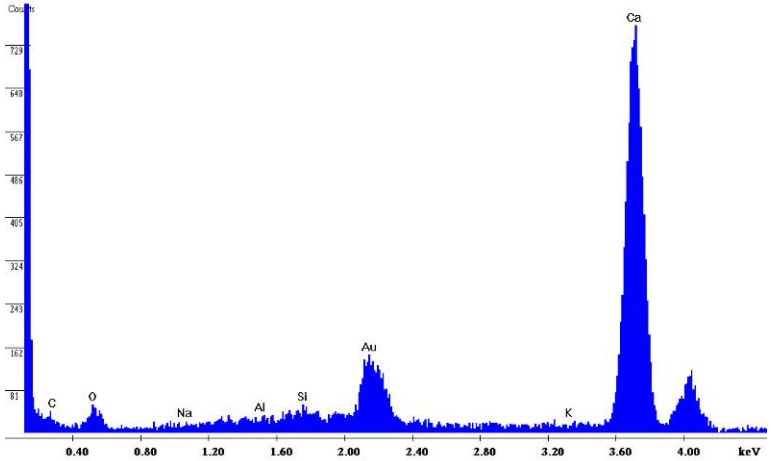

Rectangular crystals in the matrix are composed of authigenic Ca-Na feldspars (x, upper spectra). Well-cemented areas of the matrix are composed of microcrystalline calcite (y, lower spectra). (Scale bar = 10 microns)

Schlumberger Confidential

TerraTek
A Schlumberger company

1935 S. Fremont Drive • Salt Lake City, Utah 84104
Telephone (801) 584-2400
FAX (801) 584-2406

Appendix E

Chainman Shale Stratigraphic Section Mineral and Elemental Concentrations
Whole-Rock X-Ray Fluorescense Oxide Weight Percent and X-Ray Diffraction
Mineral Identification of Samples Collected from the Camp Canyon Stratigraphic Section

		X-Ray Fluorescence Major Elements												Total
Sample ID	Meters[1]	SiO_2	Al_2O_3	CaO	MgO	Na_2O	K_2O	Fe_2O_3	MnO	TiO_2	P_2O_5	SO_3	CL	Sample Wt%[2]
cc-mc-535m	535	1.97	0.44	95.60	0.87		0.17	0.45			0.27	0.02	0.01	99.98
cc-mc-9-515m	515	3.22	0.31	93.80	0.93	0.13	0.05	0.79			0.31	0.08	0.01	99.98
cc-mc-8-494m	494	5.45	0.60	84.10	1.09		0.08	7.66	0.19		0.33	0.12	0.00	99.97
cc-mc-7-486m	486	50.60	19.90	12.30	1.05	0.10	1.95	11.40	0.05	1.93	0.25	0.08	0.01	99.99
cc_mc_5_485M	485	3.38	0.88	89.20	1.44		0.12	2.51	0.77		1.15	0.20	0.01	99.76
cc-mc-4-484	484	69.50	16.70	3.88	1.00	0.07	2.54	4.12		1.79	0.11	0.03	0.03	99.99
cc-mc-3-483	483	52.30	15.00	20.60	1.16		2.61	5.37		2.39	0.18	0.06	0.01	100.05
cc-mc-6-479	479	81.90	3.18	7.72	0.51		0.21	5.36	0.05	0.57	0.12	0.02	0.01	99.96
cc-mc-458-459	458	13.70	1.94	54.30	0.99		0.12	13.40		0.27	14.10	0.15	0.00	100.03
cc-mc-1-431	431	4.80	0.16	92.40	1.10		0.06	0.75			0.26	0.04	0.01	99.98
cc-mc-8-51-281-5	282	54.40	11.90	20.80	1.29	0.21	1.99	7.49		1.38	0.14	0.07	0.01	100.04
cc-mc-8-51-281	281	31.00	3.05	58.10	0.82	0.15	0.41	4.67		0.33	0.29	0.14	0.01	99.91
cc-mc-8-49-273m	273	32.90	6.51	52.60	0.86	0.06	1.06	4.31		0.82	0.20	0.05	0.00	99.99
cc-mc-271	271	37.60	7.10	45.80	1.20	0.21	1.10	5.30		0.91	0.17	0.06	0.01	100.02
cc-mc-7-42-233m	223	27.90	6.16	57.80	1.00	0.10	0.92	4.38		0.63	0.25	0.07	0.01	100.03
cc-mc-213	213	32.70	3.72	55.10	1.54	0.11	0.62	4.35		0.55	0.35	0.12	0.01	100.01
cc-mc-193m	193	51.30	12.20	23.60	1.08	0.11	1.70	7.98		1.43	0.12	0.07	0.01	99.96
cc-mc-192m	192	33.30	3.56	55.30	0.72	0.24	0.48	4.94		0.30	0.30	0.11	0.00	99.97
cc-mc-175	175	43.30	8.61	38.20	0.96	0.08	1.07	5.84		0.95	0.22	0.07	0.00	99.94
cc-mc-7-35-173m	173	60.10	12.50	15.90	0.96	0.11	1.58	6.79		1.37	0.18	0.07		99.94
cc-mc-171	171	60.20	12.40	15.70	0.95	0.14	1.55	7.17		1.32	0.17	0.06	0.00	100.08
cc_mc_146	146	47.90	12.00	28.40	0.81	0.07	1.42	7.31		1.18	0.27	0.09	0.00	100.02
cc_mc_131	131	61.00	21.70	1.46	1.10	0.17	2.10	9.93		1.96	0.07	0.10	0.01	100.01
cc-mc-123	123	34.90	8.37	46.30	0.95	0.06	1.37	6.22		0.99	0.23	0.12	0.00	100.06
cc_mc_99	99	64.00	19.80	0.54	1.53	0.66	3.00	7.06		2.06	0.11	0.68	0.17	100.02
cc_mc_75m	76	75.80	9.56	0.98	1.11	0.09	4.58	6.01		1.14	0.07	0.18	0.00	99.99
cc_mc_75m_616	75	42.40	5.29	33.70	10.00	0.27	2.33	4.10	0.09	0.98	0.18	0.31	0.02	99.94
cc_mc_41-5	42	63.40	9.35	10.20	4.42	0.50	4.39	5.95		1.27	0.11	0.09	0.01	100.07
cc-mc-41	41	64.50	13.20	3.43	2.22	0.26	6.60	7.03		1.62	0.44	0.13	0.01	99.96
cc_mc_2_14m	14	54.40	7.77	20.00	7.01	0.40	3.44	5.22	0.05	1.08	0.12	0.36	0.02	100.00
d-ph-ch	12	22.60	2.41	47.60	0.50		1.12	3.08		0.34	21.00	0.27	0.01	99.95
cc_mc_9	9	2.98	0.26	94.00	1.03	0.11	0.07	0.82			0.28	0.08	0.01	100.00
cc-mc-7-5	7	74.70	9.92	1.10	1.18	0.05	4.87	6.26		1.01	0.09	0.33	0.01	99.97
cc_mc_1_basal_wp	1	18.80	1.34	52.50	0.22		0.53	1.43			23.60	0.34	0.01	100.27
0-30-ch	0	51.40	7.14	22.90	7.85	0.46	3.24	4.90	0.09	1.04	0.16	0.40	0.06	100.02

Note

[1] Meters are the sampling location in the Camp Canyon stratigraphic sequence from the Joanna Limestone at the base, through the members of the Chainman Shale, to the Ely Limestone at the top of the section.

[2] Samples powdered and analyzed using qualitative X-ray fluorescense analysis. Duplicate samples were prepared and analyzed to determine the reproducability and precision.

Appendix E

Chainman Shale Stratigraphic Section Mineral and Elemental Concentrations
Whole-Rock X-Ray Fluorescense Oxide Weight Percent and X-Ray Diffraction
Mineral Identification of Samples Collected from the Camp Canyon Stratigraphic Section

		X-Ray Fluorescence Trace Elements								X-Ray Diffraction Phase Analysis
Sample ID	Meters[1]	V_2O_5	Cr_2O_3	NiO	ZnO	As_2O_3	Rb_2O	SrO	Y_2O_3	[3]Approximate Sample %
cc-mc-535m	535							0.09		Calcite 93%, Quartz 7%
cc-mc-9-515m	515							0.25		Calcite 59%, Feldspar 34%, Quartz 7%
cc-mc-8-494m	494							0.24		Calcite 76%, Quartz 24%
cc-mc-7-486m	486		0.12	0.05				0.11		Chlorite 43%, Quartz 37%, Calcite 17%, clay 3%
cc_mc_5_485M	485									Calcite 89%, Muscovite 4%, Dolomite 3%, Clay Minerals 3%, Apatite 1%
cc-mc-4-484	484		0.09					0.05		Quartz 66%, Chlorite 16%, Muscovite 15%, Clay Minerals 3%
cc-mc-3-483	483		0.12	0.04				0.10		Quartz 49%, Chlorite 29%, Calcite 14%, Clay Minerals 8%
cc-mc-6-479	479	0.08	0.13					0.03		Quartz 89 %, Mica 6%, Calcite 5%
cc-mc-458-459	458		0.12	0.07	0.30			0.39	0.08	Fluorapatite 70%, Calcite 15%, Mica 9%, Quartz 6%
cc-mc-1-431	431							0.29		Calcite 66%, Dolomite 17%, Quartz 12%, Apatite 5%
cc-mc-8-51-281-5	282		0.07					0.21		Calcite 64%, Quartz 28%, Clay Minerals 8%
cc-mc-8-51-281	281		0.08		0.14			0.64		Calcite 64%, Quartz 28%, Clay Minerals 8%
cc-mc-8-49-273m	273		0.08					0.44		Calcite 66%, Quartz 25%, Gypsum 8%, Clay Minerals 1%
cc-mc-271	271							0.47		Calcite 56%, Quartz 32%, Vermiculite 10%, Biotite 2%
cc-mc-7-42-233m	223							0.72		Calcite 52%, Quartz 43%, Clay Minerals 5%
cc-mc-213	213		0.09	0.06	0.05			0.54		Calcite 44%, Quartz 31%, Dolomite 20%, Clay Minerals 5%
cc-mc-193m	193		0.07	0.04	0.03			0.12		N/A
cc-mc-192m	192		0.09					0.56		Quartz 59%, Calcite 37%, Clay Minerals 4%
cc-mc-175	175		0.10	0.05	0.03			0.38		Quartz 39%, Calcite 30%, Feldspar 29%, Clay Minerals 2%
cc-mc-7-35-173m	173		0.11		0.04			0.16		Quartz 53%, Chlorite 42%, Calcite 5%
cc-mc-171	171		0.08	0.04	0.04			0.16		Quartz 61%, Calcite 23%, Biotite 9%, Clay Minerals 7%
cc_mc_146	146		0.10		0.07			0.29		Quartz 32%, Calcite 28%, Clay Minerals 29%, Mica 11%
cc_mc_131	131		0.11	0.04	0.04		0.03	0.11		Clay Minerals 57%, Quartz 25%, Biotite 18%
cc-mc-123	123		0.11					0.34		Quartz 50%, Calcite 33%, Biotite 10%, Clay Minerals 7%
cc_mc_99	99		0.19	0.04				0.09		Quartz 60%, Muscovite 21%, Clay Minerals 19%
cc_mc_75m	76		0.14	0.06	0.05		0.03	0.09		Quartz 72%, Other Micas 18%, Muscovite 10%
cc_mc_75m_616	75		0.10					0.05		Quartz 43%, Dolomite 43%, Muscovite 8%, Biotite 6%
cc_mc_41-5	42		0.10	0.05	0.08			0.04		Quartz 82%, Biotite 15%, Clay Minerals 3%
cc-mc-41	41		0.19	0.06	0.10		0.04	0.06		Muscovite 35%, Quartz 34%, Clay Minerals 31%
cc_mc_2_14m	14							0.05		Feldspar 37%, Dolomite 36%, Quartz 22%, Biotite 6%
d-ph-ch	12	0.13		0.08	0.05			0.54	0.15	Fluorapatite 76%, Quartz 24%
cc_mc_9	9							0.25		Calcite 96%, Quartz 4%
cc-mc-7-5	7		0.11	0.05	0.06	0.03	0.03	0.08		Quartz 64%, Illite 28%, Clay Minerals 8%
cc_mc_1_basal_wp	1		0.15	0.06	0.26			0.64	0.29	Fluorapatite 75%, Quartz 25%
0-30-ch	0		0.13	0.04	0.03			0.06		Quartz 40%, Dolomite 33%, Feldspar 18%, Biotite 9%

Note

[1] Meters are the sampling location in the Camp Canyon stratigraphic sequence from the Joanna Limestone at the base, through the members of the Chainman Shale, to the Ely Limestone at the top of the section.

[3] Mineralogical assembledge identified from powdered samples. Phases identified from using PDXL software and the ICDD and COD pattern databases. Percentage of phase identified is qualitative and indicates the relative precentages of phases in the whole-rock sample.